Nano Energy 91 (2022) 106661

Contents lists available at ScienceDirect

Nano Energy

journal homepage: www.elsevier.com/locate/nanoen

Review

Recent advances in structural engineering of 2D hexagonal boron nitride electrocatalysts

Madiha Rafiq [a], Xiaozhen Hu [a], Zhiliang Ye [a], Abdul Qayum [a], Hong Xia [a], Liangsheng Hu [a,*], Fushen Lu [a,*], Paul K. Chu [b,*]

[a] Department of Chemistry and Key Laboratory for Preparation and Application of Ordered Structural Materials of Guangdong Province, Shantou University, Guangdong 515063, China

[b] Department of Physics, Department of Materials Science and Engineering, and Department of Biomedical Engineering, City University of Hong Kong, Tat Chee Avenue, Kowloon, Hong Kong, China

ARTICLE INFO

Keywords:
boron nitride
oxygen reduction reaction
hydrogen evolution reaction
oxygen evolution reaction
carbon dioxide reduction reaction
nitrogen reduction reaction

ABSTRACT

Hexagonal boron nitride (h-BN) as a type of two-dimensional (2D) materials has gained significant attention in green energy applications recently. In the past, h-BN has mainly been regarded as inert materials because of the poor conductivity and is mainly used commercially as insulators. However, recent advances in materials science and nanotechnology have unveiled exciting applications of h-BN by taking advantage of the unique chemical and electrochemical properties, high thermal stability, as well as environmental friendliness. In the energy field, h-BN has not been researched as extensively as other 2D materials such as graphene and there have been few comprehensive reviews discussing the various aspects of the materials and applications. The objective of this review is to summarize recent results and applications of this unique class of materials and to provide guidance to future research and development of green energy systems based on h-BN. We first describe the physical and chemical modification strategies to convert insulating h-BN into the desirable conductive materials suitable for energy conversion. In addition to functionalization strategies, different synthetic methods and important properties of h-BN are reviewed. We then describe recent progress and applications of h-BN as electrocatalysts in energy applications, including the oxygen reduction reaction (ORR), hydrogen evolution reaction (HER), oxygen evolution reaction (OER), carbon dioxide reduction reaction (CO_2RR), and nitrogen reduction reaction (NRR). The electrocatalytic mechanisms and impact on the materials performance are discussed and finally, the challenges and prospects for modified h-BN in the energy conversion field are discussed.

1. Introduction

Heterogeneous electrocatalysis, which a critical process in rechargeable batteries, electrochemical water splitting, and fuel cells, is an important technology to produce sustainable energy and mitigate the society's dependence on fossil fuels [1]. Electrocatalysis, a process in which electrochemical reactions on the electrode surfaces are accelerated, must be well understood, especially the fundamental mechanisms and principles, in order to benefit next-generation energy systems [2–7]. The carbon cycle, nitrogen cycle, and water cycle are the three main energy cycles in electrolysis and are essential to energy-related applications [8–10]. For example, the anodic hydrogen oxidation reaction (HOR) and cathodic oxygen reduction reaction (ORR) take place in H_2/O_2 fuel cells to release water and electrical energy, respectively. In comparison, in water splitting or electrolysis, water molecules are dissociated into hydrogen and oxygen via the hydrogen evolution reaction (HER) and oxygen evolution reaction (OER) [3,11]. In fuel cells, the electrolyzing units can be combined to form single units, referred to as regenerating fuel cells, which have promising potential in transportation applications. Organic compounds containing carbon such as formic acid, methanol, ethanol, and dimethyl ether may be utilized directly as fuels in fuel cells to produce carbon dioxide, water, and electricity. Carbon dioxide can be reduced by the CO_2 reduction reaction (CO_2RR) and converted by electrochemical reactions into value-adding fuel products such as methanol, methane, and ethanol [12–14].

Electrocatalytic techniques can also be utilized to convert biomass-derived chemical compounds such as glycerol, furan, and 5-hydroxymethyl-2-furfural into value-added products. In the nitrogen cycle,

* Corresponding authors.
E-mail addresses: lshu@stu.edu.cn (L. Hu), fslu@stu.edu.cn (F. Lu), paul.chu@cityu.edu.hk (P.K. Chu).

https://doi.org/10.1016/j.nanoen.2021.106661
Received 31 August 2021; Received in revised form 13 October 2021; Accepted 24 October 2021
Available online 29 October 2021

nitrogen fixation proceeds by the nitrogen reduction reaction (NRR) can be performed electrolytically under ambient conditions to produce ammonia to serve as the energy source in ammonia fuel cells [15]. Generally, rechargeable metal-air batteries, also referred to as metal-air fuel cells, can be prepared by ORR/OER (discharging/charging) methods [16,17]. All these technologies have one thing in common. That is, they all require high-performance electrocatalysts on the electrodes. Generally, the desirable electrocatalyst should have a large exposed surface area, excellent electrical conductance, and long-term durability. The performance of electrodes is determined mainly by the physicochemical characteristics of the electrocatalyst and electrode-electrolyte interface [6,8] and the functional life cycle of an electrocatalytic cell depends on the durability of the electrocatalysts. Unfortunately, common Pt-based electrocatalysts tend to have a limited operating lifetime in ORR due to the low tolerance to byproducts such as CO/methanol [7]. As a result, the development of next-generation and high-performance electrocatalysts is vital to energy applications.

Although noble metals and their derived transition metals-based materials are commonly used in energy conversion and storage technologies, the high disposal and recycling cost as well as environmental impact limit large-scale commercial implementation. Therefore, there have been substantial research activities in developing efficient, stable, environmentally safe, and cost-effective catalytic materials [5]. Since Novoselov and Geim demonstrated separation of graphene from graphite in 2004 [18], graphene and other two-dimensional (2D) materials have attracted enormous research interests on account of the intriguing low dimensional structure, strong charge transferability, large specific surface area, low density, and optical and electrical anisotropy [19–26]. Owing to the large charging/discharging rates and robust cycle durability, emerging 2D materials such as graphene and transition metal dichalcogenides (TMDs) offer many benefits in sustainable renewable energy conversion and storage applications [27]. Recent studies on hexagonal boron nitride (h-BN) also reveal that it is an interesting class of 2D materials for energy applications [28–30].

h-BN has a bulk crystal structure similar to graphite and the isolated layer of h-BN is almost analogous to graphene with the 2D honeycomb-like configuration. However, despite the structural similarity, the electrical properties of these two types of 2D materials differ significantly. Graphene has a zero bandgap, but the h-BN monolayer has a wide bandgap of 5.97 eV. h-BN is an insulating isomorph of graphite, in which the B and N atoms exhibit the Bernal arrangement. The boron and nitrogen atoms have different on-site energies resulting in a large bandgap (5.97 eV) and slight (1.7%) lattice difference compared to graphite [31–33]. In reality, BN as an insulator does not have significant electrochemical activity because of the wide bandgap. Nonetheless, h-BN has sparked significant scientific interests because of its superior thermal and chemical stability, high thermal conductivity, superior optoelectronic characteristics, and inherent electrical insulation [33,34]. For example, Ng et al. [35] have reported that the BN/CF/PBT hybrid shows reduced electrical conductivity and BN can be used in electrically resistive junctions to condense electrons to enhance the tensile properties and processing capability. Although h-BN is electrically insulating, there have been efforts to convert h-BN into an electrical conductor in order to expand the applications. For instance, heteroatom doping and functional group grafting are effective techniques. Depending on the dopants and functional groups (CN, NH_2, F, H, OH, CHO, CH_3, etc.), the bandgap of h-BN can be reduced theoretically [5]. Another method is edge hydroxylation which is a powerful functionalization method by reacting h-BN with hot steam to improve catalytic oxidative dehydrogenation of alkanes [36,37]. h-BN has also gained significant attention in HER and ORR by introducing defects such as B/N vacancies and impurities, and the materials can be modified by hydrogen decoration [38–41]. Single- and multi-layered h-BN nanosheets have been proposed for demanding applications such as dielectric tunneling [42], biomedicine [20,43], DUV photonic devices [44], power devices [45], fuel cells [46], and electronic packaging [47].

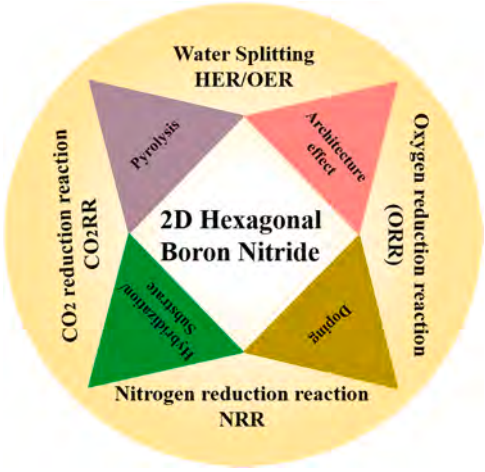

Fig. 1. Common strategies to engineer BN-based electrocatalysts for ORR, HER/OER, CO_2RR, and NRR.

Table 1
Summary of some of the important structural and physical properties of h-, c-, and w-BN.

Properties	h-BN	c-BN	w-BN
Structure	hexagonal	zinc blende	lonsdalite
Space group	$P6_3/mmc$	$F\bar{4}3m$	$P6_3mc$
Lattice parameter (Å)	a = 2.5043, c = 6.6562	a = 3.615	a = 2.55, c = 4.17
Bond length (Å)	1.44	1.57	1.55
Density (g cm^{-3})	2.20	3.45	3.48
Thermal conductivity (W cm^{-1} K^{-1})	2.35 in-plane 2.3×10^{-2} out of plane	12	–
Hardness (kg mm^{-2})	–	4500	3400
Bulk modulus (Gpa)	36.5	369–400	390, 375
Standard molar volume (cm^3 mol^{-1})	10.892	7.1183	7.145

In spite of the tremendous potential of h-BN, there are still many undiscovered aspects of h-BN hybrids and comprehensive studies have also been relatively rare. Consequently, the lack of a good understanding has impeded the development of h-BN heterostructures in the energy fields especially in electrocatalysis. Herein, we review recent advances of h-BN and our objective is to provide comprehensive information concerning the latest development of BN-based electrocatalysts and h-BN heterojunctions to guide future research and development of this important class of materials. The various synthesis and functionalization methods to convert h-BN into a conductor are described and the role of h-BN in heterostructured electrocatalysts, theoretical simulation, and potential electrocatalytic energy applications are discussed with the focus on the important reactions of ORR, HER, OER, CO_2RR, and NRR (Fig. 1). Finally, we present the prospective, main challenges, opportunities, and future research directions.

2. Boron nitride

2.1. Physical properties

BN was first synthesized by Balmain in 1842 with potassium cyanide (KCN) and molten boric acid (H_3BO_3). It has the same crystal structure as carbon and shows a variety of crystalline structures such as hexagonal BN (h-BN), cubic BN (c-BN), and wurtzite BN (w-BN). Reports on BN characterization date all the way back to 1911 [48–50] and the physical and structural characteristics of h-BN were studied even before c-BN and

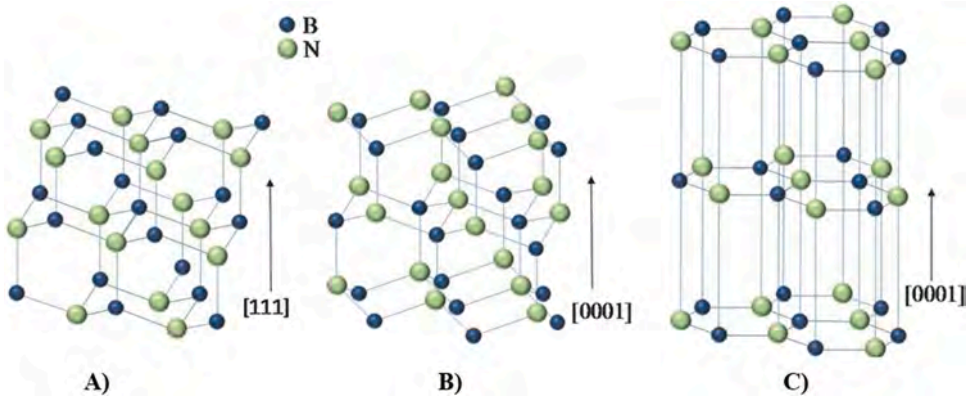

Fig. 2. Crystal structures: (A) Cubic, (B) Wurtzite, and (C) Hexagonal BN. Reproduced with permission [49]. Copyright 2017, John Wiley and Sons.

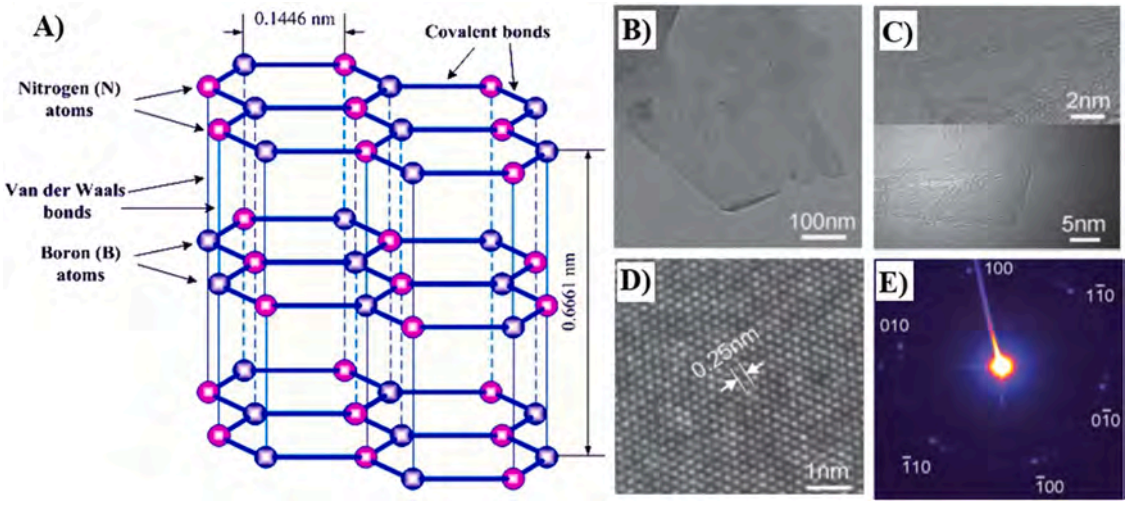

Fig. 3. (A) Crystal structure of h-BN. Reproduced with permission [72]. (B) TEM image of the BNNS. (C) TEM images showing three sheets containing 3, 4, and 5 layers of BN. (D) HR-TEM image of the BN sheet. (E) Electron diffraction pattern from a large number of milled sheets. Reproduced with permission [69]. Copyright 2011, The Royal Society of Chemistry.

w-BN, which were prepared in 1957 [51] and 1963 [52], respectively. Owing to the similarities with graphene, h-BN is also known as "white graphene". c-BN is the second hardest substance after diamond and has a structure resembling that of the diamond. w-BN is related to lonsdaleite (lonsdaleite, also called hexagonal diamond due to its crystal structure) [53] and a summary of the physical properties of h-, c-, and w-BN is presented in Table 1 [49,54,55]. Among the three BN phases (Fig. 2), h-BN with the sp^2-hybridized 2D structure is considered the most stable phase under standard conditions and the 2D layers are held together by weak Van der Waals forces. The layered h-BN structure has an interlayer distance of 3.33 Å and a lattice constant of 2.50 Å [56]. However, unlike graphene, h-BN is an insulator with a thickness-dependent bandgap. h-BN nanosheets have been used mainly as dielectric substrates for graphene and MoS_2-based heterostructures in electronic and optical devices [57,58]. By means of electronic and structural modification, h-BN possess many favorable properties such as small cytotoxicity, large surface area, abundant active sites, good thermal stability, outstanding mechanical strength, and high electrical conductivity [59]. Nevertheless, pristine h-BN has low electrocatalytic activity due to the low conductivity and as a result, various physio/chemical procedures have been proposed to convert h-BN into semi-conducting or conducting materials. For example, Uosaki and coworkers have tuned the electronic properties of h-BN by combining with Au NPs and the electrocatalyst delivers improved ORR performance mainly because of activation of adsorbed O_2 and high selectivity in the associative pathway [38,60]. The exceptional properties of h-BN render it exciting materials in many applications [48–50, 61]. In this review, leaving aside c-BN and w-BN, our focus is the current progress of 2D h-BN including fabrication techniques and applications in electrochemical energy conversion.

2.2. Two-dimensional hexagonal boron nitride

2.2.1. Structure of 2D h-BN

Analogous to graphite, h-BN is a white slippery powder with a honeycomb structure in which the B and N atoms are sp^2 hybridized and Van der Waals forces hold the layers together [62]. The B-N bond has ionic features with a length of 0.144 nm (0.142 nm in graphite) [63] and the space between the centers of adjacent hexagonal rings is 0.25 nm (0.246 nm in graphene) (Fig. 3A). To satisfy the "lip-lip" interactions in individual BN layers [64] (referred to as electrostatic or polar-polar interactions), h-BN has AA stacking in which the adjacent hexagon rings are superposed with B and N atoms alternatively located along the c axis. In contrast, graphite has the AB stacking in which each layer is shifted by half a hexagon with C atoms always located at the center of the hexagon [61,65]. Although the AA stacking is intrinsic to bulk h-BN, it may be converted to AB stacking when the top and bottom layers of the layered structure are made to slide slightly by sonication [66,67]. According to density-functional theory (DFT) calculation, free sliding is associated with bandgap modulation of ~0.6 eV [67]. Compared to graphitic C-C bonds, B-N bonds show combined ionic and covalent

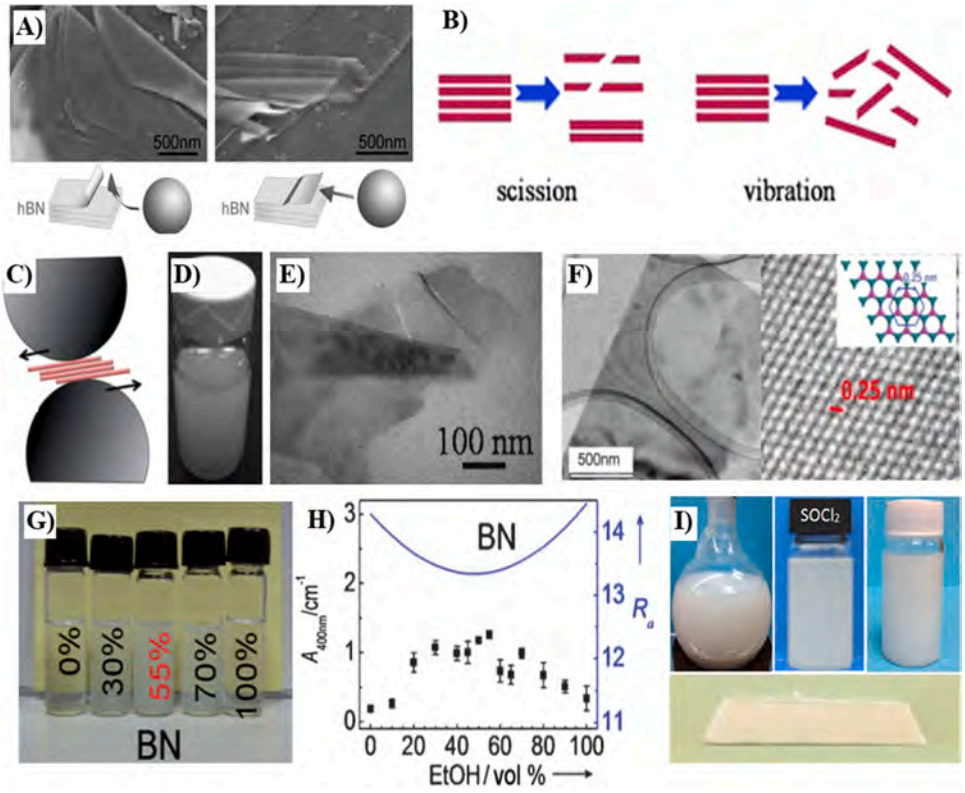

Fig. 4. (A) SEM images and diagrams showing the two exfoliating pathways in ball milling. Reproduced with permission [69]. Copyright 2011, The Royal Society of Chemistry. (B) Sonication causing scission-induced exfoliation and vibration-induced exfoliation. (C) Exfoliation of 2D nanosheets by the shear force in low-energy ball milling. (D) BNNS dispersion in SDS–water. (E) TEM image of folded BNNSs. Reproduced with permission [87]. Copyright 2012, The Royal Society of Chemistry. (F) TEM (left) and HR-TEM (right) images of BNNS exfoliated by ultra-sonication of BN powders in N, N-dimethylformamide. Reproduced with permission [89]. Copyright 2009, John Wiley and Sons. (G) h-BN dispersions in the ethanol/water mixtures. (H) Estimated Ra values presented as solid lines and absorbance of the BN suspensions in ethanol/water shown as dots (right). Reproduced with permission [90]. Copyright 2011, John Wiley and Sons. (I) BNNS suspension exfoliated in the PEI-isopropanol mixture (left), thionyl chloride (middle), and recovered and re-dispersed in acetic acid (right). The bottom image shows the BN film modified with BNNS from exfoliation in PEI-isopropanol mixture. Reproduced with permission [91]. Copyright 2017, Springer Nature.

characteristics due to the disparity in the electronegativity between B and N atoms. This can result in "lip-lip" interactions among layers [19], which stabilize the growth of open-ended BN nanotubes (BNNTs) by forming bridges between consecutive shells to evolve into a metastable energy minimum analogous to the formation of carbon nanotubes (CNTs). TEM (Fig. 3B and C) reveals exposed organized layers and atomic configurations in the h-BN nanotubes (h-BNNTs) -BNNSs [68–70]. As shown in Fig. 3D, the high-resolution TEM (HR-TEM) image shows the hexagonal atomic arrangement in the BN sheets with a 0.25 nm interplanar distance associated with the (100) and similar planes. Fig. 3E displays well-defined (100) diffraction spots with excellent AA layer stacking [69]. However, owing to layer rotation or disordered layer stacking, the dispersed regions with a circle indicate deterioration in the h-BNNS quality [71].

2.2.2. *Synthesis of 2D h-BN*

It has been reported that h-BN cannot undergo proper functionalization in its bulk form because of the small specific surface area and porosity. Zhu et al. [73] have compared the surface areas of BNNS and bulk h-BN (278 $m^2\ g^{-1}$ for BNNS and 10 $m^2\ g^{-1}$ for bulk h-BN). Herman et al. have prepared BNNTs with a larger surface area (97 $m^2\ g^{-1}$) than bulk h-BN (16 $m^2\ g^{-1}$) [74,75], and Chen et al. [76] have also reported crystalline h-BNNS with high purity, large surface area, as well as high thermal stability. Most research activities have focused on the synthesis methods of h-BN with the 2D structure, especially h-BNNS and h-BN layers with a large area, regulated thickness, and high quality. Most of the fabrication strategies are similar to those of carbon materials with slight modification. The thickness of BN nanosheets is limited to the nanoscale, whereas the other two dimensions are infinite. To date, BNNS is prepared by two main methods: top-down exfoliation and bottom-up growth. The fundamental process in the top-down technique is exfoliation of excess h-BN by eliminating the Van der Waals interactions, a process termed mechanical or chemical/liquid exfoliation [77,78]. In comparison, bottom-up techniques for BNNSs are categorized as substrate-dependent or substrate-free such as CVD, pyrolysis, or hydro/solvothermal methods.

2.2.2.1. Mechanical exfoliation. In 2004, the mechanical exfoliation method employing scotch tape was used to isolate graphene [18] and it has since been widely adopted for other 2D materials such as h-BN [79] and MoS_2 [80]. Van der Waals coupling between neighboring layers in h-BN is destroyed by mechanical exfoliation with the sticky tape due to the strong peeling force. This process produces 2D h-BN with fewer defects than chemical approaches to allow for investigation of the fundamental characteristics and exploration of a wide range of applications in electronics and optoelectronics [77]. Mechanical exfoliation involves micromechanical cleavage [77,81] and ball milling [69,82], both of which rely on shear forces to exfoliate bulk h-BN to form few-layer sheets.

The solid covalent bond in the B–N structure remains. However, this approach is inefficient for the synthesis of h-BN due to lip-lip interactions among BN planes [83]. The mechanical exfoliation yield is poor due to the more substantial contact between BN basal planes [84,85]. Li et al. [69] have proposed a precise ball milling method to fabricate h-BN with gentle shear forces instead of using direct peeling by optimizing the ball milling conditions in the N_2 atmosphere. This approach produces h-BN efficiently while causing slight structural destruction. Fig. 4A displays the SEM images of two intermediate phases of the peeled h-BNs as well as the predicted exfoliation pathway under the milling shear stress. Because the modest shear force created during milling causes minor destruction to the structure, several aspects are considered to ensure effective mechanical milling: (i) A ball mill with a regulated rolling action is preferable, (ii) a smaller milling area to enhance the actions, and (iii) the use of an adequate liquid solvent during milling to prevent the welding effect [20]. To further optimize the fabrication of h-BN nanosheets, low-energy ball milling and low-power sonication are implemented. The h-BN powder is milled with surfactants using zirconia balls and then sonicated by a low-power process [86]. Yao et al. [87] have exfoliated h-BN using sodium dodecyl sulfate (SDS) in an aqueous solution to produce mono- and

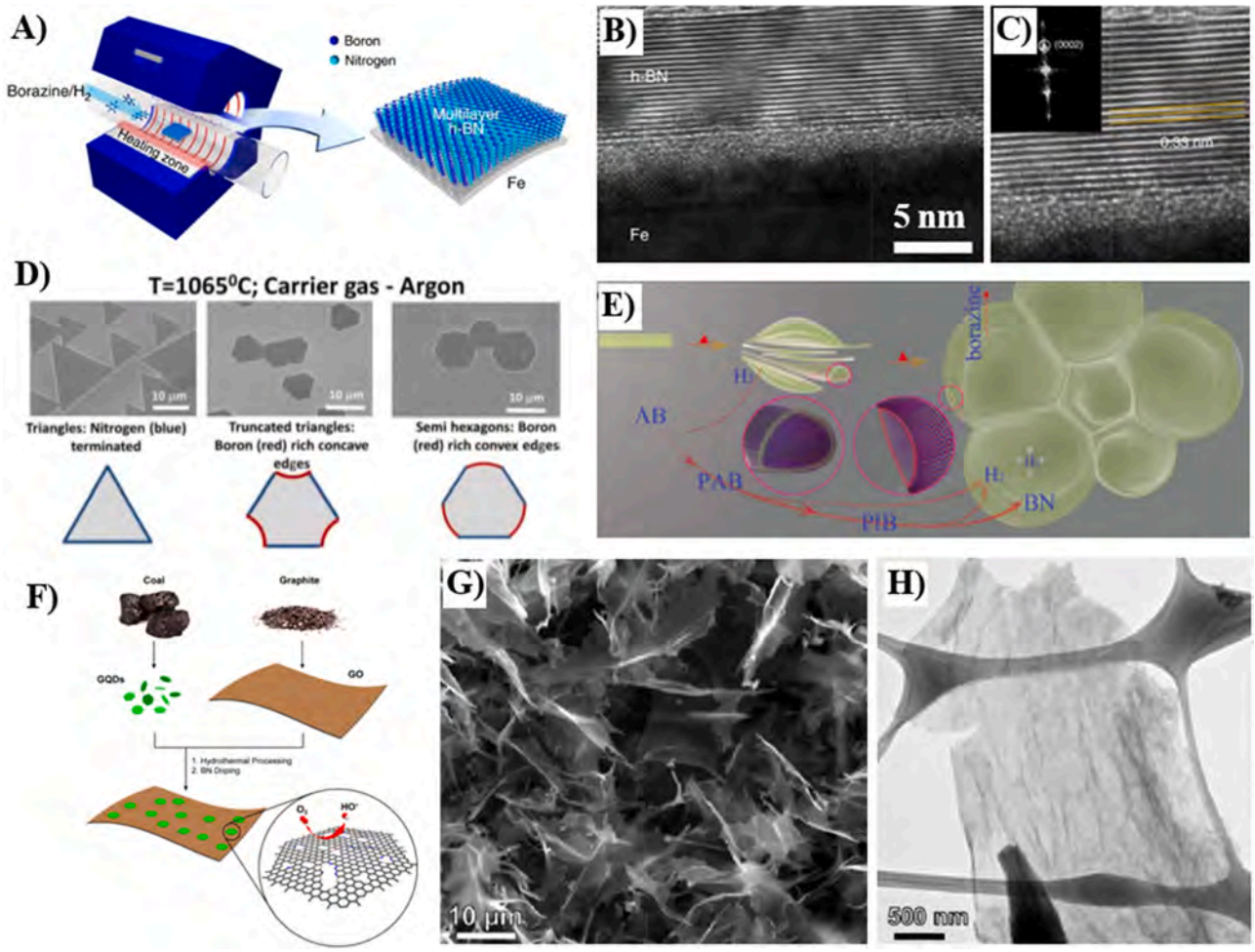

Fig. 5. (A) Schematic illustration of the CVD method to prepare h-BN on the Fe foil using a borazine precursor. (B) and (C) Cross-sectional TEM images of a multi-layered h-BN sheet grown on the Fe foil. Reproduced with permission [107]. Copyright 2015, Springer Nature. (D) SEM images of h-BN generated with argon as the buffer gas at 1065 °C and sketches of the resultant h-BN crystal on the bottom with blue representing nitrogen and red for boron. Reproduced with permission [117]. Copyright 2015, American Chemical Society. (E) Formation mechanism based on self-bubbling of B-N-H polymers during dehydrogenation into the nanostructure thin walls, where AB stands for ammonia borane, PAB stands for polymeric aminoborane, and PIB is polyiminoborane. Reproduced with permission [122]. Copyright 2011 John Wiley and Sons. (F) Schematic diagram of catalyst preparation by the hydro/solvothermal method. (G) and (H) SEM images of the BN-GQD/G nanocomposite. Reproduced with permission [123]. Copyright 2014, American Chemical Society.

multi-layer BNNSs with a quantity of about 1.2 mg mL^{-1} together with robust stability (Fig. 4B-4E). Besides the liquid phase, solid phases have been reported. Liu et al. [88] have proposed a solid exfoliation procedure to generate BNNS, in which the h-BN powder and ammonia borane (NH_3BH_3) are milled together. NH_3BH_3 adsorbs easily onto h-BN, thus reducing the dehydrogenation temperature and Van der Waals force during milling, resulting in good exfoliation and production efficiency for the h-BN nanosheets. All in all, mechanical exfoliation is the most efficient technique to generate h-BNNS, although the relatively tiny flake size restricts its use in large-area applications.

2.2.2.2. Liquid/chemical exfoliation. Exfoliation may also be performed by exploiting the volume expansion effects produced by in situ physical or chemical reactions between h-BN layers. Chemical exfoliation is mainly dependent on ultrasonication and surface tension of the organic solvents to overcome interlayered Van der Walls interactions with the aid of solvent stabilization (Fig. 4F) [89, 92–94]. Han et al. [95] have introduced the chemical exfoliation method to exfoliate mono- and multi-layer h-BNNSs, in which 0.2 mg of h-BN particles are ultrasonicated in 5 mL of the 1,2-dichloroethane solution of poly (m-phenyl-enevinylene-co-2,5-dictoxy-p-phenylenevinylene) to dis solve and reduce Van der Waals forces between h-BN layers. As chemical exfoliation takes place in a liquid, it is solvent-based exfoliation and the Coleman's Hansen solubility parameter (HSP) theory is used to study the functions of several solvents by verifying the polarity, hydrogen bonding, and interconnected energy densities so as to reduce the exfoliation energy or form robust and adequate surface tension (e.g., γ 40 mJ m^{-2}) [96]. Isopropyl alcohol (IPA) is a valuable solvent in h-BN exfoliation, producing 50% yield in the dispersions (0.06 mg mL^{-1} BNNS). According to the HSP theory, the mixed solvent approach is established by comparing the HSP space and Ra value of the various solvent compositions. For instance, Zhou et al. [90] have employed two weak solvents (water and ethanol) to exfoliate h-BN and obtained a "milky" h-BN nanosheet solution with a quantity of 0.075 ± 0.003 mg mL^{-1}, that is 37 times the concentration of exfoliated in IPA as shown in Fig. 4G-4H. Cao et al. [97] have proposed a mixed solvent sonication method with ammonia and IPA and the Lewis base characteristics of ammonia assists exfoliation (low boiling point and surface tension of 57 mJ m^{-2}). BNNS has also been exfoliated by electric field-assisted liquid exfoliation [98], molten hydroxides [99], microwave irradiation-assisted exfoliation [19], magnetic stirring-assisted ultrasonication technique [100], and layer-by-layer etching and irradiation with an electron beam [101,102]. The h-BNNS synthesized by these approaches are often unstable, lack morphological uniformity,

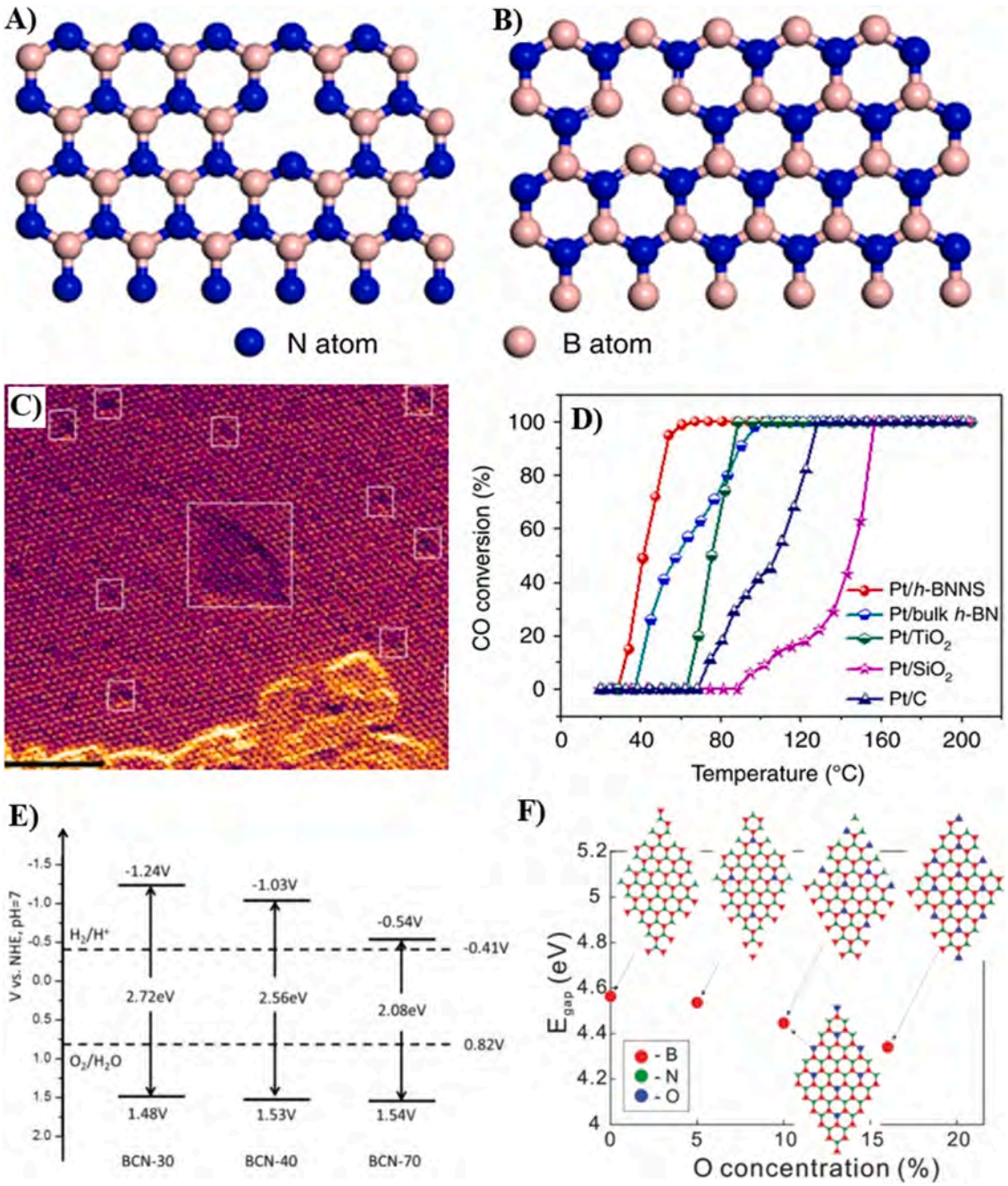

Fig. 6. (A) and (B) h-BNNS with the B vacancy and N terminated edge on the left side and with the N vacancy and B terminated edge on the right side. (C) HR-STEM image of vacancies containing h-BNNS highlighted with boxes (Scale bar = 2 nm). (D) CO oxidation light-off curves for the Pt/h-BNNS, Pt/bulk h-BN, Pt/TiO_2, Pt/SiO_2 and Pt/C, m(catalyst) = 30 mg, CO flow rate 10 mL min^{-1}. Reproduced with permission [147]. Copyright 2017, Springer Nature. (E) Band structures of the BCN-based samples. Reproduced with permission [148]. Copyright 2015, Springer Nature. (F) Dependence of the bandgap on the embedded oxygen content (random doping mode) in the infinite h-BN monolayer. Reproduced with permission [149]. Copyright 2017, John Wiley and Sons.

include impurities, and require lengthy washing and post-treatment steps [103]. Ma et al. [104] have reported that the BNNS solution starts to aggregate within 12 h after dispersion and aggregates completely after three days. Therefore, it is critical to modify the surface of BNNSs to produce a stable and uniform BNNS dispersion. Anderson et al. [91] have also studied the uniform dispersion ability of exfoliated BNNSs in several solvent systems under different conditions (Fig. 4I). All in all, despite these disadvantages, chemical techniques are easy and suitable for large-scale synthesis compared to mechanical exfoliation [105].

2.2.2.3. Chemical vapor deposition. The bottom-up growth of BNNSs may be characterized as substrate-dependent and substrate-free. The substrate-dependent ones are typically carried out by chemical vapor deposition (CVD) which is a cost-effective approach to produce high-quality h-BNNS with a regulated atomic thickness and minimal impurities [106–108]. 2D materials are often grown on a substrate by this method and the intrinsic properties of the as-grown materials and interactions between two adjacent layers can be studied. In 1990, the first h-BN monolayer was obtained by decomposing $B_3N_3H_6$ on transition metals such as Pt (111) and Ru (0001) [109]. The typical CVD technique involves one or more volatile chemicals/sources that react and dissociate on the surface of the substrate to produce the coating. h-BN is commonly obtained from metal salts and organic precursors, e.g.,

ammonia borane, boron trichloride, borazine, ammonia, and nitrogen, on transition metals such as Cu [110], Ni [111,112], Ag [113], Au [114], and Ru [115] as substrates. The TM substances act as catalysts and transform the precursors to form the h-BN monolayer. After the substrate is coated with h-BN, there is no more degradation of the precursor and the process turns into a self-limiting one [49]. Theoretical studies and experimental evidence indicate that 2D h-BN layers formed on 3d and 5d TMs are weakly attached to the metal support. However, in 4d-TMs, the h-BN-surface binding energy increases in proportion to the number of vacant states in the substrate of the d-shell. One of the concerns in controlling the thickness of the h-BN film is the solubility of boron and nitrogen atoms in the adsorbent. For instance, a monolayer h-BN film may be formed on a Cu substrate by taking advantage of the low solubility of boron and nitrogen atoms [116] and a multilayer h-BN film can be formed on an iron substrate by taking advantage of the limited solid solubility of boron and nitrogen atoms (Fig. 5 A-5C) [107]. By altering the growth conditions, h-BNs with different shapes such as triangular, asymmetric diamond, or hexagonal may be obtained. For example, Stehle et al. [117] have reported that by changing the percentage of boron to nitrogen on the Cu surface, triangular, truncated triangular, and hexagonal h-BN can be formed (Fig. 5D). Ji et al. have also observed spontaneous structure evolution of monolayer h-BN formed by CVD on a Cu foil [118], and h-BN sheets have been deposited by CVD methods such as microwave plasma CVD [119] and catalyst-assisted CVD [120]. The template-assisted CVD route described by Shelimov and Moskovits is considered to be superior to other CVD methods due to the formation of layered nanostructures with high precision and excellent crystallinity [121]. Unlike powder h-BNNS, CVD produces h-BNNS covalently bound to metallic surfaces thus requiring transfer techniques and as a result, h-BNNS synthesized by this method requires functionalization and post processing [5].

2.2.2.4. Pyrolysis. Pyrolysis is another bottom-up strategy to increase the yield of h-BN nanosheets by combining boric and nitride precursors and heating to a high temperature. Nag et al. have synthesized multilayered BN sheets by mixing urea and boric acid at 900 °C [124]. The h-BN nanosheets formed with a significant proportion of urea are predominantly 2–3 layers thick. The surface area of BN increases as the layer thickness decreases. This method often employs low-cost B- and N-containing chemicals including melamine, boric acid, boron oxide, and urea [125–127]. The unique BN micro or nanostructures may be constructed by changing the B or N sources [128]. Owing to the formation of gaseous products like CO_2, CO, and NH_3, this approach may produce porous h-BNNSs and the production of porous structures with a large surface area involves the use of a hard template rather than pyrolysis. Weng et al. have synthesized porous BN micro-sponges with a large BET surface area of 1900 $m^2 g^{-1}$ by varying the urea and boric acid molar ratios and synthesis temperature [129]. Apart from the techniques mentioned previously, several other techniques for the fabrication of h-BN nanomaterials have been proposed, for instance, chemical blowing (Fig. 5E) [122], biomass-directed carbothermal synthesis [130], hydro/solvothermal method (Fig. 5F-H) [123], pulsed laser deposition [131–133], electrodeposition [134–136], electrospinning method [137], and plasma-arc method [138,139]. Most of these processes need a large amount of input energy (>2000 °C) and so have not been studied as extensively as other techniques.

3. Functionalization of 2D h-BN

Pristine h-BN has no electrocatalytic activity and therefore, physical and chemical techniques must be implemented to change h-BN to a conductor. Lyalin et al. have reported exfoliation or functionalization to tailor the nanoscale structure, size, and morphology [140].

3.1. Defect engineering and metal doping

In the preparation of 2D h-BN, defects such as grain boundaries, vacancies, and distorted edges are created and these defects affect the properties of the materials and devices. Theoretically, the B vacancy is more thermodynamically favorable because of the smaller formation energy compared to the N vacancy [141]. Chemical activation of the BN monolayer increases significantly on account of these defect sites, which can be further amplified by doping the defects with metal atoms [142–144]. Although defect-free BN sheets have poor interactions with the deposited metal atoms due to their chemical inertness, the defective BN sheet may function as a template to produce advanced catalysts by metal doping. For example, metallic atoms such as Co [145], Fe [145], Ru [146], and Cu [142] have been incorporated into BN sheets to produce promising catalysts for CO oxidation. Zhu et al. have prepared vacancy-abundant h-BNNS doped with Pt NPs for CO oxidation by taking advantage of the electronic effects on Pt caused by the nanosheets with N and B vacancies (Fig. 6A-6D) [147].

3.2. Carbon and oxygen doping

Carbon being naturally abundant is the most common dopant to modify h-BN nanostructures. Chen et al. have proposed a simple pyrolysis method to generate carbon-doped h-BN porous materials by heating the mixture of melamine and boric acid under Ar to 800 °C and the catalyst has excellent CO_2 adsorption capability in contrast to pure h-BN [150]. Modification of h-BN with carbon changes the bandgap from 5.9 eV to 2.6 eV and is promising for non-metal photocatalysts. Huang et al. [148] have adjusted the bandgap of h-BN by adding the appropriate amount of carbon to create a ternary B-C-N hybrid which is active not only in overall water splitting but also in CO_2 reduction (Fig. 6E). Besides carbon doping, h-BNNS doped with oxygen has been studied. Weng et al. have synthesized oxygen-doped h-BNNS by a thermal reaction under ammonia at 1000 °C using boric acid and hexamethylenetetramine. The yellow h-BN catalyst has a reduced bandgap of 2.1 eV for a minimum oxygen doping concentration of 23.1 at% (Fig. 6F) [149]. Co-doping with carbon and oxygen may improve the surface, optical, and electronic properties of h-BN to produce exciting gas sorption, fluorescence, and electrochemical energy storage characteristics and applications [5,151]. In addition to defects and atomic doping, alloying and hybridization have been proven to be effective in changing the electronic structures of the materials.

3.3. Pyrolysis and hybridization

Compared to other modification methods in which functionalization is normally performed at edge or defect sites [82,92], pyrolysis can generate homogeneous heteroatom doping and produce more changes in the materials. When different types of 2D materials are combined, the structures may consist of a myriad of heterostructures and superlattices and by introducing multiple bandgaps in the heterojunctions, quantum wells satisfying the conditions for charge flow can be prepared [152, 153]. The heterostructures also facilitate the formation of defects to improve the dispersion of charge carriers and the electrochemical activity by using free electrons [154]. Furthermore, the electrocatalytic activity of h-BN can be tuned by combining the dz_2 metal orbitals with the N-pz and B-pz orbitals of h-BN in the electronic interactions with the underlying metal substrate [155,156]. The BN nanosheets with unique properties have applications as spacers, protectors for tunneling systems, transistors [157,158], deep ultraviolet luminescence [159,160], solid-state lubrication [161], and electrocatalysts in energy conversion devices [46,162]. In the following section, important electrocatalytic applications of h-BN-based heterojunctions for energy conversion including ORR, HER, OER, CO_2RR, and NRR are discussed.

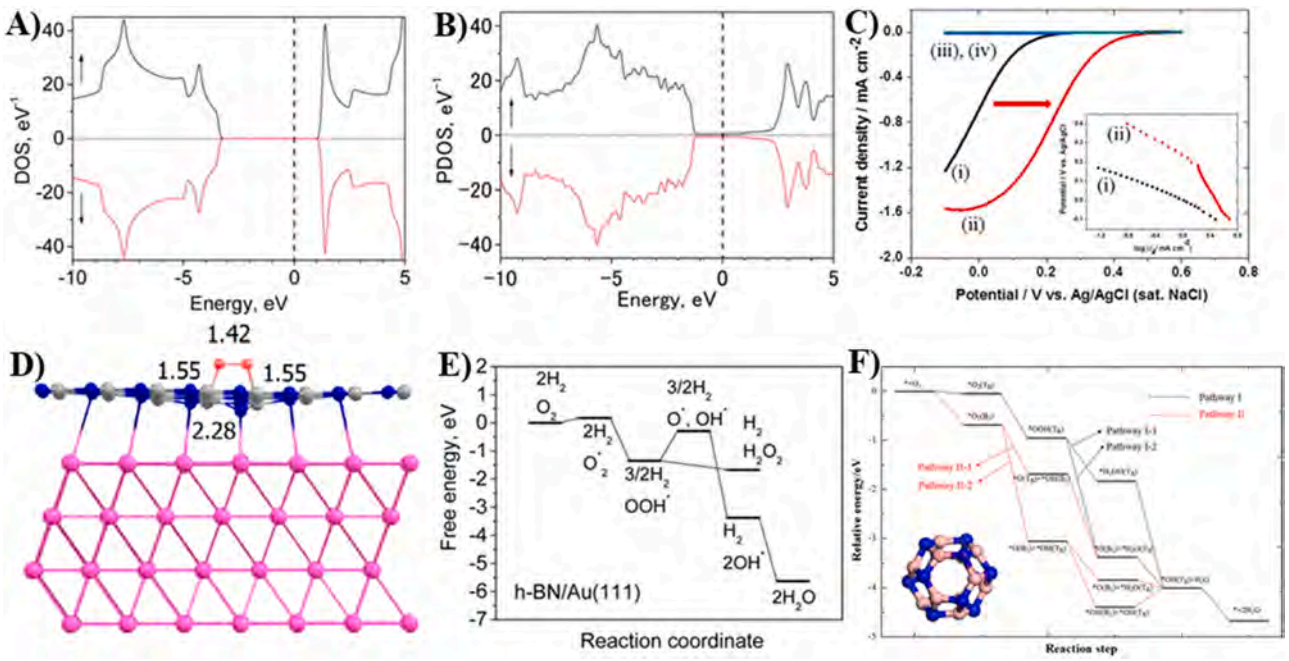

Fig. 7. Spin-polarized DOS calculation of (A) h-BN and (B) h-BN/Au (111). (C) LSVs curve for ORR of (i) Bare Au, (ii) BNNS/Au, (iii) Bare GC, and (iv) BNNS/GC; Inset is the Tafel plot of (i) Bare Au and (ii) BNNS/Au. (D) Optimized model for O_2 adsorption on h-BN/Au (111) with distances in Angstroms. (E) Free energy illustration for ORR on h-BN/Au (111). Reproduced with permission [38]. Copyright 2014, American Chemical Society. (F) Free energy diagram of all the feasible ORR pathways on $B_{12}N_{12}$; Inset shows the optimized geometry of the $B_{12}N_{12}$ nanocage. Reproduced with permission [173]. Copyright 2016, American Chemical Society.

4. Applications of 2D h-BN

4.1. Oxygen reduction reaction

Fuel cells (FCs) are mainly used as a power source in long-term applications and ORR regulates the functioning of fuel cells and metal-air batteries [38,162,163]. Thermodynamically, fuel cell degradation is analogous to ORR due to the production of water (H_2O) or hydrogen peroxide (H_2O_2) on the cathode of PEM fuel cells [164], but this problem may be addressed by employing an appropriate catalyst [165]. Normally, there are two mechanisms in ORR: (1) 4 electron reduction (dissociative route) of O_2 to H_2O in acidic media or OH^- in basic media and (2) 2 electron reduction (associative route) of O_2 to H_2O_2 in acidic media or HO_2^- in basic media [9]. In addition to possessing fewer electrons per O_2 molecule, H_2O_2 is highly corrosive when it decomposes into free radicals such as $OH^\bullet$ and $OOH^\bullet$. Pt is considered the ideal ORR catalyst for effective adsorption and reduction of molecular O_2 via the two- or four-electron mechanism. However, large-scale production is still hampered by the high cost of noble metals, time-dependent drift, fuel cross-over effect, and CO deactivation and more economical non-metal-based catalysts are demanded for ORR [7,166,167].

The underlying mechanism of metal-free ORR electrocatalysis has been studied experimentally and theoretically [7,9,168,169]. Uosaki et al. have observed that h-BNNS loaded onto the Au surface is an active

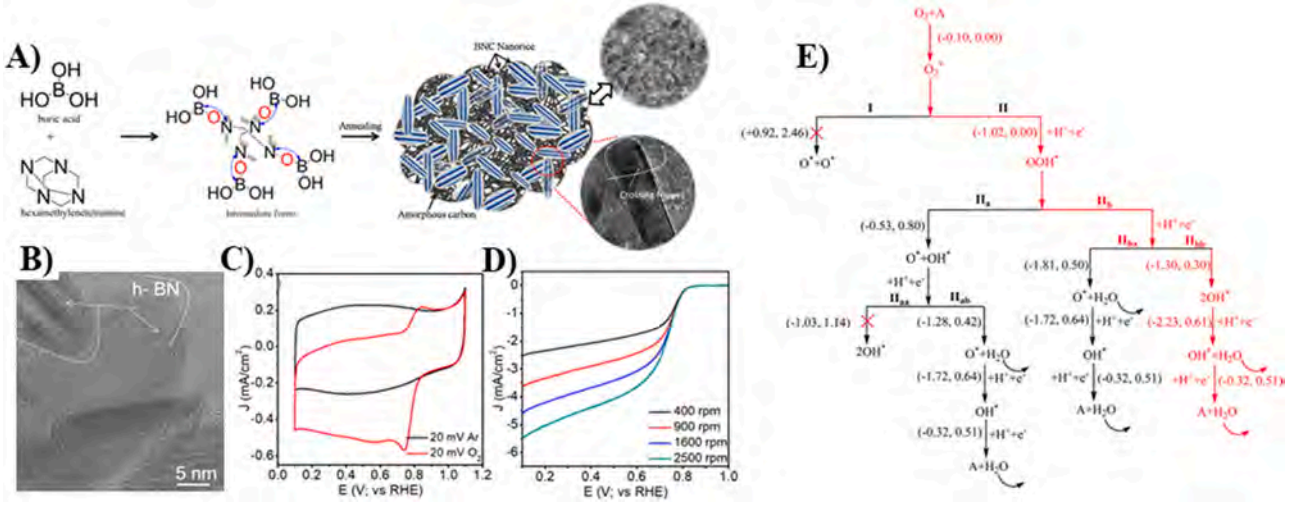

Fig. 8. (A) Schematic diagram showing stepwise preparation of BNC. (B) HR-TEM image of BNC2–850 with the nanorice structures and more defect sites. (C) CVs of the BNC2–850 catalyst in Ar- and O_2-saturated 0.1 M KOH at a sweeping rate of 20 mV s^{-1}. (D) ORR polarization curves of the BNC2–850 catalyst in O_2-saturated 0.1 M KOH at various rates. Reproduced with permission [175]. Copyright 2018, American Chemical Society. (E) Possible reaction pathways on the C_N sheet for ORR with the one in red being the most kinetically favorable pathway. Reproduced with permission [176]. Copyright 2015, American Chemical Society.

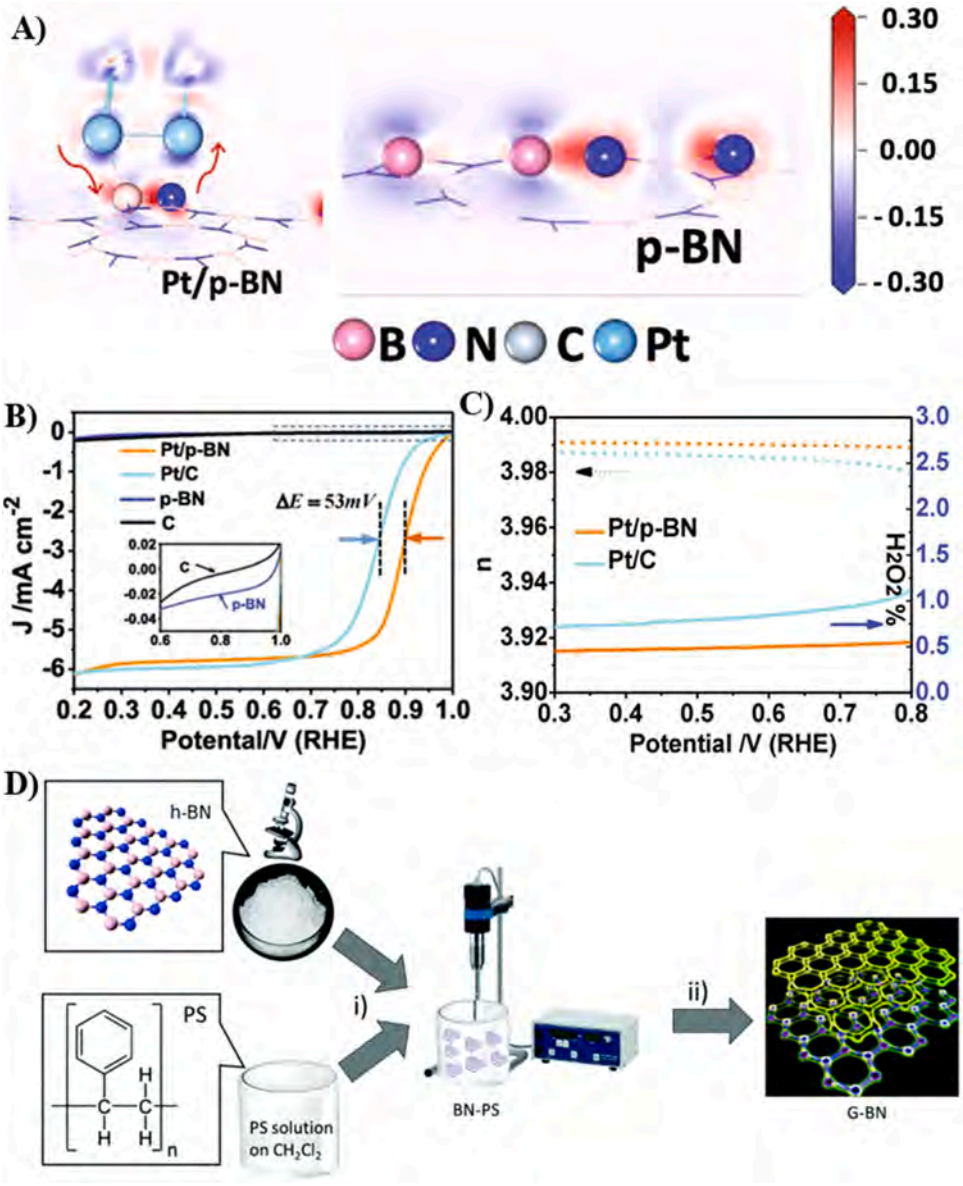

Fig. 9. (A) Schematic representation of the electron donation back-donation phenomenon in the sample with and without the Pt cluster loaded onto p-BN; Charge-density difference plots of the samples. (B) LSV curve and (C) Electron transfer number (n) and H_2O_2 yield. Reproduced with permission [186]. Copyright 2020, Elsevier. (D) Schematic diagram for the preparation of the G-BN superlattice based on exfoliating bulk BN crystals with PS. Reproduced with permission [187]. Copyright 2019, The Royal Society of Chemistry.

ORR electrocatalyst [38] and DFT studies reveal that combining the d-orbital and p-orbital of single-layer BN causes a slight shift towards the Fermi level to alter the electronic properties of h-BN (Fig. 7A and 7B). Owing to the interface created between h-BNNS and Au substrate, O_2 forms bonds with two B atoms closest to the N atom, which is located directly above the Au atoms (Fig. 7C). Besides the surface of h-BNNS/Au, the edges of h-BNNS appear to be actively engaged in ORR. According to the free energy diagram, ORR to form H_2O_2 is feasible via the two and four electron routes on h-BNNS/Au (111) (Fig. 7D). The BN nanosheets on the gold electrode may reduce the overpotential in ORR (Fig. 7E) and the activity of BN nanosheets is improved by decorating them with Au NP (Au-BNNS/Au), revealing that loading AuNPs onto BNNS not only lowers the overpotential in ORR but also enhances oxygen reduction to H_2O by 80–90% by the four-electron pathway [162, 170,171]. Crystalline h-BN has also been investigated as an ORR electrocatalyst [172].

The curvature of nanomaterials plays a substantial role in adsorption and desorption of O_2 [174] and BN nanocages show improved adsorption of O_2 and oxygen reduction intermediates due to the curvature effect. Chen et al. have theoretically evaluated and compared the ORR efficacy of $B_{12}N_{12}$ and $B_{60}N_{60}$ nanocages [173] and the results indicate that the adsorption energies of all ORR intermediates on the $B_{12}N_{12}$ catalyst are comparable to those previously reported for the Pt (111) catalyst, implying that it may be an efficient ORR catalyst with similar catalytic properties as Pt. According to the free energy diagram, the ORR process on these two BN nanocages may occur spontaneously by the dissociative route (Fig. 7F).

Pyrolysis, chemical vapor deposition, and electron beam irradiation are effective methods to dope or generate defects such as B- or N-vacancies and disrupted edges. Carbon doping can produce interesting electrocatalytic properties in h-BN. The nanorice-like carbon-doped h-BN (BNC) has been synthesized by CVD as shown in Fig. 8A and it shows promising catalytic properties such as an onset potential of + 0.83 V vs RHE in basic media (Fig. 8C and 8D). Two critical parameters including the synthesis temperature and composition affect the ORR activity. The HR-TEM image (Fig. 8B) shows that the rice-like BNC nanocrystals are consistent with the competitive growth of carbon. Despite a smaller onset potential than Pt/C, the nanorice-like C doped h-BN outperforms Pt/C in terms of reliability and resistance to methanol oxidation [175]. Zhao et al. have examined C-doped BNNS as an efficient catalyst for ORR [176] and theoretical studies demonstrate that doping BNNS with C increases the spin and electron density while decreasing the bandgap,

Table 2
Electrocatalytic characteristics of BN-based materials in ORR.

Catalysts	Electrolytes	Half-wave Potential ($E_{1/2}$ V)	Overpotential (mV)	Onset-potential (V)	Limiting Current density (mA. cm^{-2})	Tafel slope (mV dec^{-1})	Ref.
1–1-NBC	0.1 M KOH	–	590	0.87	4.18	79	[196]
AuNP(5 nm)-BNNS/Au	0.05 M H_2SO_4	–	720	–	-0.2	–	[162]
AuNP(5 nm)-BNNS/Au	0.1 M $HCLO_4$	–	760	–	-0.2	–	[162]
BN-Gas-2	0.1 M KOH	-0.20	–	-0.05	5.7	–	[197]
BCN/KBC10%	0.1 M KOH	–	–	1.01	5	72.4	[181]
Pt/p-BN	0.1 M $HCLO_4$	0.902	–	1.000	–	74.9	[186]
BCN2–850	0.1 M KOH	–	–	0.83	4.6	–	[175]
MnBN/C-75	0.1 M KOH	18	–	0.9	5.6	122	[184]
CNTBN5–750	0.1 M KOH	0.72	–	0.86	5.78	–	[198]
N,B-CNT	1.0 M KOH	-0.131	–	-0.070	1.35	55.87	[199]
GOBN5–750	0.1 M KOH	0.64	–	0.798	3.0	–	[191]
GOBN2-BM	0.1 M KOH	0.74	–	0.89	4.4	102	[190]

leading to enhanced O_2 adsorption. The chemical reactivity of the catalyst increases in ORR after substituting C for N by the four-electron OOH hydrogenation pathway as manifested by the low activation barrier of 0.61 V compared to Pt-based electrocatalysts (Fig. 8E). While defect-free BN nanostructures are highly inert and interact with metal atoms very weakly, defective BN nanostructures can be produced by metal atom doping [163,177,178]. Deng et al. have reported Co-doped boron nitride (Co/BN) as an ORR electrocatalyst [179] in which Co atoms interact with defective 2D-BN to maintain the Co/BN stability. All the ORR intermediates can adsorb on Co/BN. HOOH species are volatile and decompose into two OH species, implying that ORR occurs primarily by the direct 4 e^- mechanism on Co/BN.

Carbon-based non-metal nanomaterials doped with heteroatoms have also been investigated as electrocatalysts and the activity has been benchmarked with that of Pt/C [123,180,181]. Kahan et al. have observed that carbon substitution for both B and N gives rise to greater ORR catalytic activity than that B or N-doped graphene and DFT simulation indicates that co-doping reduces the gap between the LUMO and HOMO states [182]. Metal-supporting interactions are required in ORR activation of h-BN [183–185]. According to Li et al. [186], the donation and back-donation phenomena result in significant interactions between porous boron nitride (p-BN) and Pt NPs due to electron transfer from N atoms to Pt NPs and Pt NPs to B atoms (Fig. 9A). The Pt/p-BN catalyst exhibits outstanding catalytic activity in ORR with a 53 mV positive shift of the half-wave potential in comparison with commercial Pt/C (Fig. 9B and 9C).

Modification by doping not only increases the porosity, but also improves the overall conductivity of the electrode materials. Carbon is introduced to h-BN to form borocarbonitride ($B_xC_yN_z$) which is believed to include both graphene and h-BN domains and exhibit characteristics between those of graphene and h-BN [188]. Chen et al. [150] have synthesized porous carbon-doped boron nitride (BCN) in situ by heating the mixture of melamine and boric acid under Ar and revealed that carbon doping in BN enhances the nanopores (<0.7 nm) and structural defects. Besides, incorporation of O into porous BN results in different polarities of O-containing bonds as well as B-vacancies to boost the electron-attracting ability and adsorption capacity. Liu et al. [189] have reported the template-free synthesis of oxygen-doped mesoporous BN by pyrolysis to produce a large surface area (474.3 m^2 g^{-1}) and porosity (0.332 cm^3 g^{-1}). The presence of the distinct graphene and h-BN phases on the other hand, modifies the bandgap and charge density of the electrodes [190,191]. One of the advantages of the distinct nanoscale phase is that almost all C hexagons are linked to improving the stability of C-C and B-N bonds and Π-conjugation [192]. Rendón-Patiño et al. have proposed a reliable method to prepare the graphene-boron nitride (G-BN) heterostructure in superlattices as large-area films or powders by pyrolysis of exfoliated BN in polystyrene for ORR (Fig. 9D) [187]. Although manufacturing of monolayer G-BN is a difficult task, a variety of G-BN heterostructures have been synthesized on substrates such as Cu [193], Ir(111) [194], and Pt(111) [195] for ORR with metal-free catalysts. Table 2 summarizes the characteristics of modified BN-based ORR catalysts reported recently.

4.2. Water splitting

The scientific community has tinkered with the idea of producing energy from water for more than a century and electrocatalytic water splitting has emerged to be the technology of choice to produce fuels of the future. HER is the cathodic half-reaction in water splitting in which protons (acidic solution: $2H^+ + 2e^- \rightarrow H_2$) or water (alkaline solution: $2H_2O + 2e^- \rightarrow H_2 + 2OH^-$) are converted into molecular hydrogen. Mechanistically, three principal steps/reactions are involved in electrochemical HER: Volmer reaction ($H^+_{(aq)} + e^- \rightarrow H_{ads}$), Heyrovsky reaction ($H^+_{(aq)} + H_{ads} + e^- \rightarrow H_2$), and Tafel reaction ($H_{ads} + H_{ads} \rightarrow H_2$). Molecular H_2 forms by the Volmer–Heyrovsky or Volmer–Tafel pathway or both depending on the H_{ads} coverage on the surface of the catalyst. At low H_{ads} coverage, H_2 is produced by the Volmer–Heyrovsky pathway but at high H_{ads} coverage, H_2 is formed via the Volmer–Tafel pathway [11,200]. The reaction rate of the catalyst mainly depends on the H_{ads}—M strength (M stands for metal) in the interaction, which can be estimated theoretically by the hydrogen adsorption free energy (ΔGH_{ads}) [11,201,202]. The variation in ΔGH affects the nature of the reactions. A negative and small ΔGH* shows that the H* combines readily on the electrode surface thus favoring the initial Volmer step. However, a large absolute value of ΔGH* makes the subsequent Tafel or Heyrovsky step difficult. In contrast, a large and positive ΔGH means the whole reaction is sluggish because of weak interactions between protons and electrodes. Therefore, the ideal HER catalysts should have nearly zero ΔGH. In theory, zero voltage (0 V) is required to start a reaction but practically, it is crucial to apply a high potential to overcome the cell resistance and kinetic barriers on each electrode [203] and suitable electrocatalysts are required. Presently, noble metal catalysts such as Pt group metals are efficient electrocatalysts in HER offering low overpotentials but their low efficiency and limited resources restrict widespread use [204–206]. Consequently, the search for more suitable materials with a larger active surface area, specific activity, and particle or layer structure has increased significantly [207–213].

In many energy-related technologies like rechargeable metal-air batteries and water electrolysis, OER is a fundamental step [214–216]. Oxygen production is endothermic by nature ($\Delta H > 0$) and occurs naturally in photosynthesis via absorption of photon energy from sunlight, but it can also be generated synthetically by OER in water splitting [217–220]. Compared to HER, OER is more sluggish and generally considered the thermodynamically and kinetically demanding process in water electrolysis [221]. There are a number of possible pathways in OER as a result of the formation of a large number of adsorbed

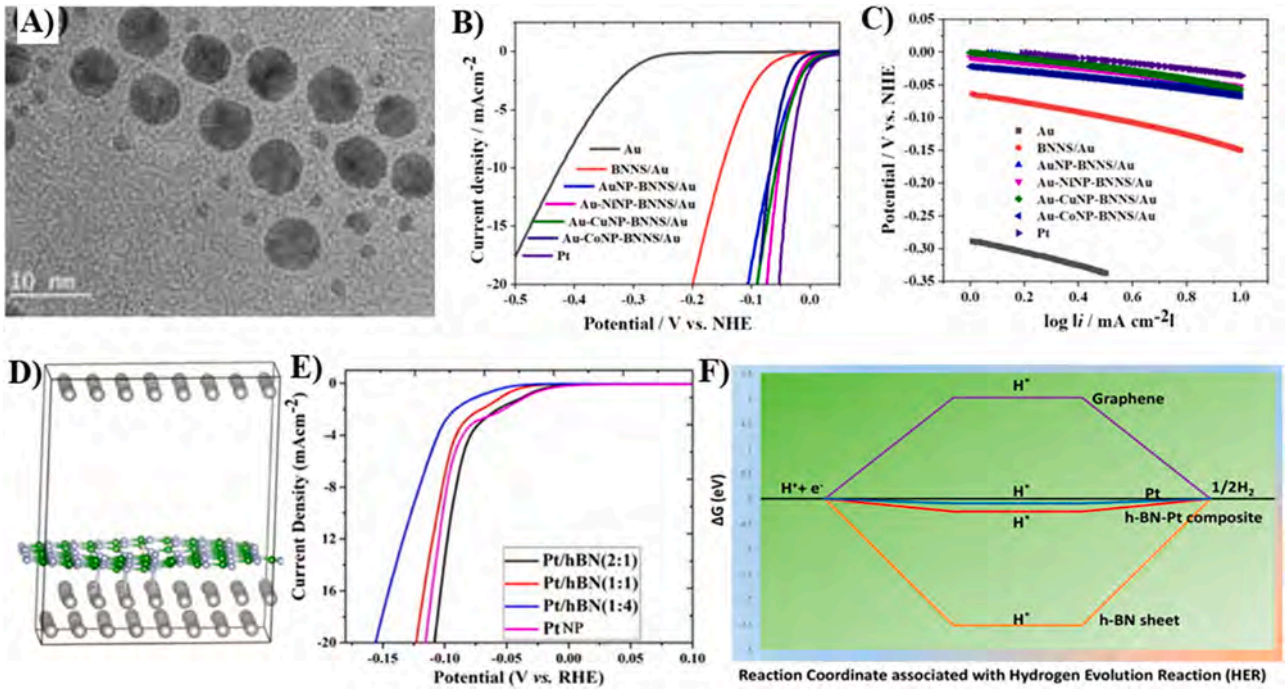

Fig. 10. (A) TEM image of Au-Ni NPs-BNNS/Au. (B) LSV curves and (C) Tafel plots of BNNS-decorated composites in comparison with Pt NPs. Reproduced with permission [230]. Copyright 2019, Elsevier. (D) Bird's eye and side views of Pt-modified h-BN. (E) LSV curves of various Pt/h-BN based catalysts. (F) Free energy diagram of Pt/h-BN, graphene, h-BN, and Pt. Reproduced with permission [231]. Copyright 2018, American Chemical Society.

intermediates (M-O, M-OH, M-OOH), as it involves transferring of 4 electrons and 4 protons [215]. The OER routes take place in different directions depending on the catalyst used and reaction medium (acidic/alkaline). However, in all directions, similar phenomena occur (adsorption/desorption of the oxide, peroxide, and superoxide intermediates). For efficient OER, IrO_2-based catalysts are considered the best but owing to the high price and limited resources, there have been extensive efforts to develop environmentally friendly, cheap, and

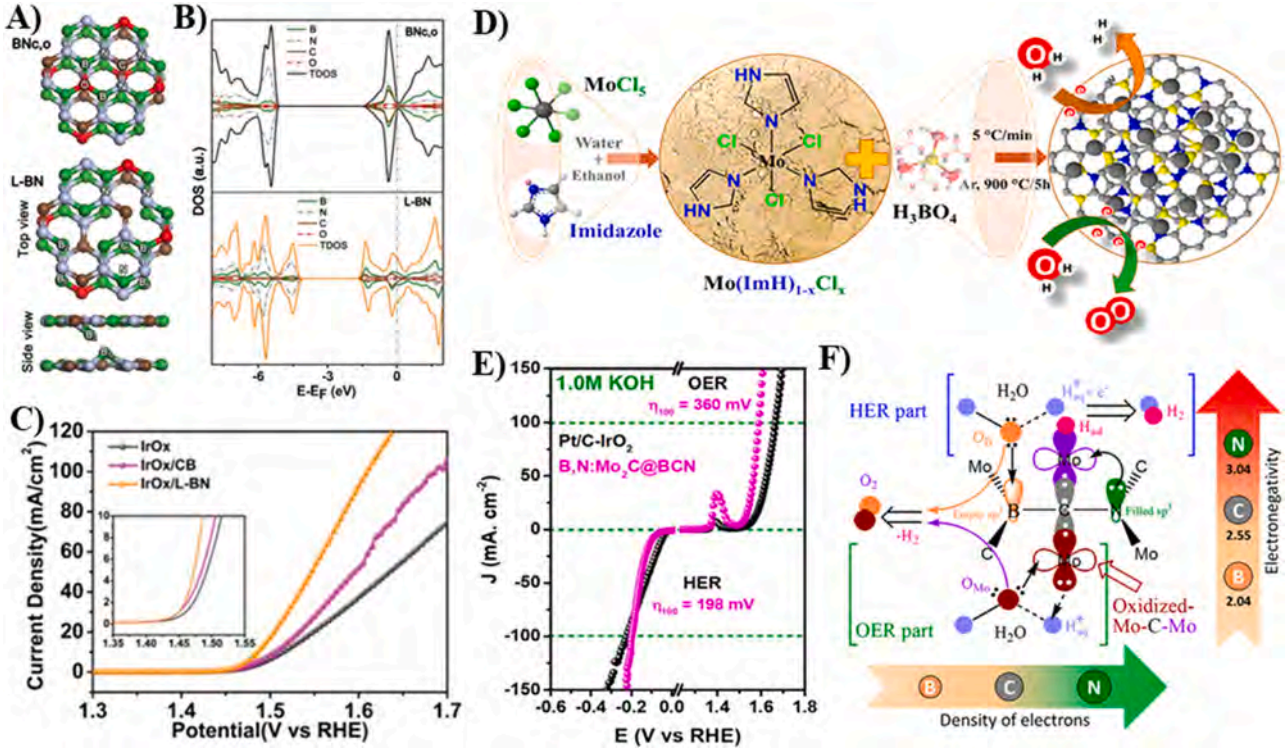

Fig. 11. (A) Schematic diagram of BNc,o and L-BN. (B) Partial densities and total density of states of L-BN and BNc,o. (C) OER polarization curves of different materials supporting IrO_x. Reproduced with permission [233]. Copyright 2020, John Wiley and Sons. (D) Schematic diagram for the preparation of the (B,N:Mo_2C@BCN) catalyst. (E) polarization curves of HER and OER in 1.0 M KOH for B,N:Mo_2C@BCN. (F) Possible mechanism for overall water splitting on the B,N:Mo_2C@BCN catalyst. Reproduced with permission [236]. Copyright 2018, American Chemical Society.

Table 3
Electrocatalytic characteristics of BN-based materials in HER/OER.

Catalysts	Electrolytes	HER/OER	Overpotential (mV)	Onset-potential (V)	Current density (mA.cm^{-2})	Tafel slope (mV dec^{-1})	Ref.
BN-Gas-2	0.1 M KOH	OER	–	0.37	10	379.3	[197]
IrO_x-L-BN	1.0 M KOH	OER	259	–	10	36.68	[233]
CNTBN5–750	0.1 M KOH	OER	0.38	–	10	122	[198]
Co_3O_4-BCN	1.0 M KOH	OER	394	0.406	10	–	[239]
1–1-NBC	0.5 M H_2SO_4	HER	590	-0.43	10	205	[196]
1–1-NBC	1.0 M KOH	HER	486	–	10	199	[196]
1–1-NBC	1.0 M PBS	HER	–	-0.4	10	256	[196]
Pt/h-BN	0.5 MH_2SO_4	HER	90	–	–	29	[231]
h-BN/Cu	0.1 M $HCLO_4$	HER	–	-0.688	10	136	[155]
h-Bn/Au	0.1 M $HCLO_5$	HER	–	-0.688	900	108	[155]
B,N:Mo_2C@BCN	1.0 M KOH	HER	100	–	10	62	[236]
B,N:Mo_2C@BCN	1.0 M KOH	OER	360	–	100	61	[236]
Ni@BCN	–	OER	0.47 V	–	–	–	[240]
Ni@BCN	–	HER	0.02 V	–	–	–	[240]

high-rate non-metal-based catalysts [215,216,222–227].

Since the electrocatalyst is a crucial component of the electrode, the HER activity depends on the properties of electrocatalysts and considerable efforts have been made to develop noble-metal free catalysts with low overpotentials and high current densities. Recently, boron nitride-based materials have attracted attention [228]. Uosaki et al. have reported improved HER activity from boron nitride nanosheets (BNNSs) prepared on a gold electrode. Theoretically, the edge sites have the most favorable hydrogen adsorption energies for HER and they experimentally verify that h-BNNSs with decreased lateral sizes exhibit a relatively low overpotential [229]. The HER activity of the same catalyst is slightly modified with Au NPs decorated on BNNSs/Au. The Au concentration in the catalyst is reduced by alloying the Au NPs with other metals such as Ni, Cu, and Co. The most efficient electrode is that modified with BNNSs and decorated with Au-Ni NPs and the HER activity is comparable to that of Pt with an overpotential of 15 mV (at 5 mA cm^{-2}) and −30 mV (at 15 mA cm^{-2}) higher than those obtained from a Pt electrode (Fig. 10A-10C) [230]. Introducing metallic surfaces to h-BN is an effective way to alter the intrinsic catalytic activity of h-BN by modulation of the band structure [155]. Guha et al. have evaluated the HER activity of the Pt electrode and Pt NPs wrapped/coated with h-BN prepared by a simple reduction method. They have shown theoretically and experimentally that the high efficiency of the catalysts arises from synergistic effects of h-BN and underneath Pt and also that the BN edge atoms offer dynamically favorable hydrogen adsorption sites (Fig. 10D). As a result, the catalyst is capable of generating an HER current density of 10 mA cm^{-2} at a 90 mV overpotential, which is 10 mV less than that of Pt NPs (Fig. 10E). Although h-BN is insulating with a bandgap of 6 eV, DFT calculation shows that when h-BN is modified with Pt NPs, the bandgap decreases drastically yielding metal-like properties. The lower ΔG is mainly due to covalent bonding between Pt and h-BN (Fig. 10F) [231] and Nguyen et al. have evaluated C-doped h-BNNS as a metal free bifunctional electrocatalyst for ORR and HER. Four geometric models of C-doped h-BNNSs are suggested, namely single and double C-doped h-BNNS in which C atom(s) occupy either the B or N site(s) and the single C-doped catalyst with dopants at the N site (CN) is more favorable for HER [196,232].

Generating boron, nitrogen, and oxygen vacancies are beneficial [233,234] and Liu et al. have synthesized conductive BNNS support by first co-doping with C and O and then using pulsed laser ablation (PLA) to generate oxygen vacancies to form L-BN (Fig. 11A) [233]. PLA modification creates interlaminar B-B dipolar interactions leading to significant electrical conductivity improvement (Fig. 11 B) and the oxygen vacancy is an active site for IrO_x loading. Consequently, when L-BN is doped with IrO_x, few electrons from Ir ions move to C atoms in N-C=N, resulting in oxidation of Ir ions to generate robust interactions between IrO_x and L-BN. The enhanced electrocatalytic performance and high stability are confirmed by the low overpotential of 259 mV at 10 mA cm^{-2} (Fig. 11C). The structural similarity between graphene and h-BN has motivated researchers to develop hybrid materials such as boron carbon nitride (BCN). Maji et al. have discovered that the graphene magnetic islands in h-BN generate a high level of chemical stimulation [235] and the magnetism in C-doped h-BN arises from the spin of unpaired 2pz electrons in the functionalized C atoms in h-BN. These valence electrons belong to an isolated carbon atom or to a graphene island, thus preventing all the carbon atoms from completing sub-shell filling and activating the catalyst in OER and ORR. DFT calculation shows the inherent relationship between chemical activation and magnetism in C-doped h-BN. Besides the magnetic island, the interface formed by combining a few exfoliated layers of graphene and BN produces synergistic effects to f-CNT and h-BN by providing the ideal site for oxygen adsorption and reduction [198].

Defective h-BN provides excellent support to design effective catalysts for both HER and OER [237]. Since water splitting consists of HER and OER, the development of bifunctional catalysts for both reactions have received increasing attention in recent years [238]. The HER and OER characteristics of some BN-based catalysts are summarized in Table 3. Anjum et al. have prepared a bifunctional Mo_2C based catalyst embedded in the BCN network by single-step annealing (Fig. 11D). The B,N:Mo_2C@BCN catalyst shows overpotentials of 198 mV for HER and 360 mV for OER at a 100 mA cm^{-2} current density (Fig. 11E), which are smaller than those of commercial Pt/C (239 mV) and IrO_2 (435 mV). The high activity primarily stems from enhanced charge transfer and wetting characteristics caused by the synergistic effects of B, N, and small Mo_2C NPs embedded in the BCN system (Fig. 11F) [236,239]. Tang et al. have compared 18 different TMs deposited on the BCN hybrid for both HER/OER [240] and the enhanced HER/OER performance of the BCN hybrid with a large BN ratio is primarily due to charge polarization and synergism rendered by graphene, BN, and Ni. Although the use of BN-based catalysts in electrocatalytic water splitting is still in the early stage, recent experimental and theoretical results have unveiled tremendous potential.

4.3. CO_2 reduction reaction

CO_2 is the primary greenhouse gas produced by fossil fuel combustion and its concentration in the atmosphere has increased steadily. CO_2 reduction combined with renewable energy generation can lead to carbon-neutral fuels and mitigate the use of industrial chemicals produced from petroleum. Electrochemical CO_2 reduction to liquid fuels and chemical feedstocks is a significant area of research [241]. Compared to other electrochemical reactions such as the OER and HER, CO_2RR differs in that it proceeds through multiple steps [242,243]. Thermodynamically, to accomplish the first step in CO_2RR (formation of key intermediates ($CO_2^{\bullet-}$)), a high negative potential of −1.90 V is required thus making the overall reaction energetically unfavorable [244]. The rate-determining step (RDS) in CO_2RR is commonly believed to be the first electron transfer to CO_2 to create the $CO_2^{\bullet-}$ intermediate

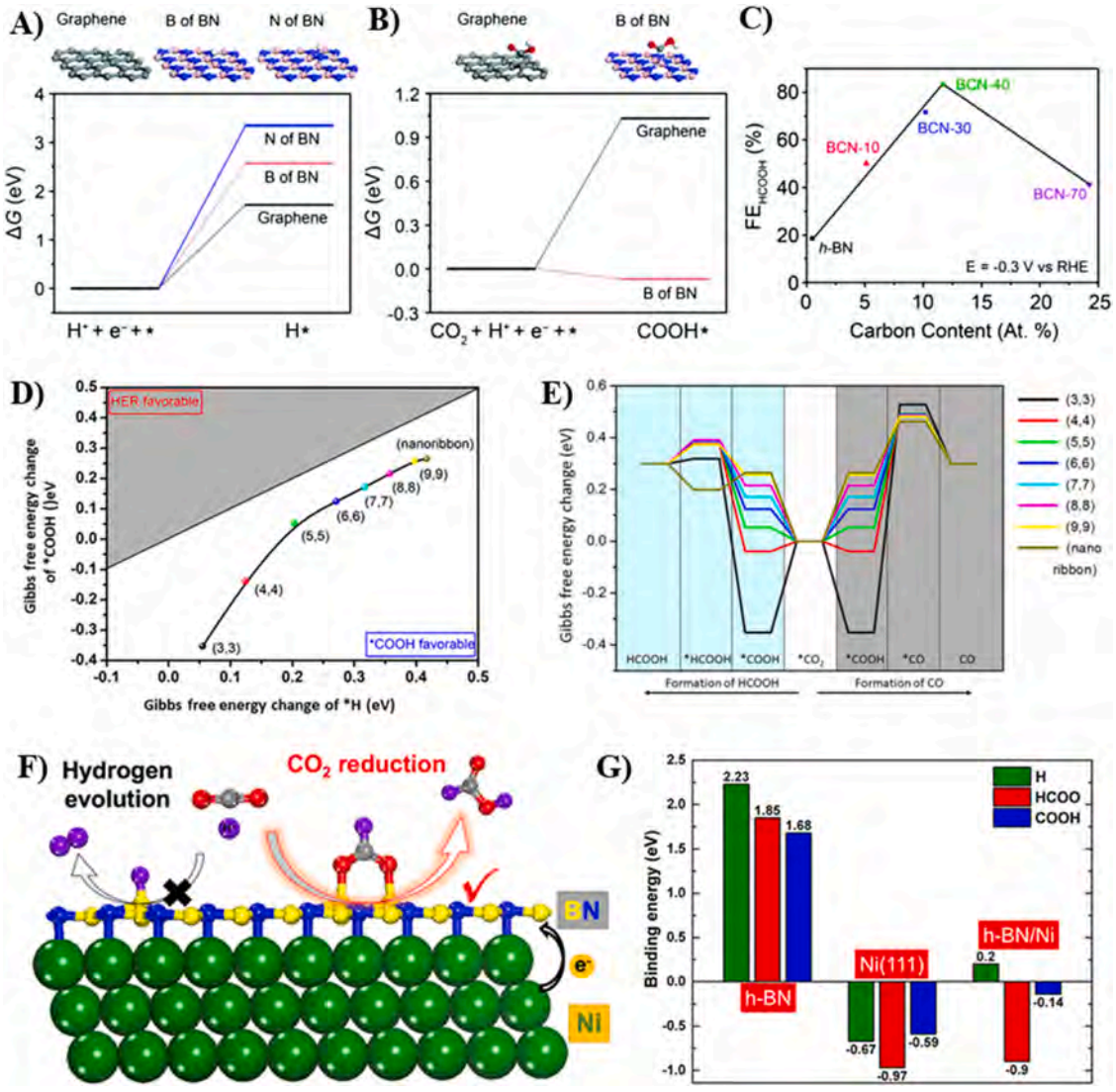

Fig. 12. Free energy diagrams for (A) Proton activation and (B) CO_2 activation at 0 V versus RHE. The crystal structures of graphene and h-BN are presented above the graph and the white, pink, gray, blue, and red balls represent H, B, C, N, and O atoms, respectively. (C) Faradaic efficiency versus carbon contents of h-BN and BCN-x catalysts in HCOOH production. Reproduced with permission [256]. Copyright 2013, The Royal Society of Chemistry. (D) Free energy diagram of *COOH and *H for comparison of HER and CO_2RR on G-BNNR (nanoribbon) and G-BNNT (nanotube). (3,3)-(9,9) represent catalysts with different indexes from (3) to G-BN (9). (E) Gibbs free energy change diagrams for the formation of CO and HCOOH molecules on the catalysts. Reproduced with permission [258]. Copyright 2020, John Wiley and Sons. (F) Optimized geometries for HCOOH on h-BN/Ni. (G) Comparison of binding energies (eV) for intermediate species such as H, HCOO, and COOH on the h-BN monolayer, Ni(111), and h-BN/Ni(111). Reproduced with permission [259]. Copyright 2018, American Chemical Society.

and the next step depends on whether the oxygen atom or carbon atom is bound to the electrode surface [242]. CO_2RR is a complicated reaction in which a wide range of products can be obtained (such as H_2, CO, methanol, CH_4, C_2H_4, ethanol, n-propanol, etc.) depending on the number of electrons transferred. CO_2RR is further complicated by the simultaneous transfer of electrons and protons giving rise to the formation of complex intermediates. These multi-step transfer processes produce slow reaction kinetics and require a significant overpotential in order to produce fuels at an acceptable rate, thereby making it inefficient for commercialization on a large scale [245]. To reduce the overpotential of CO_2RR, electrocatalysts can be used to activate CO_2. In general, a desirable electrocatalyst for CO_2 reduction must be capable of mediating multiple electron and proton transfer while suppressing the competitive hydrogen evolution reaction [244–246].

Among the common CO_2RR catalysts, copper is the only metal capable of producing large amounts of C1–C3 hydrocarbons due to the appropriate intermediate bonding strength for CO [247]. However, it suffers from poor product selectivity, high overpotential, and poor Faradaic efficiency mainly due to competitive reactions like HER [248–250]. Hence, highly active and selective CO_2RR catalysts are required for efficient CO_2RR electrocatalysis. With regard to metal catalysts, the scaling relationship of CO_2RR intermediates correlates with the d-band structure [251,252] and so synthesizing metal-free catalysts with the only s- and p-orbital contributions can disrupt the scaling interactions. In this respect, BN-like materials can be active in CO_2 chemisorption by adding an extra electron to the structure [253–255] for possible CO_2 reduction. Cao et al. have reported that carbon doping in h-BN can improve the catalytic activity in CO_2RR [256] and theoretically, an active site is formed when a graphitic C atom is surrounded by the h-BN B atom. They use a simple pyrolysis method to prepare BCN-x flakes which boast a Faradic efficiency of 83.5% for HCOOH at a small overpotential of 100 mV in addition to energy efficiency of 78.0%. According to DFT calculation, CO_2 activation is more likely to take place on B atoms, whereas proton activation occurs more frequently on C atoms (Fig. 12A-12C). Tang et al. have predicted carbon-doped boron nitride nanoribbons (BNNRs) which are active as both C1 and C2

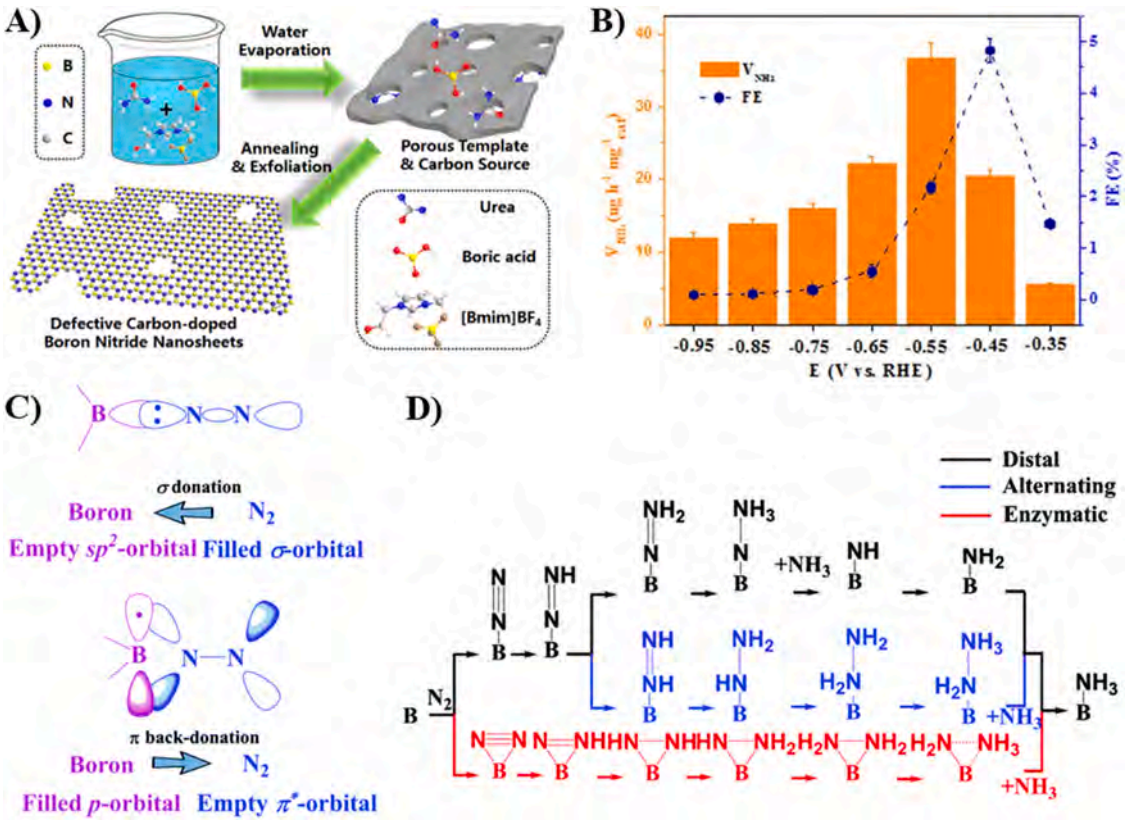

Fig. 13. (A) Schematic diagram for defective C-BN nanosheets preparation. (B) V_{NH3} and FEs of C-BN/CP at different potentials. Reproduced with permission [288]. Copyright 2020, American Chemical Society. (C) N_2 bonded to a B atom stabilized by the substrate. (D) Schematic depiction of the distal, alternating, and enzymatic mechanisms in N_2 reduction to NH_3 by B-based catalysts. Reproduced with permission [289]. Copyright 2019, The Royal Society of Chemistry.

products and the electrocatalyst converts CO_2 into CO at a relatively low overpotential of −0.5 V and forms C2 products such as C_2H_4 and C_2H_5OH with high efficiency and selectivity for C_2H_5OH by suppressing HER [257]. The selectivity for C2 products stems from the chemical bond between $*CH_2$ and CO intermediates generated from the edge B atoms and C dopant as dual active sites on BNNRs.

A potential benefit of introducing curvature to the catalyst surface is to boost the binding strength with key intermediates. Mao et al. have shown theoretically that the C-N interface on the curved surface provides highly active sites for CO_2RR as well as strong binding with *COOH groups to suppress HER (Fig. 12D and 12E) [258] and the smaller index of graphene-BN nanotubes (G-BNNTs) leads to CH_3OH formation, whereas the large index of the G-BNNTs facilitates the generation of CH_4. Hybridizing BN with metals and alloys can produce high-performance heterogeneous catalysts [162,260,261]. Hu et al. have observed the trend of the activity of catalysts for CO_2 reduction to HCOOH by monitoring the binding energies of the three intermediates of H, HCOO, and COOH [259]. By studying the h-BN interface and engineering of the monolayer on different TMs (Co, Ni, and Cu), the key intermediates produced during HER and CO_2RR possess unique chemical reactivity at the h-BN/metal interface when an electron is transferred from the metal to h-BN. Accordingly, H adsorption on the surface of h-BN/metal decreases significantly but HCOO adsorption is least affected, consequently resulting in CO_2RR selectivity control and suppressed HER (Fig. 12F and 12G). Tan et al. have compared 17 different metal surfaces from the perspective of reduction of CO_2 to CH_4 and Fe/defective BN and Pt/defective BN are promising catalysts boasting low onset potentials −0.52 V and −0.60 V in conjunction with high selectivity [262]. The high electrochemical activities arise from the mild electron affinities of the electrocatalyst for C and O, thus modifying the free energies of the electrochemical reduction intermediates in the reaction. Similarly, Cui et al. have studied catalysts consisting of B-vacancy of BN doped with 18 different metals and Mo-doped BN exhibits excellent CO_2 to CH_4 conversion together with a small limiting potential of −0.45 V [263]. The Mulliken charge analysis of the activity shows that charges are transferred from MoN_3 (Moiety 2) and BN monolayer (Moiety 3) to the $C_xH_yO_z$ (Moiety 1) (end products). The BN monolayer serves as a reservoir for electrons for donating or accepting electrons to contribute 0.626 electrons to moiety 1, whereas MoN_3 acts as the transmitter and active site for CO_2RR. Cu can catalytically produce hydrocarbons and alcohols in large amounts with low faradaic efficiency [247,264] and Sun et al. have demonstrated a 4-fold increase in the efficiency [265]. The N-based Cu(I)/C-doped boron nitride (BN-C) composites convert CO_2 into CH_3COOH (acetic acid) with a Faradaic efficiency of approximately 80.3% due to the synergistic effects between BN-C30, Cu metal center, N based ligand, and electrolyte. Qin et al. have determined the formation energy (E_f) and dissolution potential (U_{diss}) of 96 two-dimensional catalysts containing different defect sites of monoclinic crystal BN, and Ga/In@N-BN, Sn@BN, and Co@N-BN are considered the best catalysts to produce HCOOH, CO, and CH_3OH by CO_2RR, respectively [266]. The literature on catalysts for CO_2 reduction is less extensive than that on ORR due to thermodynamic and kinetic limitations plaguing CO_2 reduction. Although CO_2RR is highly complex including multiple steps and multiple products depending on the catalysts, more high-performance BN-based catalytic systems are expected to be developed in the future.

4.4. Nitrogen reduction reaction

NRR is an important process for ammonia (NH_3) synthesis vital to agriculture and renewable fuels [267]. As a carbon-free fuel, NH_3 with approximately 18% hydrogen is a safer energy source than pure hydrogen [268,269]. Although the Haber-Bosch process (HBP) is the common commercial technique to produce ammonia, the process uses

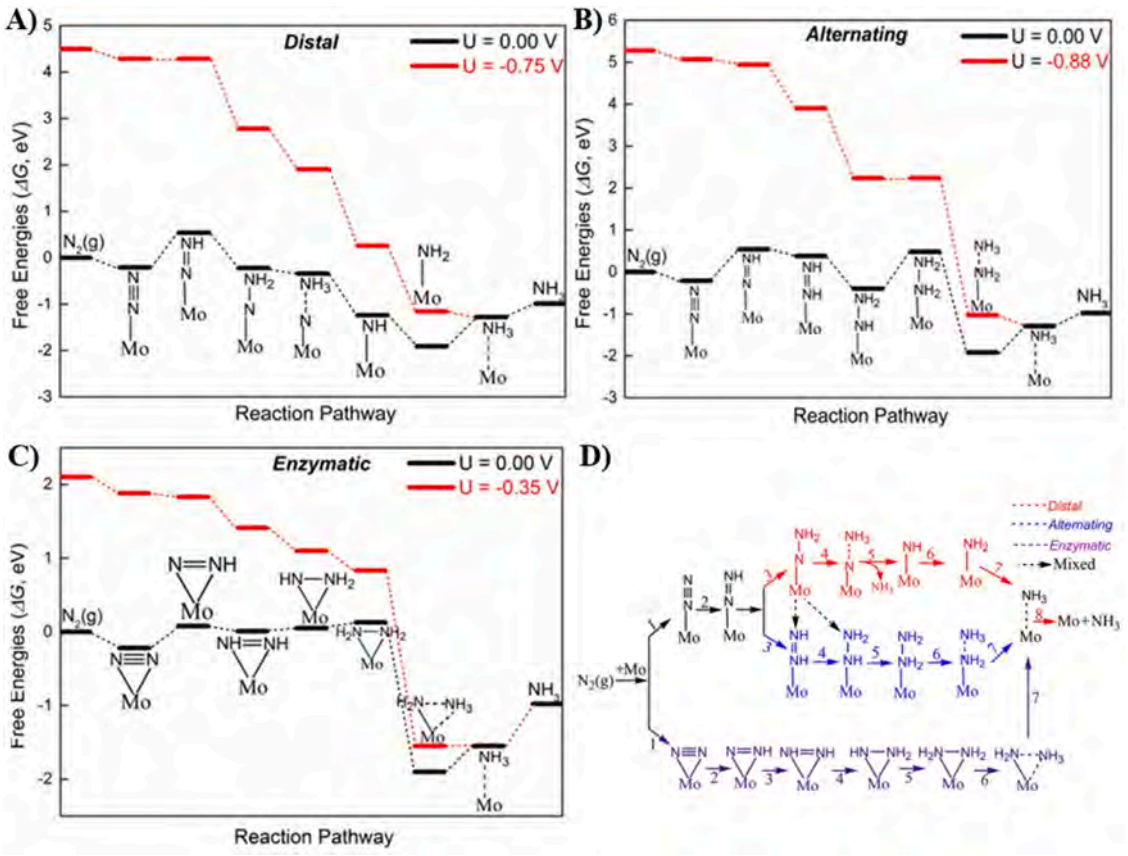

Fig. 14. Free-energy diagrams for NRR on the Mo–BN monolayer at zero and applied potentials (limiting potential) by (A) Distal, (B) Alternating, and (C) Enzymatic mechanisms. (D) Schematic depiction of the three mechanisms in N_2 electroreduction to NH_3 on the single Mo atom anchored on the defective BN monolayer. Reproduced with permission [291]. Copyright 2017, American Chemical Society.

1% of the world's energy supply, has low catalytic efficiency, and yields unwanted byproducts such as N_2H_2 and N_2H_4 in addition to generating a large amount of CO_2 [270–272]. Compared to HBP, NRR is projected to be 20% more thermodynamically energy-efficient [273,274] and compared with the ORR mechanisms, NRR mechanisms can be classified as dissociative or associative depending on the intermediates in electrocatalysis [275,276]. NRR presents several challenges, for example, low N_2 adsorption and large bond energy of N≡N (940.95 kJ/mol) cleavage, but they can be overcome by rational design of the electrocatalysts [277]. The catalyst contributes primarily to chemisorption/activation of N_2 by combining the empty and occupied d orbitals [278,279] and several metal-based catalysts containing Fe, Mo, V, Ru, Au, and Pd have been proposed [152,280–285]. Unfortunately, most of these metal-containing electrocatalysts have small or no proton adsorption free energy and produce electron donation effects which facilitate HER instead. Hence, it is challenging to balance competitive nitrogen activation and hydrogen evolution for metal-based catalysts and low NH_3 yield and Faradic efficiency (FE) frequently result.

Recently, 2D materials have become popular electrocatalysts for NRR due to low proton adsorption and small hydrogen production [286]. Zhang et al. have observed that h-BNNS prepared by liquid exfoliation can convert N_2 to NH_3 at a rate of 22.4 μg h^{-1} mg^{-1} with a Faradaic efficiency of 4.7% at −0.75 V [287] and further improvement has been made by Liu et al. with highly porous structures produced by a template-based method (Fig. 13A). The defective carbon-doped BNNSs are very active compared to reported exfoliated BNNSs, producing 36.7 μg h^{-1} mg cat^{-1} of NH_3 at −0.55 V with 6.51% faradic efficiency (Fig. 13B). The unsaturated B atom at the h-BN edge site is mainly responsible for activation of inert N_2 molecules by lowering the energy barrier for NH_3. Furthermore, doping with carbon improves the electrical conductivity of the nanosheets and increases the charge transfer rate [288]. The B atom as an electron-deficient center possesses Lewis acid like properties and so it attacks N_2 (Lewis base) to create the Lewis acid-base complexes. The outer orbital of the B atom hybridizes to generate sp^2 orbitals composed of partially occupied and vacant orbitals. The vacant sp^2 orbitals accept lone-pair electrons from N_2 molecules, while the filled sp^2 orbitals donate electrons back to the anti-bonding p* orbital of the N_2 molecules (Fig. 13C and 13D) [289]. Owing to electron acceptance and back donation, B-based materials are promising electrocatalysts for NRR. Li et al. have observed that carbon-doped hexagonal boron nitride nanoribbons (BNNRs) have excellent N_2 capturing ability originating from the edge lone pair electrons and the carbon dopant enhances the NRR catalytic activity by modulating the adsorption free energy of the NRR intermediates [290].

Design and preparation of the proper catalysts solely by experimental screening is an arduous task and computer-aided methods are highly desirable in the search for efficient NRR catalysts. Theoretical investigations not only provide assistance in designing highly efficient and novel electrocatalysts but also help to understand the NRR mechanism of different materials. Zhao et al. have prepared a stable and efficient electrocatalyst for NRR by incorporating Mo atoms into defective BN among different TM atoms. The high activity arises from high spin polarization, selective stabilization of N_2H^* species, and destabilization of NH_2^* species with a relatively low overpotential of 0.19 V (Fig. 14) [291]. BN/graphene-based hybrid nanosheets functionalized with single Mo atoms at B vacancies deliver good NRR performance. By introducing Mo atoms to B vacancies, the localized spin density and reduction in bandgap energy critical for activation of N_2 molecules reduce the overpotential for conversion of N_2 to NH_3 via an enzymatic pathway [292]. Moreover, the catalytic properties of several types of single TM

Table 4
Electrocatalytic characteristics of BN-based materials in NRR.

Catalysts	Electrolytes	V_{NH3} ($\mu g\ h^{-1}\ mg\ cat^{-1}$)	FE (%)	Ref.
Defective C-BN	0.1 M HCl	36.7	6.51	[288]
h-BNNS/CP	0.1 M HCl	22.4	4.7	[287]
B, N-doped graphene	0.1 M HCl	7.75	13.79	[296]
MBN	0.1 M Na_2SO_4	18.2	5.5	[297]
BND_2-NC/Ti	0.05 M H_2SO_4	19.1	21.2	[298]
BNS	0.1 M Na_2SO_4	13.22	4.04	[299]

atoms anchored to B vacancies of BN have been studied theoretically [293] and the curvature effect also impacts the physical and chemical properties of the catalysts. Making h-BNNSs into nanotubes and filling with TMs improve NH_3 production and according to simulation, the activity is associated with the cooperation of occupied and unoccupied boron p states, which act as electron reservoirs, consequently facilitating N_2 fixation and reduction by the enzymatic pathway [294,295]. Table 4 presents the characteristics of some common BN-based catalysts for NRR.

5. Conclusion and prospective

Significant progress has been made in the development of h-BN, including synthesis and applications, to render them efficient electrocatalysts in next-generation energy technology. Being inert materials, h-BN has not been investigated as extensively as other 2D materials in the energy conversion field. However, spurred by recent advances pertaining to physio-chemical modification and functionalization, h-BN with unique characteristics such as tunable bandgaps and high meso/microporosity has attracted much attention. In this review, the 2D h-BN structures are described and some of them are suitable catalysts without needing additional binders and supports. In fact, h-BN is an excellent supporting substrate for catalytic reactions due to its high chemical, electrochemical, and thermal stability. Moreover, the large surface area, abundant active sites, and heteroatom doping improve the properties of h-BN, so that the electronic properties as well as adsorption and desorption capabilities of reactants, intermediates, and products can be promoted from the perspectives of ORR, HER, OER, CO_2RR, and NRR.

Despite significant recent advances in 2D h-BN based electrocatalysts, there are several critical challenges, for example, large-scale production, controllability of the modification methods, electrocatalytic activity, and mechanisms, particularly in overall water splitting, CO_2RR, and NRR. Considering that modification methods affect the physio-chemical properties of h-BN, electronic manipulation and defect engineering need to be refined. In the meantime, the detailed mechanisms and relationship between these modification methods and properties of h-BN must be explored. Because most of the modification methods require a high temperature and harsh conditions, the amounts of metal dopants and grafted functional groups are difficult to control, thus creating differences between theoretical and experimental studies. Elimination of defects, particularly grain boundaries (GBs) stitching misoriented domains, is critical to the production of high-quality h-BN composites. To achieve this, the single crystal domains of h-BN can be made to be as large as possible or is fully integrated with the identical orientation [300]. In-depth knowledge of the basic growth mechanisms and substrates is required for the development of h-BN. Furthermore, the wide range of h-BN applications requires h-BN films with different thicknesses and precise control of the number of layers of h-BN films is necessary without sacrificing the crystallinity and homogeneity. Integrating h-BN layers into other 2D materials such as graphene and 2D transition metal dichalcogenides (TMDCs) to create hybrid 2D materials has aroused much interest in recent years. However, controlled manufacturing of in-plane and vertical heterostructures with crisp and clean interfaces is still a difficult task and it is still challenging to implement these methods in large-scale commercial production. Future work is expected to focus on combined theoretical and experimental approaches to develop simple and environmentally sustainable methods for large-scale synthesis of h-BN based materials. It is our belief that there is sufficient scientific interest to warrant successful development of h-BN based electrocatalysts for future green energy systems and h-BN is expected to play a vital role in our continuous endeavor to mitigate the society's reliance on fossil fuels to protect the environment.

Declaration of Competing Interest

The authors declare that they have no known competing financial interests or personal relationships that could have appeared to influence the work reported in this paper.

Acknowledgements

This work was financially supported by National Natural Science Foundation of China (NSFC 21806099 and 21671127), Guangdong Basic and Applied Basic Research Foundation (2019A1515010076 and 2019A1515012156), Scientific Research Foundation of Shantou University (NTF18009 and NTF20005), 2020 Li Ka Shing Foundation Cross-Disciplinary Research Grant (2020LKSFG09A and 2020LKSFG01A), Department of Education of Guangdong Province (2019KCXTD007, 2017KZDXM034, 2021KTSCX030, 2021LSYS009 and 2021KCXTD032), and City University of Hong Kong Strategic Research Grant (SRG) (7005505).

References

[1] P. Prabhu, V. Jose, J.-M. Lee, Design strategies for development of TMD-Based heterostructures in electrochemical energy systems, Matter 2 (2020) 526–553, https://doi.org/10.1016/j.matt.2020.01.001.
[2] Y. Sun, S. Gao, F. Lei, Y. Xie, Atomically-thin two-dimensional sheets for understanding active sites in catalysis, Chem. Soc. Rev. 44 (2015) 623–636, https://doi.org/10.1039/C4CS00236A.
[3] Y. Jiao, Y. Zheng, M. Jaroniec, S.Z. Qiao, Design of electrocatalysts for oxygen- and hydrogen-involving energy conversion reactions, Chem. Soc. Rev. 44 (2015) 2060–2086, https://doi.org/10.1039/C4CS00470A.
[4] V.R. Stamenkovic, D. Strmcnik, P.P. Lopes, N.M. Markovic, Energy and fuels from electrochemical interfaces, Nat. Mater. 16 (2017) 57–69, https://doi.org/10.1038/nmat4738.
[5] R. Han, F. Liu, X. Wang, M. Huang, W. Li, Y. Yamauchi, X. Sun, Z. Huang, Functionalised hexagonal boron nitride for energy conversion and storage, J. Mater. Chem. A 8 (2020) 14384–14399, https://doi.org/10.1039/D0TA05008C.
[6] J. Duan, S. Chen, M. Jaroniec, S.Z. Qiao, Heteroatom-doped graphene-based materials for energy-relevant electrocatalytic processes, ACS Catal. 5 (2015) 5207–5234, https://doi.org/10.1021/acscatal.5b00991.
[7] L. Dai, Y. Xue, L. Qu, H.-J. Choi, J.-B. Baek, Metal-free catalysts for oxygen reduction reaction, Chem. Rev. 115 (2015) 4823–4892, https://doi.org/10.1021/cr5003563.
[8] R. Xu, L. Du, D. Adekoya, G. Zhang, S. Zhang, S. Sun, Y. Lei, Well-defined nanostructures for electrochemical energy conversion and storage, Adv. Energy Mater. 11 (2021), 2001537, https://doi.org/10.1002/aenm.202001537.
[9] S. Zhao, D.-W. Wang, R. Amal, L. Dai, Carbon-based metal-free catalysts for key reactions involved in energy conversion and storage, Adv. Mater. 31 (2019), 1801526, https://doi.org/10.1002/adma.201801526.
[10] H. Wang, J.-M. Lee, Recent advances in structural engineering of MXene electrocatalysts, J. Mater. Chem. A 8 (2020) 10604–10624, https://doi.org/10.1039/D0TA03271A.
[11] J. Zhu, L. Hu, P. Zhao, L.Y.S. Lee, K.-Y. Wong, Recent advances in electrocatalytic hydrogen evolution using nanoparticles, Chem. Rev. 120 (2020) 851–918, https://doi.org/10.1021/acs.chemrev.9b00248.
[12] S. Nitopi, E. Bertheussen, S.B. Scott, X. Liu, A.K. Engstfeld, S. Horch, B. Seger, I.E. L. Stephens, K. Chan, C. Hahn, J.K. Nørskov, T.F. Jaramillo, I. Chorkendorff, Progress and perspectives of electrochemical CO_2 reduction on copper in aqueous electrolyte, Chem. Rev. 119 (2019) 7610–7672, https://doi.org/10.1021/acs.chemrev.8b00705.
[13] G. Wang, J. Chen, Y. Ding, P. Cai, L. Yi, Y. Li, C. Tu, Y. Hou, Z. Wen, L. Dai, Electrocatalysis for CO_2 conversion: from fundamentals to value-added products, Chem. Soc. Rev. 50 (2021) 4993–5061, https://doi.org/10.1039/D0CS00071J.
[14] P. Prabhu, V. Jose, J.-M. Lee, Heterostructured catalysts for electrocatalytic and photocatalytic carbon dioxide reduction, Adv. Funct. Mater. 30 (2020), 1910768, https://doi.org/10.1002/adfm.201910768.
[15] R. Manjunatha, A. Karajić, M. Liu, Z. Zhai, L. Dong, W. Yan, D.P. Wilkinson, J. Zhang, A review of composite/hybrid electrocatalysts and photocatalysts for nitrogen reduction reactions: advanced materials, mechanisms, challenges and

perspectives, Electrochem. Energy Rev. 3 (2020) 506–540, https://doi.org/10.1007/s41918-020-00069-0.
[16] H.A. Gasteiger, S.S. Kocha, B. Sompalli, F.T. Wagner, Activity benchmarks and requirements for Pt, Pt-alloy, and non-Pt oxygen reduction catalysts for PEMFCs, Appl. Catal. B Environ. 56 (2005) 9–35, https://doi.org/10.1016/j.apcatb.2004.06.021.
[17] Y.P. Zhu, C. Guo, Y. Zheng, S.-Z. Qiao, Surface and interface engineering of noble-metal-free electrocatalysts for efficient energy conversion processes, Acc. Chem. Res. 50 (2017) 915–923, https://doi.org/10.1021/acs.accounts.6b00635.
[18] K.S. Novoselov, A.K. Geim, S.V. Morozov, D. Jiang, Y. Zhang, S.V. Dubonos, I. V. Grigorieva, A.A. Firsov, Electric field effect in atomically thin carbon films, Science 306 (2004) 666–669, https://doi.org/10.1126/science.1102896.
[19] Z. Jiang, W. Zhu, G. Xu, X. Xu, M. Wang, H. Chen, W. Huang, X. Ge, M. Lin, Ni-nanoparticle-bound boron nitride nanosheets prepared by a radiation-induced reduction-exfoliation method and their catalytic performance, J. Mater. Chem. A 8 (2020) 9109–9120, https://doi.org/10.1039/D0TA03701J.
[20] K. Zhang, Y. Feng, F. Wang, Z. Yang, J. Wang, Two dimensional hexagonal boron nitride (2D-hBN): synthesis, properties and applications, J. Mater. Chem. C 5 (2017) 11992–12022, https://doi.org/10.1039/C7TC04300G.
[21] J. Zhu, E. Ha, G. Zhao, Y. Zhou, D. Huang, G. Yue, L. Hu, N. Sun, Y. Wang, L.Y. S. Lee, C. Xu, K.-Y. Wong, D. Astruc, P. Zhao, Recent advance in MXenes: a promising 2D material for catalysis, sensor and chemical adsorption, Coordin. Chem. Rev. 352 (2017) 306–327, https://doi.org/10.1016/j.ccr.2017.09.012.
[22] L. Hu, X. Peng, Y. Li, L. Wang, K. Huo, L.Y.S. Lee, K.Y. Wong, P.K. Chu, Direct anodic exfoliation of graphite onto high-density aligned graphene for large capacity supercapacitors, Nano Energy 34 (2017) 515–523, https://doi.org/10.1016/j.nanoen.2017.03.007.
[23] Z. Huang, Z. Chen, A. Qayum, X. Zhao, H. Xia, F. Lu, L. Hu, Enhanced photocatalytic degradation of 4-chlorophenol under visible light over carbon nitride nanosheets with carbon vacancies, Nanotechnology 32 (2021), 415704, https://doi.org/10.1088/1361-6528/ac0eac.
[24] Z. Huang, X. Zhao, H. Xia, F. Lu, L. Hu, P.K. Chu, Insights into enhancement of photocatalytic properties of g-C_3N_4 by local electric field induced by polarization of MgO(111), J. Environ. Chem. Eng. 9 (2021) 105922, https://doi.org/10.1016/j.jece.2021.105922.
[25] H. Wang, J. Chen, Y. Lin, X. Wang, J. Li, Y. Li, L. Gao, L. Zhang, D. Chao, X. Xiao, J.-M. Lee, Electronic modulation of non-van der Waals 2D electrocatalysts for efficient energy conversion, Adv. Mater. 33 (2021), 2008422, https://doi.org/10.1002/adma.202008422.
[26] P. Prabhu, J.-M. Lee, Metallenes as functional materials in electrocatalysis, Chem. Soc. Rev. 50 (2021) 6700–6719, https://doi.org/10.1039/D0CS01041C.
[27] E. Lim, C. Jo, M.S. Kim, M.-H. Kim, J. Chun, H. Kim, J. Park, K.C. Roh, K. Kang, S. Yoon, J. Lee, High-performance sodium-ion hybrid supercapacitor based on Nb_2O_5@carbon core–shell nanoparticles and reduced graphene oxide nanocomposites, Adv. Funct. Mater. 26 (2016) 3711–3719, https://doi.org/10.1002/adfm.201505548.
[28] B. Anasori, M.R. Lukatskaya, Y. Gogotsi, 2D metal carbides and nitrides (MXenes) for energy storage, Nat. Rev. Mater. 2 (2017) 16098, https://doi.org/10.1038/natrevmats.2016.98.
[29] J. Di, J. Xia, H. Li, S. Guo, S. Dai, Bismuth oxyhalide layered materials for energy and environmental applications, Nano Energy 41 (2017) 172–192, https://doi.org/10.1016/j.nanoen.2017.09.008.
[30] J. Di, J. Xiong, H. Li, Z. Liu, Ultrathin 2D photocatalysts: electronic-structure tailoring, hybridization, and applications, Adv. Mater. 30 (2018), 1704548, https://doi.org/10.1002/adma.201704548.
[31] C.R. Dean, A.F. Young, I. Meric, C. Lee, L. Wang, S. Sorgenfrei, K. Watanabe, T. Taniguchi, P. Kim, K.L. Shepard, J. Hone, Boron nitride substrates for high-quality graphene electronics, Nat. Nanotechnol. 5 (2010) 722–726, https://doi.org/10.1038/nnano.2010.172.
[32] S.N. Shirodkar, U.V. Waghmare, T.S. Fisher, R. Grau-Crespo, Engineering the electronic bandgaps and band edge positions in carbon-substituted 2D boron nitride: a first-principles investigation, Phys. Chem. Chem. Phys. 17 (2015) 13547–13552, https://doi.org/10.1039/C5CP01680K.
[33] J. Xiong, J. Di, W. Zhu, H. Li, Hexagonal boron nitride adsorbent: synthesis, performance tailoring and applications, J. Energy Chem. 40 (2020) 99–111, https://doi.org/10.1016/j.jechem.2019.03.002.
[34] L. Cao, P. Dai, J. Tang, D. Li, R. Chen, D. Liu, X. Gu, L. Li, Y. Bando, Y.S. Ok, X. Zhao, Y. Yamauchi, Spherical superstructure of boron nitride nanosheets derived from boron-containing metal–organic frameworks, J. Am. Chem. Soc. 142 (2020) 8755–8762, https://doi.org/10.1021/jacs.0c01023.
[35] H.Y. Ng, X. Lu, S.K. Lau, Thermal conductivity, electrical resistivity, mechanical, and rheological properties of thermoplastic composites filled with boron nitride and carbon fiber, Polym. Compos. 26 (2005) 66–73, https://doi.org/10.1002/pc.20076.
[36] L. Shi, D. Wang, W. Song, D. Shao, W.-P. Zhang, A.-H. Lu, Edge-hydroxylated boron nitride for oxidative dehydrogenation of propane to propylene, ChemCatChem 9 (2017) 1788–1793, https://doi.org/10.1002/cctc.201700004.
[37] F. Xiao, S. Naficy, G. Casillas, M.H. Khan, T. Katkus, L. Jiang, H. Liu, H. Li, Z. Huang, Edge-hydroxylated boron nitride nanosheets as an effective additive to improve the thermal response of hydrogels, Adv. Mater. 27 (2015) 7196–7203, https://doi.org/10.1002/adma.201502803.
[38] K. Uosaki, G. Elumalai, H. Noguchi, T. Masuda, A. Lyalin, A. Nakayama, T. Taketsugu, Boron nitride nanosheet on gold as an electrocatalyst for oxygen reduction reaction: theoretical suggestion and experimental proof, J. Am. Chem. Soc. 136 (2014) 6542–6545, https://doi.org/10.1021/ja500393g.
[39] J. Zhou, K. Lv, Q. Wang, X.S. Chen, Q. Sun, P. Jena, Electronic structures and bonding of graphyne sheet and its BN analog, J. Chem. Phys. 134 (2011), 174701, https://doi.org/10.1063/1.3583476.
[40] M. Sun, J. Dong, Y. Lv, S. Zhao, C. Meng, Y. Song, G. Wang, J. Li, Q. Fu, Z. Tian, X. Bao, Pt@h-BN core–shell fuel cell electrocatalysts with electrocatalysis confined under outer shells, Nano Res. 11 (2018) 3490–3498, https://doi.org/10.1007/s12274-018-2029-5.
[41] R. Koitz, J.K. Nørskov, F. Studt, A systematic study of metal-supported boron nitride materials for the oxygen reduction reaction, Phys. Chem. Chem. Phys. 17 (2015) 12722–12727, https://doi.org/10.1039/C5CP01384D.
[42] L. Jiang, Y. Shi, F. Hui, K. Tang, Q. Wu, C. Pan, X. Jing, H. Uppal, F. Palumbo, G. Lu, T. Wu, H. Wang, M.A. Villena, X. Xie, P.C. McIntyre, M. Lanza, Dielectric breakdown in chemical vapor deposited hexagonal boron nitride, ACS Appl. Mater. Interfaces 9 (2017) 39758–39770, https://doi.org/10.1021/acsami.7b10948.
[43] D. Chimene, D.L. Alge, A.K. Gaharwar, Two-dimensional nanomaterials for biomedical applications: emerging trends and future prospects, Adv. Mater. 27 (2015) 7261–7284, https://doi.org/10.1002/adma.201502422.
[44] D.A. Laleyan, S. Zhao, S.Y. Woo, H.N. Tran, H.B. Le, T. Szkopek, H. Guo, G. A. Botton, Z. Mi, AlN/h-BN heterostructures for Mg dopant-free deep ultraviolet photonics, Nano Lett. 17 (2017) 3738–3743, https://doi.org/10.1021/acs.nanolett.7b01068.
[45] G.C. Constantinescu, N.D.M. Hine, Multipurpose black-phosphorus/hBN heterostructures, Nano Lett. 16 (2016) 2586–2594, https://doi.org/10.1021/acs.nanolett.6b00154.
[46] W. Jia, B. Tang, P. Wu, Novel composite proton exchange membrane with connected long-range ionic nanochannels constructed via exfoliated nafion–boron nitride nanocomposite, ACS Appl. Mater. Interfaces 9 (2017) 14791–14800, https://doi.org/10.1021/acsami.7b00858.
[47] N. Yang, X. Zeng, J. Lu, R. Sun, C.-P. Wong, Effect of chemical functionalization on the thermal conductivity of 2D hexagonal boron nitride, Appl. Phys. Lett. 113 (2018), 171904, https://doi.org/10.1063/1.5050293.
[48] C. Yu, J. Zhang, W. Tian, X. Fan, Y. Yao, Polymer composites based on hexagonal boron nitride and their application in thermally conductive composites, RSC Adv. 8 (2018) 21948–21967, https://doi.org/10.1039/C8RA02685H.
[49] N. Izyumskaya, D.O. Demchenko, S. Das, Ü. Özgür, V. Avrutin, H. Morkoç, Recent development of boron nitride towards electronic applications, Adv. Electron. Mater. 3 (2017), 1600485, https://doi.org/10.1002/aelm.201600485.
[50] V. Sharma, H.L. Kagdada, P.K. Jha, P. Śpiewak, K.J. Kurzydłowski, Thermal transport properties of boron nitride based materials: a review, Renew. Sust. Energ. Rev. 120 (2020) 109622, https://doi.org/10.1016/j.rser.2019.109622.
[51] R.H. Wentorf, Cubic form of boron nitride, J. Chem. Phys. 26 (1957) 956–957. https://aip.scitation.org/doi/pdf/10.1063/1.1745964.
[52] F.P. Bundy, R.H. Wentorf, Direct transformation of hexagonal boron nitride to denser forms, J. Chem. Phys. 38 (1963) 1144–1149, https://doi.org/10.1063/1.1733815.
[53] P. Németh, L.A.J. Garvie, T. Aoki, N. Dubrovinskaia, L. Dubrovinsky, P.R. Buseck, Lonsdaleite is faulted and twinned cubic diamond and does not exist as a discrete material, Nat. Commun. 5 (2014) 5447, https://doi.org/10.1038/ncomms6447.
[54] H. Wang, Y. Zhao, Y. Xie, X. Ma, X. Zhang, Recent progress in synthesis of two-dimensional hexagonal boron nitride, J. Semicond. 38 (2017), 031003, https://doi.org/10.1088/1674-4926/38/3/031003.
[55] C.B. Samantaray, R.N. Singh, Review of synthesis and properties of cubic boron nitride (c-BN) thin films, Int. Mater. Rev. 50 (2005) 313–344, https://doi.org/10.1179/174328005X67160.
[56] R. Geick, C.H. Perry, G. Rupprecht, Normal modes in hexagonal boron nitride, Phys. Rev. 146 (1966) 543–547, https://doi.org/10.1103/PhysRev.146.543.
[57] G.-H. Lee, Y.-J. Yu, X. Cui, N. Petrone, C.-H. Lee, M.S. Choi, D.-Y. Lee, C. Lee, W. J. Yoo, K. Watanabe, T. Taniguchi, C. Nuckolls, P. Kim, J. Hone, Flexible and transparent MoS_2 field-effect transistors on hexagonal boron nitride-graphene heterostructures, ACS Nano 7 (2013) 7931–7936, https://doi.org/10.1021/nn402954e.
[58] M.P. Levendorf, C.-J. Kim, L. Brown, P.Y. Huang, R.W. Havener, D.A. Muller, J. Park, Graphene and boron nitride lateral heterostructures for atomically thin circuitry, Nature 488 (2012) 627–632, https://doi.org/10.1038/nature11408.
[59] D. Fan, X. Lv, J. Feng, S. Zhang, J. Bai, R. Lu, J. Liu, Cobalt nickel nanoparticles encapsulated within hexagonal boron nitride as stable, catalytic dehydrogenation nanoreactor, Int. J. Hydrog. Energy 42 (2017) 11312–11320, https://doi.org/10.1016/j.ijhydene.2017.03.139.
[60] H. Jin, C. Guo, X. Liu, J. Liu, A. Vasileff, Y. Jiao, Y. Zheng, S.-Z. Qiao, Emerging two-dimensional nanomaterials for electrocatalysis, Chem. Rev. 118 (2018) 6337–6408, https://doi.org/10.1021/acs.chemrev.7b00689.
[61] Z. Zheng, M. Cox, B. Li, Surface modification of hexagonal boron nitride nanomaterials: a review, J. Mater. Sci. 53 (2018) 66–99, https://doi.org/10.1007/s10853-017-1472-0.
[62] M.S. Qayyum, H. Hayat, R.K. Matharu, T.A. Tabish, M. Edirisinghe, Boron nitride nanoscrolls: structure, synthesis, and applications, Appl. Phys. Rev. 6 (2019), 021310, https://doi.org/10.1063/1.5092547.
[63] X.-F. Jiang, Q. Weng, X.-B. Wang, X. Li, J. Zhang, D. Golberg, Y. Bando, Recent progress on fabrications and applications of boron nitride nanomaterials: a review, J. Mater. Sci. Technol. 31 (2015) 589–598, https://doi.org/10.1016/j.jmst.2014.12.008.
[64] D. Golberg, Y. Bando, Y. Huang, T. Terao, M. Mitome, C. Tang, C. Zhi, Boron nitride nanotubes and nanosheets, ACS Nano 4 (2010) 2979–2993, https://doi.org/10.1021/nn1006495.

[65] F. Lu, F. Wang, L. Cao, C.Y. Kong, X. Huang, Hexagonal boron nitride nanomaterials: advances towards bioapplications, Nanosci. Nanotechnol. Lett. 4 (2012) 949–961, https://doi.org/10.1166/nnl.2012.1444.
[66] R.M. Ribeiro, N.M.R. Peres, Stability of boron nitride bilayers: ground-state energies, interlayer distances, and tight-binding description, Phys. Rev. B 83 (2011) 235312, https://doi.org/10.1103/PhysRevB.83.235312.
[67] N. Marom, J. Bernstein, J. Garel, A. Tkatchenko, E. Joselevich, L. Kronik, O. Hod, Stacking and registry effects in layered materials: the case of hexagonal boron nitride, Phys. Rev. Lett. 105 (2010) 046801, https://doi.org/10.1103/PhysRevLett.105.046801.
[68] S. Chatterjee, Z. Luo, M. Acerce, D.M. Yates, A.T.C. Johnson, L.G. Sneddon, Chemical vapor deposition of boron nitride nanosheets on metallic substrates via decaborane/ammonia reactions, Chem. Mater. 23 (2011) 4414–4416, https://doi.org/10.1021/cm201955v.
[69] L.H. Li, Y. Chen, G. Behan, H. Zhang, M. Petravic, A.M. Glushenkov, Large-scale mechanical peeling of boron nitride nanosheets by low-energy ball milling, J. Mater. Chem. 21 (2011) 11862–11866, https://doi.org/10.1039/C1JM11192B.
[70] G. Lu, T. Wu, Q. Yuan, H. Wang, H. Wang, F. Ding, X. Xie, M. Jiang, Synthesis of large single-crystal hexagonal boron nitride grains on Cu–Ni alloy, Nat. Commun. 6 (2015) 6160, https://doi.org/10.1038/ncomms7160.
[71] L. Qin, J. Yu, M. Li, F. Liu, X. Bai, Catalyst-free growth of mono- and few-atomic-layer boron nitride sheets by chemical vapor deposition, Nanotechnology 22 (2011), 215602, https://doi.org/10.1088/0957-4484/22/21/215602.
[72] S. Majety, X.K. Cao, R. Dahal, B.N. Pantha, J. Li, J.Y. Lin, H.X. Jiang, Semiconducting hexagonal boron nitride for deep ultraviolet photonics, in: Proc. SPIE, 2012.
[73] W. Zhu, X. Gao, Q. Li, H. Li, Y. Chao, M. Li, S.M. Mahurin, H. Li, H. Zhu, S. Dai, Controlled gas exfoliation of boron nitride into few-layered nanosheets, Angew. Chem. Int. Ed. 55 (2016) 10766–10770, https://doi.org/10.1002/anie.201605515.
[74] A.M. Love, B. Thomas, S.E. Specht, M.P. Hanrahan, J.M. Venegas, S.P. Burt, J. T. Grant, M.C. Cendejas, W.P. McDermott, A.J. Rossini, I. Hermans, Probing the transformation of boron nitride catalysts under oxidative dehydrogenation conditions, J. Am. Chem. Soc. 141 (2019) 182–190, https://doi.org/10.1021/jacs.8b08165.
[75] J.T. Grant, C.A. Carrero, F. Goeltl, J. Venegas, P. Mueller, S.P. Burt, S.E. Specht, W.P. McDermott, A. Chieregato, I. Hermans, Selective oxidative dehydrogenation of propane to propene using boron nitride catalysts, Science 354 (2016) 1570–1573, https://doi.org/10.1126/science.aaf7885.
[76] H. Chen, Z. Yang, Z. Zhang, Z. Chen, M. Chi, S. Wang, J. Fu, S. Dai, Construction of a nanoporous highly crystalline hexagonal boron nitride from an amorphous precursor for catalytic dehydrogenation, Angew. Chem. Int. Ed. 58 (2019) 10626–10630, https://doi.org/10.1002/anie.201904996.
[77] D. Pacilé, J.C. Meyer, Ç.Ö. Girit, A. Zettl, The two-dimensional phase of boron nitride: few-atomic-layer sheets and suspended membranes, Appl. Phys. Lett. 92 (2008), 133107, https://doi.org/10.1063/1.2903702.
[78] W. Sun, Y. Meng, Q. Fu, F. Wang, G. Wang, W. Gao, X. Huang, F. Lu, High-yield production of boron nitride nanosheets and its uses as a catalyst support for hydrogenation of nitroaromatics, ACS Appl. Mater. Interfaces 8 (2016) 9881–9888, https://doi.org/10.1021/acsami.6b01008.
[79] Y. Huang, E. Sutter, N.N. Shi, J. Zheng, T. Yang, D. Englund, H.-J. Gao, P. Sutter, Reliable exfoliation of large-area high-quality flakes of graphene and other two-dimensional materials, ACS Nano 9 (2015) 10612–10620, https://doi.org/10.1021/acsnano.5b04258.
[80] K.S. Novoselov, D. Jiang, F. Schedin, T.J. Booth, V.V. Khotkevich, S.V. Morozov, A.K. Geim, Two-dimensional atomic crystals, Proc. Natl. Acad. Sci. USA 102 (2005) 10451–10453,, https://doi.org/10.1073/pnas.0502848102.
[81] F. Lu, F. Wang, W. Gao, X. Huang, X. Zhang, Y. Li, Aqueous soluble boron nitride nanosheets via anionic compound-assisted exfoliation, Mater. Express 3 (2013) 144–150, https://doi.org/10.1166/mex.2013.1110.
[82] W. Lei, V.N. Mochalin, D. Liu, S. Qin, Y. Gogotsi, Y. Chen, Boron nitride colloidal solutions, ultralight aerogels and freestanding membranes through one-step exfoliation and functionalization, Nat. Commun. 6 (2015) 8849, https://doi.org/10.1038/ncomms9849.
[83] T. Guo, P. Nikolaev, A.G. Rinzler, D. Tomanek, D.T. Colbert, R.E. Smalley, Self-assembly of tubular fullerenes, J. Phys. Chem. 99 (1995) 10694–10697, https://doi.org/10.1021/j100027a002.
[84] M. Xu, T. Liang, M. Shi, H. Chen, Graphene-like two-dimensional materials, Chem. Rev. 113 (2013) 3766–3798, https://doi.org/10.1021/cr300263a.
[85] A. Pakdel, C. Zhi, Y. Bando, D. Golberg, Low-dimensional boron nitride nanomaterials, Mater. Today 15 (2012) 256–265, https://doi.org/10.1016/S1369-7021(12)70116-5.
[86] Z. Lin, A. McNamara, Y. Liu, K.-S. Moon, C.-P. Wong, Exfoliated hexagonal boron nitride-based polymer nanocomposite with enhanced thermal conductivity for electronic encapsulation, Compos. Sci. Technol. 90 (2014) 123–128, https://doi.org/10.1016/j.compscitech.2013.10.018.
[87] Y. Yao, Z. Lin, Z. Li, X. Song, K.-S. Moon, C.-p Wong, Large-scale production of two-dimensional nanosheets, J. Mater. Chem. 22 (2012) 13494–13499, https://doi.org/10.1039/C2JM30587A.
[88] L. Liu, Z. Xiong, D. Hu, G. Wu, B. Liu, P. Chen, Solid exfoliation of hexagonal boron nitride crystals for the synthesis of few-layer boron nitride nanosheets, Chem. Lett. 42 (2013) 1415–1416, https://doi.org/10.1246/cl.130562.
[89] C. Zhi, Y. Bando, C. Tang, H. Kuwahara, D. Golberg, Large-scale fabrication of boron nitride nanosheets and their utilization in polymeric composites with improved thermal and mechanical properties, Adv. Mater. 21 (2009) 2889–2893, https://doi.org/10.1002/adma.200900323.
[90] K.-G. Zhou, N.-N. Mao, H.-X. Wang, Y. Peng, H.-L. Zhang, A mixed-solvent strategy for efficient exfoliation of inorganic graphene analogues, Angew. Chem. Int. Ed. 50 (2011) 10839–10842, https://doi.org/10.1002/anie.201105364.
[91] A. Anderson, Z.-L. Hou, W.-L. Song, M.J. Meziani, P. Wang, F. Lu, J. Lee, L. Xu, Y.-P. Sun, Towards nanostructured boron nitride films, J. Mater. Sci.: Mater. Electron. 28 (2017) 9048–9055, https://doi.org/10.1007/s10854-017-6637-8.
[92] Y. Lin, T.V. Williams, T.-B. Xu, W. Cao, H.E. Elsayed-Ali, J.W. Connell, Aqueous dispersions of few-layered and monolayered hexagonal boron nitride nanosheets from sonication-assisted hydrolysis: critical role of water, J. Phys. Chem. C 115 (2011) 2679–2685, https://doi.org/10.1021/jp110985w.
[93] Y. Wang, Z. Shi, J. Yin, Boron nitride nanosheets: large-scale exfoliation in methanesulfonic acid and their composites with polybenzimidazole, J. Mater. Chem. 21 (2011) 11371–11377, https://doi.org/10.1039/C1JM10342C.
[94] R.J. Smith, P.J. King, M. Lotya, C. Wirtz, U. Khan, S. De, A. O'Neill, G. S. Duesberg, J.C. Grunlan, G. Moriarty, J. Chen, J. Wang, A.I. Minett, V. Nicolosi, J.N. Coleman, Large-Scale exfoliation of inorganic layered compounds in aqueous surfactant solutions, Adv. Mater. 23 (2011) 3944–3948, https://doi.org/10.1002/adma.201102584.
[95] W.-Q. Han, L. Wu, Y. Zhu, K. Watanabe, T. Taniguchi, Structure of chemically derived mono- and few-atomic-layer boron nitride sheets, Appl. Phys. Lett. 93 (2008), 223103, https://doi.org/10.1063/1.3041639.
[96] J.N. Coleman, M. Lotya, A. O'Neill, S.D. Bergin, P.J. King, U. Khan, K. Young, A. Gaucher, S. De, R.J. Smith, I.V. Shvets, S.K. Arora, G. Stanton, H.-Y. Kim, K. Lee, G.T. Kim, G.S. Duesberg, T. Hallam, J.J. Boland, J.J. Wang, J.F. Donegan, J.C. Grunlan, G. Moriarty, A. Shmeliov, R.J. Nicholls, J.M. Perkins, E. M. Grieveson, K. Theuwissen, D.W. McComb, P.D. Nellist, V. Nicolosi, Two-dimensional nanosheets produced by liquid exfoliation of layered, Mater., Sci. 331 (2011) 568–571, https://doi.org/10.1126/science.1194975.
[97] L. Cao, S. Emami, K. Lafdi, Large-scale exfoliation of hexagonal boron nitride nanosheets in liquid phase, Mater. Express 4 (2014) 165–171, https://doi.org/10.1166/mex.2014.1155.
[98] A. Sokołowska, J. Rudnicki, M. Kostecki, S. Wojtkiewicz, P. Sawosz, R. Chodun, K. Zdunek, A. Olszyna, Electric field used as the substitute for ultrasounds in the liquid exfoliation of hexagonal boron nitride, Microelectron. Eng. 126 (2014) 124–128, https://doi.org/10.1016/j.mee.2014.06.025.
[99] X. Li, X. Hao, M. Zhao, Y. Wu, J. Yang, Y. Tian, G. Qian, Exfoliation of hexagonal boron nitride by molten hydroxides, Adv. Mater. 25 (2013) 2200–2204, https://doi.org/10.1002/adma.201204031.
[100] G. Zhao, Y. Wu, Y. Shao, X. Hao, Large-quantity and continuous preparation of two-dimensional nanosheets, Nanoscale 8 (2016) 5407–5411, https://doi.org/10.1039/C5NR07950K.
[101] C. Jin, F. Lin, K. Suenaga, S. Iijima, Fabrication of a freestanding boron nitride single layer and its defect assignments, Phys. Rev. Lett. 102 (2009) 195505, https://doi.org/10.1103/PhysRevLett.102.195505.
[102] J.C. Meyer, A. Chuvilin, G. Algara-Siller, J. Biskupek, U. Kaiser, Selective sputtering and atomic resolution imaging of atomically thin boron nitride membranes, Nano Lett. 9 (2009) 2683–2689, https://doi.org/10.1021/nl9011497.
[103] J. Yin, J. Li, Y. Hang, J. Yu, G. Tai, X. Li, Z. Zhang, W. Guo, Boron nitride nanostructures: fabrication, functionalization and applications, Small 12 (2016) 2942–2968, https://doi.org/10.1002/smll.201600053.
[104] P. Ma, J.T. Spencer, Non-covalent stabilization and functionalization of boron nitride nanosheets (BNNSs) by organic polymers: formation of complex BNNSs-containing structures, J. Mater. Sci. 50 (2015) 313–323, https://doi.org/10.1007/s10853-014-8590-8.
[105] Y. Xue, Q. Liu, G. He, K. Xu, L. Jiang, X. Hu, J. Hu, Excellent electrical conductivity of the exfoliated and fluorinated hexagonal boron nitride nanosheets, Nanoscale Res. Lett. 8 (2013) 49, https://doi.org/10.1186/1556-276X-8-49.
[106] M.H. Khan, H.K. Liu, X. Sun, Y. Yamauchi, Y. Bando, D. Golberg, Z. Huang, Few-atomic-layered hexagonal boron nitride: CVD growth, characterization, and applications, Mater. Today 20 (2017) 611–628, https://doi.org/10.1016/j.mattod.2017.04.027.
[107] S.M. Kim, A. Hsu, M.H. Park, S.H. Chae, S.J. Yun, J.S. Lee, D.-H. Cho, W. Fang, C. Lee, T. Palacios, M. Dresselhaus, K.K. Kim, Y.H. Lee, J. Kong, Synthesis of large-area multilayer hexagonal boron nitride for high material performance, Nat. Commun. 6 (2015) 8662, https://doi.org/10.1038/ncomms9662.
[108] Z. Liu, Y. Gong, W. Zhou, L. Ma, J. Yu, J.C. Idrobo, J. Jung, A.H. MacDonald, R. Vajtai, J. Lou, P.M. Ajayan, Ultrathin high-temperature oxidation-resistant coatings of hexagonal boron nitride, Nat. Commun. 4 (2013) 2541, https://doi.org/10.1038/ncomms3541.
[109] M.T. Paffett, R.J. Simonson, P. Papin, R.T. Paine, Borazine adsorption and decomposition at Pt(111) and Ru(001) surfaces, Surf. Sci. 232 (1990) 286–296, https://doi.org/10.1016/0039-6028(90)90121-N.
[110] B.N. Feigelson, V.M. Bermudez, J.K. Hite, Z.R. Robinson, V.D. Wheeler, K. Sridhara, S.C. Hernández, Growth and spectroscopic characterization of monolayer and few-layer hexagonal boron nitride on metal substrates, Nanoscale 7 (2015) 3694–3702, https://doi.org/10.1039/C4NR05557H.
[111] A. Ismach, H. Chou, D.A. Ferrer, Y. Wu, S. McDonnell, H.C. Floresca, A. Covacevich, C. Pope, R. Piner, M.J. Kim, R.M. Wallace, L. Colombo, R.S. Ruoff, Toward the controlled synthesis of hexagonal boron nitride films, ACS Nano 6 (2012) 6378–6385, https://doi.org/10.1021/nn301940k.
[112] R.Y. Tay, H. Li, S.H. Tsang, M. Zhu, M. Loeblein, L. Jing, F.N. Leong, E.H.T. Teo, Trimethylamine borane: a new single-source precursor for monolayer h-BN single

crystals and h-BCN thin films, Chem. Mater. 28 (2016) 2180–2190, https://doi.org/10.1021/acs.chemmater.6b00114.
[113] F. Müller, S. Grandthyll, Monolayer formation of hexagonal boron nitride on Ag (001), Surf. Sci. 617 (2013) 207–210, https://doi.org/10.1016/j.susc.2013.07.024.
[114] Z. Zhang, X. Ji, J. Shi, X. Zhou, S. Zhang, Y. Hou, Y. Qi, Q. Fang, Q. Ji, Y. Zhang, M. Hong, P. Yang, X. Liu, Q. Zhang, L. Liao, C. Jin, Z. Liu, Y. Zhang, Direct chemical vapor deposition growth and band-gap characterization of MoS_2/h-BN van der Waals heterostructures on Au foils, ACS Nano 11 (2017) 4328–4336, https://doi.org/10.1021/acsnano.7b01537.
[115] P. Sutter, J. Lahiri, P. Albrecht, E. Sutter, Chemical vapor deposition and etching of high-quality monolayer hexagonal boron nitride films, ACS Nano 5 (2011) 7303–7309, https://doi.org/10.1021/nn202141k.
[116] K.K. Kim, A. Hsu, X. Jia, S.M. Kim, Y. Shi, M. Hofmann, D. Nezich, J.F. Rodriguez-Nieva, M. Dresselhaus, T. Palacios, J. Kong, Synthesis of monolayer hexagonal boron nitride on Cu foil using chemical vapor deposition, Nano Lett. 12 (2012) 161–166, https://doi.org/10.1021/nl203249a.
[117] Y. Stehle, H.M. Meyer, R.R. Unocic, M. Kidder, G. Polizos, P.G. Datskos, R. Jackson, S.N. Smirnov, I.V. Vlassiouk, Synthesis of hexagonal boron nitride monolayer: control of nucleation and crystal morphology, Chem. Mater. 27 (2015) 8041–8047, https://doi.org/10.1021/acs.chemmater.5b03607.
[118] Y. Ji, B. Calderon, Y. Han, P. Cueva, N.R. Jungwirth, H.A. Alsalman, J. Hwang, G. D. Fuchs, D.A. Muller, M.G. Spencer, Chemical vapor deposition growth of large single-crystal mono-, bi-, tri-layer hexagonal boron nitride and their interlayer stacking, ACS Nano 11 (2017) 12057–12066, https://doi.org/10.1021/acsnano.7b04841.
[119] J. Yu, L. Qin, Y. Hao, S. Kuang, X. Bai, Y.-M. Chong, W. Zhang, E. Wang, Vertically aligned boron nitride nanosheets: chemical vapor synthesis, ultraviolet light emission, and superhydrophobicity, ACS Nano 4 (2010) 414–422, https://doi.org/10.1021/nn901204c.
[120] A. Pakdel, X. Wang, C. Zhi, Y. Bando, K. Watanabe, T. Sekiguchi, T. Nakayama, D. Golberg, Facile synthesis of vertically aligned hexagonal boron nitride nanosheets hybridized with graphitic domains, J. Mater. Chem. 22 (2012) 4818–4824, https://doi.org/10.1039/C2JM15109J.
[121] K.B. Shelimov, M. Moskovits, Composite nanostructures based on template-grown boron nitride nanotubules, Chem. Mater. 12 (2000) 250–254, https://doi.org/10.1021/cm9905996.
[122] X. Wang, C. Zhi, L. Li, H. Zeng, C. Li, M. Mitome, D. Golberg, Y. Bando, "Chemical Blowing" of thin-walled bubbles: high-throughput fabrication of large-area, few-layered BN and Cx-BN nanosheets, Adv. Mater. 23 (2011) 4072–4076, https://doi.org/10.1002/adma.201101788.
[123] H. Fei, R. Ye, G. Ye, Y. Gong, Z. Peng, X. Fan, E.L.G. Samuel, P.M. Ajayan, J. M. Tour, Boron- and nitrogen-doped graphene quantum dots/graphene hybrid nanoplatelets as efficient electrocatalysts for oxygen reduction, ACS Nano 8 (2014) 10837–10843, https://doi.org/10.1021/nn504637y.
[124] A. Nag, K. Raidongia, K.P.S.S. Hembram, R. Datta, U.V. Waghmare, C.N.R. Rao, Graphene analogues of BN: novel synthesis and properties, ACS Nano 4 (2010) 1539–1544, https://doi.org/10.1021/nn9018762.
[125] R. Gao, L. Yin, C. Wang, Y. Qi, N. Lun, L. Zhang, Y.-X. Liu, L. Kang, X. Wang, High-yield synthesis of boron nitride nanosheets with strong ultraviolet cathodoluminescence emission, J. Phys. Chem. C 113 (2009) 15160–15165, https://doi.org/10.1021/jp904246j.
[126] S. Marchesini, X. Wang, C. Petit, Porous boron nitride materials: influence of structure, chemistry and stability on the adsorption of organics, Front. Chem. 7 (2019) 160, https://doi.org/10.3389/fchem.2019.00160.
[127] P. Wu, W. Zhu, Y. Chao, J. Zhang, P. Zhang, H. Zhu, C. Li, Z. Chen, H. Li, S. Dai, A template-free solvent-mediated synthesis of high surface area boron nitride nanosheets for aerobic oxidative desulfurization, Chem. Commun. 52 (2016) 144–147, https://doi.org/10.1039/C5CC07830J.
[128] W. Lei, D. Portehault, D. Liu, S. Qin, Y. Chen, Porous boron nitride nanosheets for effective water cleaning, Nat. Commun. 4 (2013) 1777, https://doi.org/10.1038/ncomms2818.
[129] Q. Weng, X. Wang, Y. Bando, D. Golberg, One-step template-free synthesis of highly porous boron nitride microsponges for hydrogen storage, Adv. Energy Mater. 4 (2014), 1301525, https://doi.org/10.1002/aenm.201301525.
[130] X.-B. Wang, Q. Weng, X. Wang, X. Li, J. Zhang, F. Liu, X.-F. Jiang, H. Guo, N. Xu, D. Golberg, Y. Bando, Biomass-directed synthesis of 20 g high-quality boron nitride nanosheets for thermoconductive polymeric composites, ACS Nano 8 (2014) 9081–9088, https://doi.org/10.1021/nn502486x.
[131] D. Velázquez, R. Seibert, H. Man, L. Spentzouris, J. Terry, Pulsed laser deposition of single layer, hexagonal boron nitride (white graphene, h-BN) on fiber-oriented Ag(111)/$SrTiO_3$(001), J. Appl. Phys. 119 (2016), 095306, https://doi.org/10.1063/1.4943174.
[132] R. Arenal, O. Stephan, J.-L. Cochon, A. Loiseau, Root-growth mechanism for single-walled boron nitride nanotubes in laser vaporization technique, J. Am. Chem. Soc. 129 (2007) 16183–16189, https://doi.org/10.1021/ja076135n.
[133] N.R. Glavin, M.L. Jespersen, M.H. Check, J. Hu, A.M. Hilton, T.S. Fisher, A. A. Voevodin, Synthesis of few-layer, large area hexagonal-boron nitride by pulsed laser deposition, Thin Solid Films 572 (2014) 245–250, https://doi.org/10.1016/j.tsf.2014.07.059.
[134] S. Saha, P. Samanta, N.C. Murmu, N.H. Kim, T. Kuila, J.H. Lee, Electrochemical functionalization and in-situ deposition of the SAA@rGO/h-BN@Ni electrode for supercapacitor applications, J. Ind. Eng. Chem. 52 (2017) 321–330, https://doi.org/10.1016/j.jiec.2017.04.005Get rights and content.
[135] Y. Göncü, M. Geçgin, F. Bakan, N. Ay, Electrophoretic deposition of hydroxyapatite-hexagonal boron nitride composite coatings on Ti substrate, Mater. Sci. Eng. C 79 (2017) 343–353, https://doi.org/10.1016/j.msec.2017.05.023.
[136] H. Han, J. Lyu, L. Zhu, G. Wang, C. Ma, H. Ma, Fabrication of BN modified Ti/PbO_2 electrodes with tunable hydrophobic characteristics and their electrocatalytic performance, J. Alloy Compd. 828 (2020) 154049, https://doi.org/10.1016/j.jallcom.2020.154049.
[137] Y. Qiu, J. Yu, J. Yin, C. Tan, X. Zhou, X. Bai, E. Wang, Synthesis of continuous boron nitride nanofibers by solution coating electrospun template fibers, Nanotechnology 20 (2009), 345603, https://doi.org/10.1088/0957-4484/20/34/345603.
[138] N.G. Chopra, R.J. Luyken, K. Cherrey, V.H. Crespi, M.L. Cohen, S.G. Louie, A. Zettl, Boron nitride nanotubes, Science 269 (1995) 966–967, https://doi.org/10.1126/science.269.5226.966.
[139] J. Cumings, A. Zettl, Mass-production of boron nitride double-wall nanotubes and nanococoons, Chem. Phys. Lett. 316 (2000) 211–216, https://doi.org/10.1016/S0009-2614(99)01277-4.
[140] A. Lyalin, M. Gao, T. Taketsugu, When inert becomes active: a fascinating route for catalyst design, Chem. Rec. 16 (2016) 2324–2337, https://doi.org/10.1002/tcr.201600035.
[141] A. Du, Y. Chen, Z. Zhu, R. Amal, G.Q. Lu, S.C. Smith, Dots versus antidots: computational exploration of structure, magnetism, and half-metallicity in boron−nitride nanostructures, J. Am. Chem. Soc. 131 (2009) 17354–17359, https://doi.org/10.1021/ja9071942.
[142] X. Liu, T. Duan, Y. Sui, C. Meng, Y. Han, Copper atoms embedded in hexagonal boron nitride as potential catalysts for CO oxidation: a first-principles investigation, RSC Adv. 4 (2014) 38750–38760, https://doi.org/10.1039/C4RA06436D.
[143] D. Xu, Y.-j Liu, J.-x Zhao, Q.-h Cai, X.-z Wang, Theoretical study of the deposition of pt clusters on defective hexagonal boron nitride (h-BN) sheets: morphologies, electronic structures, and interactions with O, J. Phys. Chem. C 118 (2014) 8868–8876, https://doi.org/10.1021/jp4087943.
[144] Q. Fu, Y. Meng, Z. Fang, Q. Hu, L. Xu, W. Gao, X. Huang, Q. Xue, Y.-P. Sun, F. Lu, Boron nitride nanosheet-anchored Pd–Fe core–shell nanoparticles as highly efficient catalysts for Suzuki–Miyaura coupling reactions, ACS Appl. Mater. Interfaces 9 (2017) 2469–2476, https://doi.org/10.1021/acsami.6b13570.
[145] S. Lin, X. Ye, R.S. Johnson, H. Guo, First-principles investigations of metal (Cu, Ag, Au, Pt, Rh, Pd, Fe, Co, and Ir) doped hexagonal boron nitride nanosheets: stability and catalysis of CO oxidation, J. Phys. Chem. C 117 (2013) 17319–17326, https://doi.org/10.1021/jp4055445.
[146] C. Huang, X. Ye, C. Chen, S. Lin, D. Xie, A computational investigation of CO oxidation on ruthenium-embedded hexagonal boron nitride nanosheet, Comput. Theor. Chem. 1011 (2013) 5–10, https://doi.org/10.1016/j.comptc.2013.02.004.
[147] W. Zhu, Z. Wu, G.S. Foo, X. Gao, M. Zhou, B. Liu, G.M. Veith, P. Wu, K. L. Browning, H.N. Lee, H. Li, S. Dai, H. Zhu, Taming interfacial electronic properties of platinum nanoparticles on vacancy-abundant boron nitride nanosheets for enhanced catalysis, Nat. Commun. 8 (2017) 15291, https://doi.org/10.1038/ncomms15291.
[148] C. Huang, C. Chen, M. Zhang, L. Lin, X. Ye, S. Lin, M. Antonietti, X. Wang, Carbon-doped BN nanosheets for metal-free photoredox catalysis, Nat. Commun. 6 (2015) 7698, https://doi.org/10.1038/ncomms8698.
[149] Q. Weng, D.G. Kvashnin, X. Wang, O. Cretu, Y. Yang, M. Zhou, C. Zhang, D.-M. Tang, P.B. Sorokin, Y. Bando, D. Golberg, Tuning of the optical, electronic, and magnetic properties of boron nitride nanosheets with oxygen doping and functionalization, Adv. Mater. 29 (2017), 1700695, https://doi.org/10.1002/adma.201700695.
[150] S. Chen, P. Li, S. Xu, X. Pan, Q. Fu, X. Bao, Carbon doping of hexagonal boron nitride porous materials toward CO_2 capture, J. Mater. Chem. A 6 (2018) 1832–1839, https://doi.org/10.1039/C7TA08515J.
[151] Q. Weng, X. Wang, X. Wang, D. Liu, X. Jiang, C. Zhi, Y. Bando, D. Golberg, Preparation and hydrogen sorption performances of BCNO porous microbelts with ultra-narrow and tunable pore widths, Chem. Asian J. 8 (2013) 2936–2939, https://doi.org/10.1002/asia.201300940.
[152] S. Saha, M. Jana, P. Khanra, P. Samanta, H. Koo, N.C. Murmu, T. Kuila, Band gap engineering of boron nitride by graphene and its application as positive electrode material in asymmetric supercapacitor device, ACS Appl. Mater. Interfaces 7 (2015) 14211–14222, https://doi.org/10.1021/acsami.5b03562.
[153] H. Li, X. Duan, X. Wu, X. Zhuang, H. Zhou, Q. Zhang, X. Zhu, W. Hu, P. Ren, P. Guo, L. Ma, X. Fan, X. Wang, J. Xu, A. Pan, X. Duan, Growth of alloy $MoS_{2x}Se_{2(1-x)}$ nanosheets with fully tunable chemical compositions and optical properties, J. Am. Chem. Soc. 136 (2014) 3756–3759, https://doi.org/10.1021/ja500069b.
[154] S. Saha, M. Jana, P. Khanra, P. Samanta, H. Koo, N. Chandra Murmu, T. Kuila, Band gap modified boron doped NiO/Fe_3O_4 nanostructure as the positive electrode for high energy asymmetric supercapacitors, RSC Adv. 6 (2016) 1380–1387, https://doi.org/10.1039/C5RA20928E.
[155] D.-Q. Liu, B. Tao, H.-C. Ruan, C.L. Bentley, P.R. Unwin, Metal support effects in electrocatalysis at hexagonal boron nitride, Chem. Commun. 55 (2019) 628–631, https://doi.org/10.1039/C8CC08517J.
[156] M. Gao, A. Lyalin, T. Taketsugu, Oxygen activation and dissociation on h-BN supported Au atoms, Int. J. Quantum Chem. 113 (2013) 443–452, https://doi.org/10.1002/qua.24066.
[157] W. Pan, J. Xiao, J. Zhu, C. Yu, G. Zhang, Z. Ni, K. Watanabe, T. Taniguchi, Y. Shi, X. Wang, Biaxial compressive strain engineering in graphene/boron nitride heterostructures, Sci. Rep. 2 (2012) 893, https://doi.org/10.1038/srep00893.
[158] L. Britnell, R.V. Gorbachev, R. Jalil, B.D. Belle, F. Schedin, M.I. Katsnelson, L. Eaves, S.V. Morozov, A.S. Mayorov, N.M.R. Peres, A.H. Castro Neto, J. Leist, A. K. Geim, L.A. Ponomarenko, K.S. Novoselov, Electron tunneling through ultrathin

boron nitride crystalline barriers, Nano Lett. 12 (2012) 1707–1710, https://doi.org/10.1021/nl3002205.
[159] K. Watanabe, T. Taniguchi, T. Niiyama, K. Miya, M. Taniguchi, Far-ultraviolet plane-emission handheld device based on hexagonal boron nitride, Nat. Photonics 3 (2009) 591–594, https://doi.org/10.1038/nphoton.2009.167.
[160] X. Wang, A. Pakdel, C. Zhi, K. Watanabe, T. Sekiguchi, D. Golberg, Y. Bando, High-yield boron nitride nanosheets from 'chemical blowing': towards practical applications in polymer composites, J. Phys.: Condens. Matter 24 (2012), 314205, https://doi.org/10.1088/0953-8984/24/31/314205.
[161] C. Lee, Q. Li, W. Kalb, X.-Z. Liu, H. Berger, R.W. Carpick, J. Hone, Frictional characteristics of atomically thin sheets, Science 328 (2010) 76–80, https://doi.org/10.1126/science.1184167.
[162] G. Elumalai, H. Noguchi, H.C. Dinh, K. Uosaki, An efficient electrocatalyst for oxygen reduction to water - boron nitride nanosheets decorated with small gold nanoparticles (~5nm) of narrow size distribution on gold substrate, J. Electroanal. Chem. 819 (2018) 107–113, https://doi.org/10.1016/j.jelechem.2017.09.033.
[163] M.D. Esrafili, P. Nematollahi, Potential of Si-doped boron nitride nanotubes as a highly active and metal-free electrocatalyst for oxygen reduction reaction: a DFT study, Synth. Met. 226 (2017) 129–138, https://doi.org/10.1016/j.synthmet.2017.02.011.
[164] O.T. Holton, J.W. Stevenson, The role of platinum in proton exchange membrane fuel cells, platin, Met. Rev. 57 (2013) 259–271, https://doi.org/10.1595/147106713X671222.
[165] A.F. Khan, M.P. Down, G.C. Smith, C.W. Foster, C.E. Banks, Surfactant-exfoliated 2D hexagonal boron nitride (2D-hBN): role of surfactant upon the electrochemical reduction of oxygen and capacitance applications, J. Mater. Chem. A 5 (2017) 4103–4113, https://doi.org/10.1039/C6TA09999H.
[166] M. Winter, R.J. Brodd, What are batteries, fuel cells, and supercapacitors? Chem. Rev. 104 (2004) 4245–4270, https://doi.org/10.1021/cr020730k.
[167] H. Wang, J. Li, K. Li, Y. Lin, J. Chen, L. Gao, V. Nicolosi, X. Xiao, J.-M. Lee, Transition metal nitrides for electrochemical energy applications, Chem. Soc. Rev. 50 (2021) 1354–1390, https://doi.org/10.1039/D0CS00415D.
[168] S. Guo, S. Zhang, S. Sun, Tuning nanoparticle catalysis for the oxygen reduction reaction, Angew. Chem. Int. Ed. 52 (2013) 8526–8544, https://doi.org/10.1002/anie.201207186.
[169] D. Roy, K. Panigrahi, B.K. Das, U.K. Ghorui, S. Bhattacharjee, M. Samanta, S. Sarkar, K.K. Chattopadhyay, Boron vacancy: a strategy to boost the oxygen reduction reaction of hexagonal boron nitride nanosheet in hBN–MoS_2 heterostructure, Nanoscale Adv. 3 (2021) 4739–4749, https://doi.org/10.1039/D1NA00304F.
[170] G. Elumalai, H. Noguchi, K. Uosaki, Electrocatalytic activity of various types of h-BN for the oxygen reduction reaction, Phys. Chem. Chem. Phys. 16 (2014) 13755–13761, https://doi.org/10.1039/C4CP00402G.
[171] G. Elumalai, H. Noguchi, A. Lyalin, T. Taketsugu, K. Uosaki, Gold nanoparticle decoration of insulating boron nitride nanosheet on inert gold electrode toward an efficient electrocatalyst for the reduction of oxygen to water, Electrochem. Commun. 66 (2016) 53–57, https://doi.org/10.1016/j.elecom.2016.02.021.
[172] A.F. Khan, E.P. Randviir, D.A.C. Brownson, X. Ji, G.C. Smith, C.E. Banks, 2D hexagonal boron nitride (2D-hBN) explored as a potential electrocatalyst for the oxygen reduction reaction, Electroanalysis 29 (2017) 622–634, https://doi.org/10.1002/elan.201600462.
[173] X. Chen, J. Chang, H. Yan, D. Xia, Boron nitride nanocages as high activity electrocatalysts for oxygen reduction reaction: synergistic catalysis by dual active sites, J. Phys. Chem. C 120 (2016) 28912–28916, https://doi.org/10.1021/acs.jpcc.6b08560.
[174] P. Zhang, X. Hou, S. Li, D. Liu, M. Dong, Curvature effect of O_2 adsorption and dissociation on SiC nanotubes and nanosheet, Chem. Phys. Lett. 619 (2015) 92–96, https://doi.org/10.1016/j.cplett.2014.11.057.
[175] P. Marbaniang, I. Patil, M. Lokanathan, H. Parse, D. Catherin Sesu, S. Ingavale, B. Kakade, Nanorice-like structure of carbon-doped hexagonal boron nitride as an efficient metal-free catalyst for oxygen electroreduction, ACS Sustain. Chem. Eng. 6 (2018) 11115–11122, https://doi.org/10.1021/acssuschemeng.8b02609.
[176] J. Zhao, Z. Chen, Carbon-doped boron nitride nanosheet: an efficient metal-free electrocatalyst for the oxygen reduction reaction, J. Phys. Chem. C 119 (2015) 26348–26354, https://doi.org/10.1021/acs.jpcc.5b09037.
[177] L.-y Feng, Y.-j Liu, J.-x Zhao, Iron-embedded boron nitride nanosheet as a promising electrocatalyst for the oxygen reduction reaction (ORR): A density functional theory (DFT) study, J. Power Sources 287 (2015) 431–438, https://doi.org/10.1016/j.jpowsour.2015.04.094.
[178] Q. Li, T. Zhang, X. Yu, X. Wu, X. Zhang, Z. Lu, X. Yang, Y. Huang, L. Li, Isolated Au atom anchored on porous boron nitride as a promising electrocatalyst for oxygen reduction reaction (ORR): a DFT study, Front. Chem. 7 (2019) 674, https://doi.org/10.3389/fchem.2019.00674.
[179] C. Deng, R. He, D. Wen, W. Shen, M. Li, Theoretical study on the origin of activity for the oxygen reduction reaction of metal-doped two-dimensional boron nitride materials, Phys. Chem. Chem. Phys. 20 (2018) 10240–10246, https://doi.org/10.1039/C8CP00838H.
[180] S. Chen, Z. Chen, S. Siahrostami, D. Higgins, D. Nordlund, D. Sokaras, T.R. Kim, Y. Liu, X. Yan, E. Nilsson, R. Sinclair, J.K. Nørskov, T.F. Jaramillo, Z. Bao, Designing boron nitride islands in carbon materials for efficient electrochemical synthesis of hydrogen peroxide, J. Am. Chem. Soc. 140 (2018) 7851–7859, https://doi.org/10.1021/jacs.8b02798.
[181] P. Marbaniang, S. Ingavale, D. Catherin, N. Ramgir, A. Swami, B. Kakade, Forming a BB bond in boron carbon nitride composite: a way for metal free electrocatalyst for oxygen reduction reaction in alkaline medium, J. Catal. 378 (2019) 104–112, https://doi.org/10.1016/j.jcat.2019.08.021.
[182] R.J. Kahan, W. Hirunpinyopas, J. Cid, M.J. Ingleson, R.A.W. Dryfe, Well-defined boron/nitrogen-doped polycyclic aromatic hydrocarbons are active electrocatalysts for the oxygen reduction reaction, Chem. Mater. 31 (2019) 1891–1898, https://doi.org/10.1021/acs.chemmater.8b04027.
[183] M. Weber, N. Tuleushova, J. Zgheib, C. Lamboux, I. Iatsunskyi, E. Coy, V. Flaud, S. Tingry, D. Cornu, P. Miele, M. Bechelany, Y. Holade, Enhanced electrocatalytic performance triggered by atomically bridged boron nitride between palladium nanoparticles and carbon fibers in gas-diffusion electrodes, Appl. Catal. B Environ. 257 (2019) 117917, https://doi.org/10.1016/j.apcatb.2019.117917.
[184] I.M. Patil, A. Swami, R. Chavan, M. Lokanathan, B. Kakade, Hexagonal boron nitride-supported crystalline manganese oxide nanorods/carbon: a tunable nanocomposite catalyst for dioxygen electroreduction, ACS Sustain. Chem. Eng. 6 (2018) 16886–16895, https://doi.org/10.1021/acssuschemeng.8b04241.
[185] Y. Chen, J. Cai, P. Li, G. Zhao, G. Wang, Y. Jiang, J. Chen, S.X. Dou, H. Pan, W. Sun, Hexagonal boron nitride as a multifunctional support for engineering efficient electrocatalysts toward the oxygen reduction reaction, Nano Lett. 20 (2020) 6807–6814, https://doi.org/10.1021/acs.nanolett.0c02782.
[186] Q. Li, L. Li, X. Yu, X. Wu, Z. Xie, X. Wang, Z. Lu, X. Zhang, Y. Huang, X. Yang, Ultrafine platinum particles anchored on porous boron nitride enabling excellent stability and activity for oxygen reduction reaction, Chem. Eng. J. 399 (2020) 125827, https://doi.org/10.1016/j.apcatb.2019.117917.
[187] A. Rendón-Patiño, A. Doménech, H. García, A. Primo, A reliable procedure for the preparation of graphene-boron nitride superlattices as large area (cm × cm) films on arbitrary substrates or powders (gram scale) and unexpected electrocatalytic properties, Nanoscale 11 (2019) 2981–2990, https://doi.org/10.1039/C8NR08377K.
[188] J. Pang, Y. Chao, H. Chang, H. Li, J. Xiong, M. He, Q. Zhang, H. Li, W. Zhu, Tuning electronic properties of boron nitride nanoplate via doping carbon for enhanced adsorptive performance, J. Colloid Interf. Sci. 508 (2017) 121–128, https://doi.org/10.1016/j.jcis.2017.08.012.
[189] F. Liu, S. Li, D. Yu, Y. Su, N. Shao, Z. Zhang, Template-free synthesis of oxygen-doped bundlelike porous boron nitride for highly efficient removal of heavy metals from wastewater, ACS Sustain Chem. Eng. 6 (2018) 16011–16020, https://doi.org/10.1021/acssuschemeng.8b01936.
[190] Indrajit M. Patil, C.P. Jijil, M. Lokanathan, A. Swami, B. Kakade, Mechanical activation in reduced graphite oxide/boron nitride nanocomposite electrocatalysts for significant improvement in dioxygen reduction, Sustain. Energ. Fuels 2 (2018) 252–261, https://doi.org/10.1039/C7SE00461C.
[191] I.M. Patil, M. Lokanathan, B. Kakade, Three dimensional nanocomposite of reduced graphene oxide and hexagonal boron nitride as an efficient metal-free catalyst for oxygen electroreduction, J. Mater. Chem. A 4 (2016) 4506–4515, https://doi.org/10.1039/C6TA00525J.
[192] Q. Sun, C. Sun, A. Du, S. Dou, Z. Li, In-plane graphene/boron-nitride heterostructures as an efficient metal-free electrocatalyst for the oxygen reduction reaction, Nanoscale 8 (2016) 14084–14091, https://doi.org/10.1039/C6NR03288E.
[193] L. Liu, J. Park, D.A. Siegel, K.F. McCarty, K.W. Clark, W. Deng, L. Basile, J. C. Idrobo, A.-P. Li, G. Gu, Heteroepitaxial growth of two-dimensional hexagonal boron nitride templated by graphene edges, Science 343 (2014) 163–167, https://doi.org/10.1126/science.1246137 189.
[194] M. Liu, Y. Li, P. Chen, J. Sun, D. Ma, Q. Li, T. Gao, Y. Gao, Z. Cheng, X. Qiu, Y. Fang, Y. Zhang, Z. Liu, Quasi-freestanding monolayer heterostructure of graphene and hexagonal boron nitride on Ir(111) with a zigzag boundary, Nano Lett. 14 (2014) 6342–6347, https://doi.org/10.1021/nl502780u.
[195] S. Nappini, I. Píš, T.O. Menteş, A. Sala, M. Cattelan, S. Agnoli, F. Bondino, E. Magnano, Formation of a quasi-free-standing single layer of graphene and hexagonal boron nitride on Pt(111) by a single molecular precursor, Adv. Funct. Mater. 26 (2016) 1120–1126, https://doi.org/10.1002/adfm.201503591.
[196] L. Qu, Z. Zhang, H. Zhang, H. Zhang, S. Dong, Transformation from graphitic C_3N_4 to nitrogen-boron-carbon ternary nanosheets as efficient metal-free bifunctional electrocatalyst for oxygen reduction reaction and hydrogen evolution reaction, Appl. Surf. Sci. 448 (2018) 618–627, https://doi.org/10.1016/j.apsusc.2018.04.174.
[197] W. Chen, L. Xu, Y. Tian, H. Li, K. Wang, Boron and nitrogen co-doped graphene aerogels: facile preparation, tunable doping contents and bifunctional oxygen electrocatalysis, Carbon 137 (2018) 458–466, https://doi.org/10.1016/j.carbon.2018.05.061.
[198] I.M. Patil, M. Lokanathan, B. Ganesan, A. Swami, B. Kakade, Carbon nanotube/boron nitride nanocomposite as a significant bifunctional electrocatalyst for oxygen reduction and oxygen evolution reactions, Chem. Eur. J. 23 (2017) 676–683, https://doi.org/10.1002/chem.201604231.
[199] T. Huang, S. Mao, M. Qiu, O. Mao, C. Yuan, J. Chen, Nitrogen-boron dipolar-doped nanocarbon as a high-efficiency electrocatalyst for oxygen reduction reaction, Electrochim. Acta 222 (2016) 481–487, https://doi.org/10.1016/j.electacta.2016.10.201.
[200] W. Yaseen, N. Ullah, M. Xie, B.A. Yusuf, Y. Xu, C. Tong, J. Xie, Ni-Fe-Co based mixed metal/metal-oxides nanoparticles encapsulated in ultrathin carbon nanosheets: a bifunctional electrocatalyst for overall water splitting, Surf. Interfaces 26 (2021) 101361, https://doi.org/10.1016/j.surfin.2021.101361.
[201] Z.W. Seh, J. Kibsgaard, C.F. Dickens, I. Chorkendorff, J.K. Nørskov, T. F. Jaramillo, Combining theory and experiment in electrocatalysis: Insights into materials design, Science 355 (2017) eaad4998, https://doi.org/10.1126/science.aad4998.

[202] T.R. Cook, D.K. Dogutan, S.Y. Reece, Y. Surendranath, T.S. Teets, D.G. Nocera, Solar energy supply and storage for the legacy and nonlegacy worlds, Chem. Rev. 110 (2010) 6474–6502, https://doi.org/10.1021/cr100246c.

[203] D. Wang, Y. Song, H. Zhang, X. Yan, J. Guo, Recent advances in transition metal borides for electrocatalytic oxygen evolution reaction, J. Electroanal. Chem. 861 (2020), 113953, https://doi.org/10.1016/j.jelechem.2020.113953.

[204] C.C.L. McCrory, S. Jung, I.M. Ferrer, S.M. Chatman, J.C. Peters, T.F. Jaramillo, Benchmarking hydrogen evolving reaction and oxygen evolving reaction electrocatalysts for solar water splitting devices, J. Am. Chem. Soc. 137 (2015) 4347–4357, https://doi.org/10.1021/ja510442p.

[205] H. Wang, X. Xiao, S. Liu, C.-L. Chiang, X. Kuai, C.-K. Peng, Y.-C. Lin, X. Meng, J. Zhao, J. Choi, Y.-G. Lin, J.-M. Lee, L. Gao, Structural and electronic optimization of MoS_2 edges for hydrogen evolution, J. Am. Chem. Soc. 141 (2019) 18578–18584, https://doi.org/10.1021/jacs.9b09932.

[206] H. Wang, Y. Lin, S. Liu, J. Li, L. Bu, J. Chen, X. Xiao, J.-H. Choi, L. Gao, J.-M. Lee, Confined growth of pyridinic N–Mo_2C sites on MXenes for hydrogen evolution, J. Mater. Chem. A 8 (2020) 7109–7116, https://doi.org/10.1039/D0TA01697G.

[207] M. Görlin, P. Chernev, J. Ferreira de Araújo, T. Reier, S. Dresp, B. Paul, R. Krähnert, H. Dau, P. Strasser, Oxygen evolution reaction dynamics, faradaic charge efficiency, and the active metal redox states of Ni–Fe oxide water splitting electrocatalysts, J. Am. Chem. Soc. 138 (2016) 5603–5614, https://doi.org/10.1021/jacs.6b00332.

[208] S.A. Bonke, A.M. Bond, L. Spiccia, A.N. Simonov, Parameterization of water electrooxidation catalyzed by metal oxides using fourier transformed alternating current voltammetry, J. Am. Chem. Soc. 138 (2016) 16095–16104, https://doi.org/10.1021/jacs.6b10304.

[209] X. Peng, L. Hu, L. Wang, X. Zhang, J. Fu, K. Huo, L.Y.S. Lee, K.-Y. Wong, P.K. Chu, Vanadium carbide nanoparticles encapsulated in graphitic carbon network nanosheets: a high-efficiency electrocatalyst for hydrogen evolution reaction, Nano Energy 26 (2016) 603–609, https://doi.org/10.1016/j.nanoen.2016.06.020.

[210] X. Peng, A.M. Qasim, W. Jin, L. Wang, L. Hu, Y. Miao, W. Li, Y. Li, Z. Liu, K. Huo, K.-y Wong, P.K. Chu, Ni-doped amorphous iron phosphide nanoparticles on TiN nanowire arrays: an advanced alkaline hydrogen evolution electrocatalyst, Nano Energy 53 (2018) 66–73, https://doi.org/10.1016/j.nanoen.2018.08.028.

[211] X. Yang, J. Chen, L. Hu, J. Wei, M. Shuai, D. Huang, G. Yue, D. Astruc, P. Zhao, Palladium separation by Pd-catalyzed gel formation via alkyne coupling, Chem. Mater. 31 (2019) 7386–7394, https://doi.org/10.1021/acs.chemmater.9b02031.

[212] Y. Yang, Y. Yang, Z. Pei, K.-H. Wu, C. Tan, H. Wang, L. Wei, A. Mahmood, C. Yan, J. Dong, S. Zhao, Y. Chen, Recent progress of carbon-supported single-atom catalysts for energy conversion and storage, Matter 3 (2020) 1442–1476, https://doi.org/10.1016/j.matt.2020.07.032.

[213] W. Yaseen, N. Ullah, M. Xie, W. Wei, Y. Xu, M. Zahid, C.J. Oluigbo, B.A. Yusuf, J. Xie, Cobalt–Iron nanoparticles encapsulated in mesoporous carbon nanosheets: a one-pot synthesis of highly stable electrocatalysts for overall water splitting, Int. J. Hydrog. Energy 46 (2021) 5234–5249, https://doi.org/10.1016/j.ijhydene.2020.11.041.

[214] Y. Cheng, S.P. Jiang, Advances in electrocatalysts for oxygen evolution reaction of water electrolysis-from metal oxides to carbon nanotubes, Prog. Nat. Sci. 25 (2015) 545–553, https://doi.org/10.1016/j.pnsc.2015.11.008.

[215] N.-T. Suen, S.-F. Hung, Q. Quan, N. Zhang, Y.-J. Xu, H.M. Chen, Electrocatalysis for the oxygen evolution reaction: recent development and future perspectives, Chem. Soc. Rev. 46 (2017) 337–365, https://doi.org/10.1039/C6CS00328A.

[216] J. Shan, C. Ye, S. Chen, T. Sun, Y. Jiao, L. Liu, C. Zhu, L. Song, Y. Han, M. Jaroniec, Y. Zhu, Y. Zheng, S.-Z. Qiao, Short-range ordered iridium single atoms integrated into cobalt oxide spinel structure for highly efficient electrocatalytic water oxidation, J. Am. Chem. Soc. 143 (2021) 5201–5211, https://doi.org/10.1021/jacs.1c01525.

[217] J. Sun, J. Zhang, M. Zhang, M. Antonietti, X. Fu, X. Wang, Bioinspired hollow semiconductor nanospheres as photosynthetic nanoparticles, Nat. Commun. 3 (2012) 1139, https://doi.org/10.1038/ncomms2152.

[218] J.L. Boyer, D.E. Polyansky, D.J. Szalda, R. Zong, R.P. Thummel, E. Fujita, Effects of a proximal base on water oxidation and proton reduction catalyzed by geometric isomers of $[Ru(tpy)(pynap)(OH_2)]^{2+}$, Angew. Chem. Int. Ed. 50 (2011) 12600–12604, https://doi.org/10.1002/anie.201102648.

[219] B.S. Yeo, A.T. Bell, Enhanced activity of gold-supported cobalt oxide for the electrochemical evolution of oxygen, J. Am. Chem. Soc. 133 (2011) 5587–5593, https://doi.org/10.1021/ja200559j.

[220] Y. Lin, H. Wang, C.-K. Peng, L. Bu, C.-L. Chiang, K. Tian, Y. Zhao, J. Zhao, Y.-G. Lin, J.-M. Lee, L. Gao, Co-induced electronic optimization of hierarchical NiFe LDH for oxygen evolution, Small 16 (2020), 2002426, https://doi.org/10.1002/smll.202002426.

[221] M. Li, H. Li, X. Jiang, M. Jiang, X. Zhan, G. Fu, J.-M. Lee, Y. Tang, Gd-induced electronic structure engineering of a NiFe-layered double hydroxide for efficient oxygen evolution, J. Mater. Chem. A 9 (2021) 2999–3006, https://doi.org/10.1039/D0TA10740A.

[222] X. Peng, L. Wang, L. Hu, Y. Li, B. Gao, H. Song, C. Huang, X. Zhang, J. Fu, K. Huo, P.K. Chu, In situ segregation of cobalt nanoparticles on VN nanosheets via nitriding of $Co_2V_2O_7$ nanosheets as efficient oxygen evolution reaction electrocatalysts, Nano Energy 34 (2017) 1–7, https://doi.org/10.1016/j.nanoen.2017.02.016.

[223] Y. Li, L. Hu, W. Zheng, X. Peng, M. Liu, P.K. Chu, L.Y.S. Lee, Ni/Co-based nanosheet arrays for efficient oxygen evolution reaction, Nano Energy 52 (2018) 360–368, https://doi.org/10.1016/j.nanoen.2018.08.010.

[224] X. Peng, X. Jin, N. Liu, P. Wang, Z. Liu, B. Gao, L. Hu, P.K. Chu, A high-performance electrocatalyst composed of nickel clusters encapsulated with a carbon network on TiN nanaowire arrays for the oxygen evolution reaction, Appl. Surf. Sci. 567 (2021) 150779, https://doi.org/10.1016/j.apsusc.2021.150779.

[225] J. Song, C. Wei, Z.-F. Huang, C. Liu, L. Zeng, X. Wang, Z.J. Xu, A review on fundamentals for designing oxygen evolution electrocatalysts, Chem. Soc. Rev. 49 (2020) 2196–2214, https://doi.org/10.1039/C9CS00607A.

[226] W. Liu, D. Zheng, T. Deng, Q. Chen, C. Zhu, C. Pei, H. Li, F. Wu, W. Shi, S.-W. Yang, Y. Zhu, X. Cao, Boosting electrocatalytic activity of 3d-block metal (Hydro)oxides by Ligand-induced conversion, Angew. Chem. Int. Ed. 60 (2021) 10614–10619, https://doi.org/10.1002/anie.202100371.

[227] S. Zhao, C. Tan, C.-T. He, P. An, F. Xie, S. Jiang, Y. Zhu, K.-H. Wu, B. Zhang, H. Li, J. Zhang, Y. Chen, S. Liu, J. Dong, Z. Tang, Structural transformation of highly active metal–organic framework electrocatalysts during the oxygen evolution reaction, Nat. Energy 5 (2020) 881–890, https://doi.org/10.1038/s41560-020-00709-1.

[228] S. Wirth, F. Harnisch, M. Weinmann, U. Schröder, Comparative study of IVB–VIB transition metal compound electrocatalysts for the hydrogen evolution reaction, Appl. Catal. B Environ. 126 (2012) 225–230, https://doi.org/10.1016/j.apcatb.2012.07.023.

[229] K. Uosaki, G. Elumalai, H.C. Dinh, A. Lyalin, T. Taketsugu, H. Noguchi, Highly efficient electrochemical hydrogen evolution reaction at insulating boron nitride nanosheet on inert gold substrate, Sci. Rep. 6 (2016) 32217, https://doi.org/10.1038/srep32217.

[230] G. Elumalai, H. Noguchi, K. Uosaki, Boron nitride nanosheets decorated with Au, Au-Ni, Au-Cu, or Au-Co nanoparticles as efficient electrocatalysts for hydrogen evolution reaction, J. Electroanal. Chem. 848 (2019) 113312, https://doi.org/10.1016/j.jelechem.2019.113312.

[231] A. Guha, T. Veettil Vineesh, A. Sekar, S. Narayanaru, M. Sahoo, S. Nayak, S. Chakraborty, T.N. Narayanan, Mechanistic insight into enhanced hydrogen evolution reaction activity of ultrathin hexagonal boron nitride-modified Pt electrodes, ACS Catal. 8 (2018) 6636–6644, https://doi.org/10.1021/acscatal.8b00938.

[232] D.B. Nguyen, L.N. Tran, Assessment of electrocatalytic performance of metal-free C-doped BN nanoflakes for oxygen reduction and hydrogen evolution reactions: a comparative study, J. Phys. Chem. C. 122 (2018) 21124–21131, https://doi.org/10.1021/acs.jpcc.8b04073.

[233] H. Liu, X.-H. Zhang, Y.-X. Li, X. Li, C.-K. Dong, D.-Y. Wu, C.-C. Tang, S.-L. Chou, F. Fang, X.-W. Du, Conductive boron nitride as promising catalyst support for the oxygen evolution reaction, Adv. Energy Mater. 10 (2020), 1902521, https://doi.org/10.1002/aenm.201902521.

[234] M. Gao, M. Nakahara, A. Lyalin, T. Taketsugu, Catalytic activity of gold clusters supported on the h-BN/Au(111) surface for the hydrogen evolution reaction, J. Phys. Chem. C 125 (2021) 1334–1344, https://doi.org/10.1021/acs.jpcc.0c08826.

[235] R. Maji, J. Bhattacharjee, Synergistic view of magnetism, chemical activation, and oxygen reduction reaction as well as oxygen evolution reaction catalysis of carbon-doped hexagonal boron nitride from first principles, J. Phys. Chem. C 123 (2019) 16731–16740, https://doi.org/10.1021/acs.jpcc.9b03229.

[236] M.A.R. Anjum, M.H. Lee, J.S. Lee, Boron- and nitrogen-codoped molybdenum carbide nanoparticles imbedded in a BCN network as a bifunctional electrocatalyst for hydrogen and oxygen evolution reactions, ACS Catal. 8 (2018) 8296–8305, https://doi.org/10.1021/acscatal.8b01794.

[237] D.N. Sredojević, M.R. Belić, Ž. Šljivančanin, Hydrogen evolution reaction over single-atom catalysts based on metal adatoms at defected graphene and h-BN, J. Phys. Chem. C 124 (2020) 16860–16867, https://doi.org/10.1021/acs.jpcc.0c01151.

[238] H. Abdelsalam, W.O. Younis, V.A. Saroka, N.H. Teleb, S. Yunoki, Q. Zhang, Interaction of hydrated metals with chemically modified hexagonal boron nitride quantum dots: wastewater treatment and water splitting, Phys. Chem. Chem. Phys. 22 (2020) 2566–2579, https://doi.org/10.1039/C9CP06823F.

[239] T. Balakrishnan, M. Anis, S. Arun, M. Kumar, S. Arun kumar, S. Mayavan, BCN–Co_3O_4 hybrid – a highly efficient catalyst for the oxygen evolution reaction and dye degradation, RSC Adv. 6 (2016) 79448–79451, https://doi.org/10.1039/C6RA16058A.

[240] S. Tang, X. Zhou, T. Liu, S. Zhang, T. Yang, Y. Luo, E. Sharman, J. Jiang, Single nickel atom supported on hybridized graphene–boron nitride nanosheet as a highly active bi-functional electrocatalyst for hydrogen and oxygen evolution reactions, J. Mater. Chem. A 7 (2019) 26261–26265, https://doi.org/10.1039/C9TA10500J.

[241] D.T. Whipple, P.J.A. Kenis, Prospects of CO_2 utilization via direct heterogeneous electrochemical reduction, J. Phys. Chem. Lett. 1 (2010) 3451–3458, https://doi.org/10.1021/jz1012627.

[242] R. Kortlever, J. Shen, K.J.P. Schouten, F. Calle-Vallejo, M.T.M. Koper, Catalysts and reaction pathways for the electrochemical reduction of carbon dioxide, J. Phys. Chem. Lett. 6 (2015) 4073–4082, https://doi.org/10.1021/acs.jpclett.5b01559.

[243] D.D. Zhu, J.L. Liu, S.Z. Qiao, Recent advances in inorganic heterogeneous electrocatalysts for reduction of carbon dioxide, Adv. Mater. 28 (2016) 3423–3452, https://doi.org/10.1002/adma.201504766.

[244] J. Schneider, H. Jia, J.T. Muckerman, E. Fujita, Thermodynamics and kinetics of CO_2, CO, and H^+ binding to the metal centre of CO_2 reductioncatalysts, Chem. Soc. Rev. 41 (2012) 2036–2051, https://doi.org/10.1039/C1CS15278E.

[245] H.-R.M. Jhong, S. Ma, P.J.A. Kenis, Electrochemical conversion of CO_2 to useful chemicals: current status, remaining challenges, and future opportunities, Curr. Opin. Chem. Eng. 2 (2013) 191–199, https://doi.org/10.1016/j.coche.2013.03.005.

[246] J. Shen, R. Kortlever, R. Kas, Y.Y. Birdja, O. Diaz-Morales, Y. Kwon, I. Ledezma-Yanez, K.J.P. Schouten, G. Mul, M.T.M. Koper, Electrocatalytic reduction of carbon dioxide to carbon monoxide and methane at an immobilized cobalt protoporphyrin, Nat. Commun. 6 (2015) 8177, https://doi.org/10.1038/ncomms9177.
[247] K.P. Kuhl, E.R. Cave, D.N. Abram, T.F. Jaramillo, New insights into the electrochemical reduction of carbon dioxide on metallic copper surfaces, Energy Environ. Sci. 5 (2012) 7050–7059, https://doi.org/10.1039/C2EE21234J.
[248] Y.-X. Duan, F.-L. Meng, K.-H. Liu, S.-S. Yi, S.-J. Li, J.-M. Yan, Q. Jiang, Amorphizing of Cu nanoparticles toward highly efficient and robust electrocatalyst for CO_2 reduction to liquid fuels with high faradaic efficiencies, Adv. Mater. 30 (2018), 1706194, https://doi.org/10.1002/adma.201706194.
[249] D.-H. Lim, J.H. Jo, D.Y. Shin, J. Wilcox, H.C. Ham, S.W. Nam, Carbon dioxide conversion into hydrocarbon fuels on defective graphene-supported Cu nanoparticles from first principles, Nanoscale 6 (2014) 5087–5092, https://doi.org/10.1039/C3NR06539A.
[250] C.W. Li, M.W. Kanan, CO_2 reduction at low overpotential on Cu electrodes resulting from the reduction of thick Cu_2O films, J. Am. Chem. Soc. 134 (2012) 7231–7234, https://doi.org/10.1021/ja3010978.
[251] F. Abild-Pedersen, J. Greeley, F. Studt, J. Rossmeisl, T.R. Munter, P.G. Moses, E. Skúlason, T. Bligaard, J.K. Nørskov, Scaling properties of adsorption energies for hydrogen-containing molecules on transition-metal surfaces, Phys. Rev. Lett. 99 (2007) 016105, https://doi.org/10.1103/PhysRevLett.99.016105.
[252] S. Back, J. Lim, N.-Y. Kim, Y.-H. Kim, Y. Jung, Single-atom catalysts for CO_2 electroreduction with significant activity and selectivity improvements, Chem. Sci. 8 (2017) 1090–1096, https://doi.org/10.1039/C6SC03911A.
[253] Q. Sun, Z. Li, D.J. Searles, Y. Chen, G. Lu, A. Du, Charge-controlled switchable CO_2 capture on boron nitride nanomaterials, J. Am. Chem. Soc. 135 (2013) 8246–8253, https://doi.org/10.1021/ja400243r.
[254] H. Guo, W. Zhang, N. Lu, Z. Zhuo, X.C. Zeng, X. Wu, J. Yang, CO_2 capture on h-BN sheet with high selectivity controlled by external electric field, J. Phys. Chem. C 119 (2015) 6912–6917, https://doi.org/10.1021/acs.jpcc.5b00681.
[255] L.M. Azofra, D.R. MacFarlane, C. Sun, An intensified π-hole in berylium-doped boron nitride meshes: its determinant role in CO_2 conversion into hydrocarbon fuels, Chem. Commun. 52 (2016) 3548–3551, https://doi.org/10.1039/C5CC07942J.
[256] Y. Cao, Z. Geng, W. Chen, F. Cai, G. Wang, Z. Wang, J. Zeng, Introduction of carbon–boron atomic groups as an efficient strategy to boost formic acid production toward CO_2 electrochemical reduction, Chem. Commun. 54 (2018) 3367–3370, https://doi.org/10.1039/C8CC00644J.
[257] S. Tang, X. Zhou, S. Zhang, X. Li, T. Yang, W. Hu, J. Jiang, Y. Luo, Metal-free boron nitride nanoribbon catalysts for electrochemical CO_2 reduction: combining high activity and selectivity, ACS Appl. Mater. Interfaces 11 (2019) 906–915, https://doi.org/10.1021/acsami.8b18505.
[258] X. Mao, D. Wijethunge, L. Zhang, S. Wang, C. Yan, Z. Zhu, A. Du, Metal-free graphene/boron nitride heterointerface for CO_2 reduction: surface curvature controls catalytic activity and selectivity, EcoMat 2 (2020), e12013, https://doi.org/10.1002/eom2.12013.
[259] G. Hu, Z. Wu, S. Dai, D.-E. Jiang, Interface engineering of earth-abundant transition metals using boron nitride for selective electroreduction of CO_2, ACS Appl. Mater. Interfaces 10 (2018) 6694–6700, https://doi.org/10.1021/acsami.7b17600.
[260] B. Huang, Y. Wu, Y. Luo, N. Zhou, Double atom-anchored defective boron nitride catalyst for efficient electroreduction of CO_2 to CH_4: a first principles study, Chem. Phys. Lett. 756 (2020) 137852, https://doi.org/10.1016/j.cplett.2020.137852.
[261] L. Fu, G. Chen, N. Jiang, J. Yu, C.-T. Lin, A. Yu, In situ growth of metal nanoparticles on boron nitride nanosheets as highly efficient catalysts, J. Mater. Chem. A 4 (2016) 19107–19115, https://doi.org/10.1039/C6TA06409D.
[262] X. Tan, H.A. Tahini, H. Arandiyan, S.C. Smith, Electrocatalytic reduction of carbon dioxide to methane on single transition metal atoms supported on a defective boron nitride monolayer: first principle study, Adv. Theor. Simul. 2 (2019), 1800094, https://doi.org/10.1002/adts.201800094.
[263] Q. Cui, G. Qin, W. Wang, L. Sun, A. Du, Q. Sun, Mo-doped boron nitride monolayer as a promising single-atom electrocatalyst for CO_2 conversion, Beilstein J. Nanotechnol. 10 (2019) 540–548, https://doi.org/10.3762/bjnano.10.55.
[264] A.A. Peterson, F. Abild-Pedersen, F. Studt, J. Rossmeisl, J.K. Nørskov, How copper catalyzes the electroreduction of carbon dioxide into hydrocarbon fuels, Energ. Environ. Sci. 3 (2010) 1311–1315, https://doi.org/10.1039/C0EE00071J.
[265] X. Sun, Q. Zhu, X. Kang, H. Liu, Q. Qian, J. Ma, Z. Zhang, G. Yang, B. Han, Design of a Cu(i)/C-doped boron nitride electrocatalyst for efficient conversion of CO_2 into acetic acid, Green Chem. 19 (2017) 2086–2091, https://doi.org/10.1039/C7GC00503B.
[266] B. Qin, Y.-H. Li, Q. Zhang, G. Yang, H. Wang, Y. Zhang, F. Peng, Mechanistic insights into the electrochemical reduction of CO_2 and N_2 on the regulation of a boron nitride defect-derived two-dimensional catalyst using density functional theory calculations, J. Phys. Chem. Lett. 12 (2021) 7151–7158, https://doi.org/10.1021/acs.jpclett.1c01920.
[267] V. Rosca, M. Duca, M.T. de Groot, M.T.M. Koper, Nitrogen cycle electrocatalysis, Chem. Rev. 109 (2009) 2209–2244, https://doi.org/10.1021/cr8003696.
[268] J.G. Chen, R.M. Crooks, L.C. Seefeldt, K.L. Bren, R.M. Bullock, M.Y. Darensbourg, P.L. Holland, B. Hoffman, M.J. Janik, A.K. Jones, M.G. Kanatzidis, P. King, K. M. Lancaster, S.V. Lymar, P. Pfromm, W.F. Schneider, R.R. Schrock, Beyond fossil fuel–driven nitrogen transformations, Science 360 (2018) eaar6611, https://doi.org/10.1126/science.aar6611.
[269] D.J. Little, I.I.I.M.R. Smith, T.W. Hamann, Electrolysis of liquid ammonia for hydrogen generation, Energ, Environ. Sci. 8 (2015) 2775–2781, https://doi.org/10.1039/C5EE01840D.
[270] A.E. Shilov, Catalytic reduction of molecular nitrogen in solutions, Russ. Chem. Bull. 52 (2003) 2555–2562, https://doi.org/10.1023/B:RUCB.0000019873.81002.60.
[271] J.W. Erisman, M.A. Sutton, J. Galloway, Z. Klimont, W. Winiwarter, How a century of ammonia synthesis changed the world, Nat. Geosci. 1 (2008) 636–639, https://doi.org/10.1038/ngeo325.
[272] N. Bauer, Theoretical pathways for the reduction of N_2 molecules in aqueous media: thermodynamics of N_2H_n[1], J. Phys. Chem. 64 (1960) 833–837, https://doi.org/10.1021/j100836a001.
[273] C. Ling, Y. Ouyang, Q. Li, X. Bai, X. Mao, A. Du, J. Wang, A general two-step strategy–based high-throughput screening of single atom catalysts for nitrogen fixation, Small Methods 3 (2019), 1800376, https://doi.org/10.1002/smtd.201800376.
[274] L. Yang, T. Wu, R. Zhang, H. Zhou, L. Xia, X. Shi, H. Zheng, Y. Zhang, X. Sun, Insights into defective TiO_2 in electrocatalytic N_2 reduction: combining theoretical and experimental studies, Nanoscale 11 (2019) 1555–1562, https://doi.org/10.1039/C8NR09564G.
[275] C.J.M. van der Ham, M.T.M. Koper, D.G.H. Hetterscheid, Challenges in reduction of dinitrogen by proton and electron transfer, Chem. Soc. Rev. 43 (2014) 5183–5191, https://doi.org/10.1039/C4CS00085D.
[276] M.A. Shipman, M.D. Symes, Recent progress towards the electrosynthesis of ammonia from sustainable resources, Catal. Today 286 (2017) 57–68, https://doi.org/10.1016/j.cattod.2016.05.008.
[277] X. Cui, C. Tang, Q. Zhang, A review of electrocatalytic reduction of dinitrogen to ammonia under ambient conditions, Adv. Energy Mater. 8 (2018), 1800369, https://doi.org/10.1002/aenm.201800369.
[278] R.J. Burford, M.D. Fryzuk, Examining the relationship between coordination mode and reactivity of dinitrogen, Nat. Rev. Chem. 1 (2017) 0026, https://doi.org/10.1038/s41570-017-0026.
[279] N. Hazari, Homogeneous iron complexes for the conversion of dinitrogen into ammonia and hydrazine, Chem. Soc. Rev. 39 (2010) 4044–4056, https://doi.org/10.1039/B919680N.
[280] J. Wang, L. Yu, L. Hu, G. Chen, H. Xin, X. Feng, Ambient ammonia synthesis via palladium-catalyzed electrohydrogenation of dinitrogen at low overpotential, Nat. Commun. 9 (2018) 1795, https://doi.org/10.1038/s41467-018-04213-9.
[281] L. Han, X. Liu, J. Chen, R. Lin, H. Liu, F. Lü, S. Bak, Z. Liang, S. Zhao, E. Stavitski, J. Luo, R.R. Adzic, H.L. Xin, Atomically dispersed molybdenum catalysts for efficient ambient nitrogen fixation, Angew. Chem. Int. Ed. 58 (2019) 2321–2325, https://doi.org/10.1002/anie.201811728.
[282] H. Tao, C. Choi, L.-X. Ding, Z. Jiang, Z. Han, M. Jia, Q. Fan, Y. Gao, H. Wang, A. W. Robertson, S. Hong, Y. Jung, S. Liu, Z. Sun, Nitrogen fixation by ru single-atom electrocatalytic reduction, Chem 5 (2019) 204–214, https://doi.org/10.1016/j.chempr.2018.10.007.
[283] X. Yang, S. Kattel, J. Nash, X. Chang, J.H. Lee, Y. Yan, J.G. Chen, B. Xu, Quantification of active sites and elucidation of the reaction mechanism of the electrochemical nitrogen reduction reaction on vanadium nitride, Angew. Chem. Int. Ed. 58 (2019) 13768–13772, https://doi.org/10.1002/anie.201906449.
[284] Q. Qin, T. Heil, M. Antonietti, M. Oschatz, Single-site gold catalysts on hierarchical N-doped porous noble carbon for enhanced electrochemical reduction of nitrogen, Small Methods 2 (2018), 1800202, https://doi.org/10.1002/smtd.201800202.
[285] S. Zhao, X. Lu, L. Wang, J. Gale, R. Amal, Carbon-based metal-free catalysts for electrocatalytic reduction of nitrogen for synthesis of ammonia at ambient conditions, Adv. Mater. 31 (2019), 1805367, https://doi.org/10.1002/adma.201805367.
[286] W. Zhang, J. Low, R. Long, Y. Xiong, Metal-free electrocatalysts for nitrogen reduction reaction, EnergyChem 2 (2020) 100040, https://doi.org/10.1016/j.enchem.2020.100040.
[287] Y. Zhang, H. Du, Y. Ma, L. Ji, H. Guo, Z. Tian, H. Chen, H. Huang, G. Cui, A. M. Asiri, F. Qu, L. Chen, X. Sun, Hexagonal boron nitride nanosheet for effective ambient N_2 fixation to NH_3, Nano Res. 12 (2019) 919–924, https://doi.org/10.1007/s12274-019-2323-x.
[288] Z. Liu, M. Zhang, H. Wang, D. Cang, X. Ji, B. Liu, W. Yang, D. Li, J. Liu, Defective carbon-doped boron nitride nanosheets for highly efficient electrocatalytic conversion of N_2 to NH_3, ACS Sustain Chem. Eng. 8 (2020) 5278–5286, https://doi.org/10.1021/acssuschemeng.0c00330.
[289] X. Mao, S. Zhou, C. Yan, Z. Zhu, A. Du, A single boron atom doped boron nitride edge as a metal-free catalyst for N_2 fixation, Phys. Chem. Chem. Phys. 21 (2019) 1110–1116, https://doi.org/10.1039/C8CP07064D.
[290] Y. Li, D. Gao, S. Zhao, Y. Xiao, Z. Guo, Y. Fang, J. Lin, Z. Liu, Y. Huang, K. Guo, C. Tang, Carbon doped hexagonal boron nitride nanoribbon as efficient metal-free electrochemical nitrogen reduction catalyst, Chem. Eng. J. 410 (2021) 128419, https://doi.org/10.1016/j.cej.2021.128419.
[291] J. Zhao, Z. Chen, Single Mo atom supported on defective boron nitride monolayer as an efficient electrocatalyst for nitrogen fixation: a computational study, J. Am. Chem. Soc. 139 (2017) 12480–12487, https://doi.org/10.1021/jacs.7b05213.
[292] Y. Huang, T. Yang, L. Yang, R. Liu, G. Zhang, J. Jiang, Y. Luo, P. Lian, S. Tang, Graphene–boron nitride hybrid-supported single Mo atom electrocatalysts for efficient nitrogen reduction reaction, J. Mater. Chem. A 7 (2019) 15173–15180, https://doi.org/10.1039/C9TA02947H.
[293] Z. Ma, Z. Cui, C. Xiao, W. Dai, Y. Lv, Q. Li, R. Sa, Theoretical screening of efficient single-atom catalysts for nitrogen fixation based on a defective BN monolayer, Nanoscale 12 (2020) 1541–1550, https://doi.org/10.1039/C9NR08969A.

[294] S. Zhou, X. Yang, X. Xu, S.X. Dou, Y. Du, J. Zhao, Boron nitride nanotubes for ammonia synthesis: activation by filling transition metals, J. Am. Chem. Soc. 142 (2020) 308–317, https://doi.org/10.1021/jacs.9b10588.
[295] C.V.S. Kumar, V. Subramanian, Can boron antisites of BNNTs be an efficient metal-free catalyst for nitrogen fixation? – a DFT investigation, Phys. Chem. Chem. Phys. 19 (2017) 15377–15387, https://doi.org/10.1039/C7CP02220D.
[296] C. Chen, D. Yan, Y. Wang, Y. Zhou, Y. Zou, Y. Li, S. Wang, B.-N. Pairs, Enriched defective carbon nanosheets for ammonia synthesis with high efficiency, Small 15 (2019), 1805029, https://doi.org/10.1002/smll.201805029.
[297] J. Zhao, X. Ren, X. Li, D. Fan, X. Sun, H. Ma, Q. Wei, D. Wu, High-performance N_2-to-NH_3 fixation by a metal-free electrocatalyst, Nanoscale 11 (2019) 4231–4235, https://doi.org/10.1039/C8NR10401H.
[298] B. Liu, Y. Zheng, H.-Q. Peng, B. Ji, Y. Yang, Y. Tang, C.-S. Lee, W. Zhang, Nanostructured and boron-doped diamond as an electrocatalyst for nitrogen fixation, ACS Energy Lett. 5 (2020) 2590–2596, https://doi.org/10.1021/acsenergylett.0c01317.
[299] X. Zhang, T. Wu, H. Wang, R. Zhao, H. Chen, T. Wang, P. Wei, Y. Luo, Y. Zhang, X. Sun, Boron nanosheet: an elemental two-dimensional (2D) material for ambient electrocatalytic N_2-to-NH_3 fixation in neutral media, ACS Catal. 9 (2019) 4609–4615, https://doi.org/10.1021/acscatal.8b05134.
[300] M. Jana, R.N. Singh, Progress in CVD synthesis of layered hexagonal boron nitride with tunable properties and their applications, Int. Mater. Rev. 63 (2018) 162–203, https://doi.org/10.1080/09506608.2017.1322833.

Madiha Rafiq is currently a Ph.D. scholar in Shantou University under the supervision of Prof. Fushen Lu & Prof. Liangsheng Hu. She received her M.S./M.Phil. degree in chemistry from the University of Agriculture Faisalabad, Pakistan. Her research interests include controlled synthesis of functionalized 2D hexagonal boron nitride nanomaterials and their applications in green energy-related fields.

Xiaozhen Hu received her bachelor's degree from Jinggangshan University and master's degree in chemistry from Shantou University in 2015. Her research mainly focuses on functionalization of boron nitride sheets and nanocomposites fabrication. She is a staff member of the Intellectual Property Protection Center int Shenzhen, China.

Zhiliang Ye received his bachelor's degree from Dongguan University of Technology and master's degree in chemistry from Shantou University in 2015. His research mainly focuses on the preparation of doped boron nitride nanomaterials for catalytic applications.

Abdul Qayum received his Ph.D. degree from School of Chemistry and Chemical Engineering, Shandong University in 2020. He then joined Shantou University as a postdoc fellow work in the research group of Prof. Fushen Lu & Prof. Liangsheng Hu. His research focuses on the development of functional materials for (photo)electrochemical water splitting and wastewater treatment.

Hong Xia received her Ph.D. degree from Tianjin University in 2017 and at Tianjin University as a postdoc research fellow in 2017–2019 before becoming a lecturer in the School of Science of Shantou University. Her research interests are nanostructured functional materials and their application in sustainable energy and clean environment technologies.

Liangsheng Hu received his Ph.D. in chemistry from The Hong Kong Polytechnic University in 2018 and is an associate professor at Shantou University. His research focuses on the synthesis and application of functional nanomaterials for electrochemical and photochemical catalysis, clean energy production, and biosensing.

Fushen Lu received his Ph.D. in 2005 from the Institute of Chemistry, Chinese Academy of Sciences. He worked as a postdoctoral fellow in 2005–2010 at Clemson University, USA. He is a professor in Shantou University working on carbon and boron nitride nanomaterials for novel catalytic and energetic applications.

Paul K. Chu received his Ph.D. in Chemistry from Cornell University. He is Chair Professor of Materials Engineering in the Department of Physics, Department of Materials Science, and Department of Biomedical Engineering in City University of Hong Kong. He is Fellow of the American Physical Society (APS), American Vacuum Society (AVS), Institute of Electrical and Electronics Engineers (IEEE), Materials Research Society (MRS), and Hong Kong Institution of Engineers (HKIE). He is also Fellow and Council Member of the Hong Kong Academy of Engineering Sciences (HKAES). His research interests are quite diverse encompassing plasma surface engineering, materials science and engineering, surface science, and functional materials. He is a highly-cited researcher according to Clarivate Analytics of the Web of Science.